UNIVERSIDADE DE LISBOA
FACULDADE DE CIÊNCIAS
DEPARTAMENTO DE FÍSICA

Chiral nematic liquid crystals at interfaces and substrates

Francisco Ferreira Verdasca Moreira Braz

Mestrado em Física
Especialização em Estatística e não linear

Dissertação orientada por:
Prof. Doutora Margarida Telo da Gama
Prof. Doutor Nuno Silvestre

2017

UNIVERSIDADE DE LISBOA

FACULDADE DE CIÊNCIAS

DEPARTAMENTO DE FÍSICA

Chiral nematic liquid crystals at interfaces and substrates

Francisco Ferreira Verdasca Moreira Braz

Mestrado em Física

Especialização em Estatística e não linear

Dissertação orientada por:

Prof. Doutora Margarida Telo da Gama

Prof. Doutor Nuno Silvestre

2017

Acknowledgements

I would like to express my deepest gratitude to my supervisors Margarida Telo da Gama and Nuno M. Silvestre, for their guidance and support, and to Nelson R. Bernardino, who brought me into the Center of Theoretical and Computational Physics and without whom I wouldn't have had the pleasure of working in such a magnificent theme. Through the course of the past two years I was guided not only with knowledge but with heart. They provided me unrestrained insight in how to overcome the problems that I came across and had, in any occasion, a mammoth patience to discuss the many naive ideas that I strafed them with. I acknowledge the financial support of the Portuguese Foundation for Science and Technology for the grant, PTDC/FIS/119162/2010, under the supervision of Nelson R. Bernardino. To all the CFTC staff and to those with whom I shared office, I would also like to dedicate a special thank, for all the advice, appreciation and friendship. I also acknowledge the unparalleled work conditions that I was provided with in CFTC during the course of this work.

To my family and friends, I cannot express how grateful I am to have you by my side and I would not have gotten this far without your incommensurable love and support. Thank you.

”When modern physics exerts itself to establish the world’s formula, what occurs is this: the being of entities has resolved itself into the method of the totally calculable”

Martin Heidegger

Abstract

For the past decade, one of the trends in liquid crystal studies has been the development of the fundamental understanding of interfacial and wetting phenomena of different liquid crystal phases. The reason to do so lays on the complexity and richness behind the characteristic anisotropic properties of liquid crystals that represent a viable path to the creation of novel applications, so far inaccessible with the use simple isotropic liquids. A pictorial example of the usefulness of these properties is that they allow a controlled assembly from surfaces of immersed particles in liquid crystals. These surfaces can be lithographic controlled substrates or interfaces. Thus, each of these systems has been subject to systematic and progressive study in order to complete the comprehension of this field. This thesis is inserted on this trend and is focused on the study of the Blue Phase (BP) interface with the Isotropic (I) and the Cholesteric (C) phases at the mesoscale with respect to their surface tension and interface roughness. Such study is developed for the triple coexistence, using the Landau-de Gennes (LdG) phenomenological model.

As a first result of this study it was found at the triple phase coexistence line a hyperbolic relation between the two constant approximation LdG rescaled elastic constant and the pitch. Moreover, regardless of the position in the phase diagram, the blue phase periodicity has a linear relation with that of the cholesteric phase. For the BP-I coexistence it is observed that the interface equilibrium configuration has a zig-zag arrangement of *double-twist* cells and that the undulation profile has two distinct roughness behaviours, depending on the pitch. The transition between behaviours occurs due to an interface anchoring transition, in which for low pitch values cells have small deformations and have planar anchoring while for high pitch values cells are highly deformed and have homeotropic anchoring. Moreover, it is observed that it is possible to have a continuous transition between the roughness profiles of the BP-I and C-I interfaces over the triple phase line. For the BP-C coexistence it is found that the interface equilibrium configuration has a linear arrangement of undistorted *double-twist* cells with cholesteric layers tilted by $\pi/4$, regardless of the pitch values, and that there is no anchoring transition like in the BP-I interface. It is also observed that for low pitch values only the BP-I can coexist. An introductory study of the behaviour of rough substrate confined cholesterics is also presented, showing that for a sawtooth substrate weak planar anchoring the cholesteric layers adopt a parallel orientation at the substrate regardless of the substrate aperture.

Keywords: Liquid Crystal, Chiral Nematic, Nematic, Cholesteric, Blue Phase, Landau-de Gennes Model, Frank-Oseen Model, Interface, Surface Tension, Roughness, Substrate

Resumo

Ao longo da última década, uma das tendências no estudo de Cristais Líquidos baseou-se no desenvolvimento da compreensão fundamental dos fenómenos interfaciais e de molhagem de diferentes fases. A razão para tal assenta na complexidade e riqueza por de trás das propriedades anisotrópicas características destes materiais, a partir das quais poderá vir a ser aberto um caminho viável para a criação de novas aplicações, até agora inacessíveis com o uso the líquidos isotrópicos. Um exemplo pitoresco da utilidade das propriedades destes sistemas é o de permitirem a montagem controlada de estruturas de partículas imersas que crescem a partir das superfícies do cristal líquido. Estas superfícies podem ser substratos controlados por processos litográficos ou interfaces. Como tal, cada um destes sistemas tem vindo a ser sujeito a um estudo esquematizado e progressivo a fim de completar a compreensão fundamental do ramo. Esta tese está inserida nesta tendência e foca-se no estudo de interfaces à mesoescala de um sistema em coexistência tripla entre a Blue Phase o Colestérico e o Isotrópico em relação à tensão de superfície e rugosidade das interfaces usando o modelo fenomenológico de Landau de-Gennes.

Como primeiro resultado vê-se que na coexistência tripla de fases existe uma relação hiperbólica entre a constante elática rescalada de LdG e o pitch. Além disso observa-se que, independentemente da posição no diagrama de fases, a periodicidade da blue phase tem uma relação linear com a periodicidade do colestérico. Para a coexistência entre a BP-I, é observado que a configuração de equilíbrio da interface tem um arrajo em zig-zag das células de *double-twist* e que o perfil de ondulações tem dois comportamentos de rugosidade distintos, dependendo do pitch. A transição entre comportamentos ocorre devido a uma transição de ancoramento da interface, em que para valores baixos de pitch as células são pouco deformadas e o ancoramento é paralelo e em que para valores elevados de pitch as células são altamente deformadas e o ancoramento é homeotrópico. É também observado que é possível ter uma transição contínua entre os perfis de rugosidade das interfaces BP-I e C-I sobre a linha de coexistência tripla. Para a coexistência entre a blue phase e o colestérico, é observado que a configuração de equilíbrio da interface tem um arranjo linear das células de *double-twist* com as camadas de colestérico a fazer um ângulo de $\pi/4$ na superfície, independentemente do pitch, e que não há transição de ancoramento como na interface BP-I. É também observado que para valores baixos do pitch apenas pode ocorrer a coexistência entre a blue phase e o isotrópico. Um estudo introdutório sobre o comportamento do colestérico confinado por um substrato rugoso é apresentado, mostrando que para um susbtrato dente de serra com ancoramento planar fraco, as camadas de colestérico adoptam uma orientação paralela ao substrato, indepentemente da abertura do substrato.

O Capítulo 1 é dedicado à motivação por trás do desenvolvimento desta tese. É feita a distinção conceptual entre líquidos convencionais e cristais líquidos através do desenvolvimento das ideias de ordem posicional e ordem orientacional. Em função dos diferentes tipos de ordem são apresentadas várias fases de cristais líquidos e o que as distingue fundamentalmente. Feita esta distinção apresentam-se as fases que serão estudadas nesta tese, nemáticos quirais, e de que forma elas se relacionam através das suas propriedades elásticas e quiralidade. Em seguida é introduzida a ideia de campo orientacional usada para descrever cada uma destas fases e de que forma a sua quebra de simetria se manifesta, ou em defeitos topológicos ou em interfaces. São também apresentados alguns exemplos da necessidade e da utilidade de estudar as manifestações da quebra de simetria do campo orientacional. Por fim apresentam-se alguns avanços nos estudos das fases nemático, colestérico e blue phase, com respeito à presença de colóides, substratos e interfaces.

No Capítulo 2 desenvolvem-se tanto conceptualmente como analiticamente os conceitos apresentados no capítulo anterior. Começa-se por desenvolver as noções de campo orientacional e simetria uniaxial e biaxial nos nemáticos. Acrescenta-se então a influência da quiralidade nestes compostos e de que forma o nemático pode ser visto como um limite do colestérico. Partindo da presença de quiralidade explora-se a forma em como esta está envolvida nas frustrações no campo orientacional e como através da nucleação de defeitos topológicos ocorre o aparecimento da blue phase. Para explorar de forma analítca a estabilidade e o perfil orientacional de cada uma destas fases, é desenvolvido o primeiro modelo contínuo de cristais líquidos, o modelo de Frank-Oseen. Este modelo permite ver como a energia livre do sistema está relacionada com distorções do campo orientacional, através do *splay*, *twist*, *bend* e *saddle-splay*. Mostra-se também de que forma este modelo pode contemplar a presença de células de *double-twist*. Em seguida, explora-se este modelo sob a presença de defeitos topológicos e qual é a forma típica das suas penalizações energéticas. Estabelece-se também a ponte entre estas penalizações e a forma em como as diferentes fases da blue phase estão organizadas face às suas frustrações intrínsecas do campo orientacional. Dado que este modelo falha na explicação do sistema na presença de interfaces é introduzido o conceito de parâmetro de ordem que serve de base para o modelo de Landau para transições de fase. Explora-se de que forma a diferença entre transições de fase de primeira e segunda ordem permitem ligar este modelo aos cristais líquidos no modelo de Landau-de Gennes que usa parâmetros de ordem escalar e tensorial. Por consistência e de forma a dar uma interpretação intuitiva deste modelo, estabelece-se a ligação com o modelo de Frank-Oseen para diferentes aproximações na degenerescência entra as constantes elásticas. De forma a obter um modelo transversal a qualquer composto líquido cristalino, realiza-se o rescalamento da energia livre neste modelo. Por fim, faz-se uma breve extensão deste modelo aos efeitos da presença de uma superfície ordenada.

No Capítulo 3, é explicada em primeiro lugar a equação de Euler-Lagrange do funcional de energia livre do modelo de Landau-de Gennes para obter o estado de equilíbrio, a partir do qual é possível fazer a leitura da tensão de superfície para os diferentes parâmetros do sistema. Este estado é dado em função do perfil do parâmetro de ordem tensorial em todo o sistema, que expressa o perfil do campo orientacional, permitindo portanto estudar a estrutura das diferentes interfaces. Em seguida é feita uma breve passagem sobre as ideias envolvidas no método computacional de Elementos Finitos e de que forma são obtidas as soluções numéricas das equações de Euler Lagrange dos diferentes termos do tensor de ordem.

Desenvolvidos todos os conceitos e ferramentas necessárias, o Capítulo 4 é então dedicado à revisão dos resultados obtidos nos estudos da interface C-I. A interface C-I foi estudada em função da tensão de superfície e do perfil ondulatório da superfície, que aparece devido à presença do pitch. Observou-se que quando o ancoramento é homeotrópico a configuração de equilíbrio da interface, i.e, com a menor tensão de superfície, ocorre quando as camadas de colestérico se orientam perpendicularmente à superfície e a amplitude das ondulações tem um crescimento sub-linear com a raiz quadrada do pitch. Já quando o ancoramento é planar a configuração de equilíbrio da interface ocorre quando as camadas de colestérico se orientam paralelamente à superfície e não há ondulações na interface. Para o caso do ancoramento homeotrópico observou-se adicionalmente que para valores pequenos de pitch ocorria a nucleação de células junto da interface, ou seja, que ocorria uma transição de fase para a blue phase.

Por fim, nos Capítulos 5 e 6 são apresentados os novos resultados. Começa-se por construir um diagrama de fases (triplo) para definir para que valores do pitch e constantes elásticas do colestérico é que, à temperatura de coexistência com o isotrópico, o isotrópico, o colestérico e a blue phase coexistem. Desta forma é então possível estudar separadamente cada interface sobre a linha tripla. As interfaces BP-I e BP-C são estudadas para cada uma das suas duas configurações em função da tensão de superfície e perfil de ondulações. Para concluir o trabalho, explora-se o comportamento de um colestérico confinado

por um substrato em forma de dente de serra com ancoramento planar fraco para diferentes ângulos das camadas do colestérico, dimensões dos dentes do substrato e valores de pitch, com elasticidade fixa.

Palavras-chave: Cristais Líquidos, Nemático Quiral, Nemático, Colestérico, Fase Azul, Modelo de Landau-de Gennes, Modelo de Frank-Oseen, Interface, Tensão de Superfície, Rugosidade, Substrato

Contents

List of Figures

Chapter 1

Introduction

Transitions from solid to liquid are of universal familiarity through everyday experience. Among the usual daily materials, one would hardly expect anything different from a simple transition to happen. However, beyond usual materials, there are some organic compounds that exhibit more than a simple transition from solid to liquid and can instead go through a set of intermediate transitions between the solid and liquid phases [1].

One of the first experimental evidences of such behaviour, was provided by Friedrich Reinitzer, back in 1888. He observed that a sample of cholesteryl benzoate did not simply melt from solid to liquid, but instead it went through intermediate states (mesophases) as temperature was gradually raised, from a solid into a cloudy liquid and then into a clear transparent liquid [2]. Solids with crystalline organization are characterized by magnetic and electric anisotropic susceptibilities while liquids are characterized by viscosity and the inability to support shear. It was not long after the discovery of the peculiar cholesteryl benzoate phase transitions that other materials exhibited the intermediate phase transitions and the necessity to characterize the mesophases regarding crystalline or liquid properties came up. Surprisingly, observations indicated that these mesophases had both crystalline and liquid properties and it was Otto Lehmannm, back in 1889, who defined this new and exotic materials as "liquid crystals", a new state of matter [3].

Liquid crystals can be either temperature or concentration dependent. Those whose physical properties go through an abrupt change from one phase to the other at a given transition temperature are called thermotropic. Others may depend on the material concentration in a solvent to go through such a transition and are called lyotropic liquid crystals [4].

A crystal has a lattice with three-dimensional periodicity, i.e, it has three-dimensional long range positional order. If instead of spherical molecules, some other kind of geometry should be associated to them, long range orientational order may also be present. When orientational order exists, it means that molecules are aligned according to an orientational distribution. Thus, in a crystal both kinds of order can coexist. However, if one kind of order is somehow degraded, the other kind may be unaffected. If some degree of fluidity is present in a crystal, long range positional order is reduced to lower dimensions, but orientational order may be preserved. This is the core idea to understand liquid crystals (LC) and why their mixed properties are a result of the constituent molecular geometry and the way they organize, both in position and orientation.

Different liquid crystal phases exist and their definition is based on the dimensionality of their positional order and on the orientational number of axes. The nematic phase has no long range positional order, Fig. 1.1 (a), the smectic phase has one-dimensional long range positional order, Fig. 1.1 (b), and the columnar phase has two-dimensional long range positional order Fig. 1.1 (c). Liquid crystal

molecules are uniaxially symmetric when they are rod-like, Fig. 1.1 (a.1), or disk-like, Fig. 1.1 (a.2), while biaxially symmetric molecules are brick-like, Fig. 1.1 (a.3) or boomerang-like. For phases with uniaxial orientational order, molecules have a global mean orientation along some unique direction, while for phases with biaxial orientational order, molecules have two global mean orientations, along the direction of a short and a long distinct axis [5].

Although preserving the same symmetry, there are certain features that change from material to material, such as elasticity, that is but the macroscopic expression of molecular interactions. Among the different elastic features is the twist. In the particular case of nematics, when molecules have chiral features, twist elastic deformations are enhanced by the amount of chirality. Hence, they are called chiral nematics. Chiral nematics with intermediate degrees of chirality, or simply cholesterics, Fig. 1.1 (a.1) and Fig. 1.2 (b), are distinct from regular nematics in that the molecules chiral features lead to a twist axis of the orientational order. This axis has a direction perpendicular to the molecules mean orientation and creates successive equidistant parallel planes with the same orientation, separated by a characteristic distance defined by the chirality degree, called the pitch. To some extent nematics can be interpreted as cholesterics, when the twist is negligible and when the pitch is infinite. Chirality in nematic liquid crystals may be controlled through different processes, however none of them lead to discontinuous phase transitions from the nematic to the cholesteric [6]. Chiral nematics with high degrees of chirality Fig. 1.2 (c) exhibit another phase, the blue phase, or as it is commonly designated, *double twist* phase. It is observed at temperatures immediately below the discontinuous transition from the isotropic phase to the cholesteric phase where a degeneracy of the cholesteric anisotropic singular twist axis into multiple twist axes is observed [7]. The phase is characterized by a mixed arrangement of *double-twist* cylinders and a lattice of topological defects, in which the periodicity of the cylinders and the structure of the defect lattice depend on the degree of chirality [8].

Elasticity provides liquid crystals the mechanisms to deform under thermal fluctuations, external fields or constraints imposed by the system boundaries, leading them to reorganize in more stable configurations. However, for strong enough perturbations, regions where the smooth behaviour of the orientational order is broken may be induced, topological defects, interfaces, or both. The main focus of this thesis is to understand interfaces of chiral nematic liquid crystals, between the blue phase and isotropic phases (BP-I) and between the blue phase and cholesteric phases (BP-C).

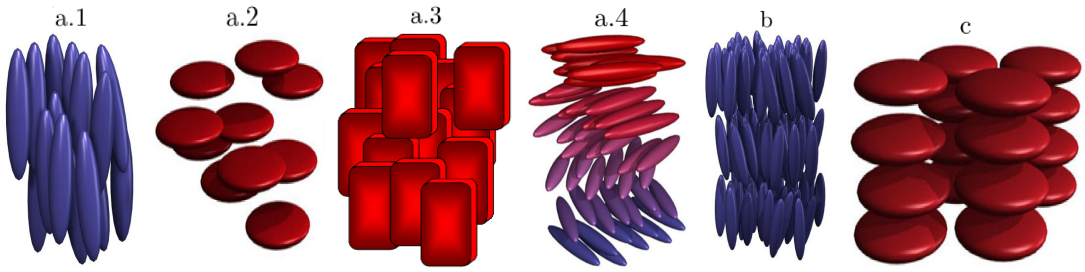

Fig. 1.1: Schematic representation of: (a) Nematic liquid crystal phases: (a.1) rod-like molecules with uniaxial symmetry; (a.2) disk-like molecules with uniaxial symmetry; (a.3) brick-like molecules with biaxial symmetry; (a.4) rod-like molecules with uniaxial symmetry and a twist axis (chiral nematic or cholesteric) (b) Smectic liquid crystal phase for rod-like molecules with uniaxial symmetry; (c) Columnar liquid crystal phase for disk-like molecules with uniaxial symmetry [9].

Topological defects, or simply disclinations, are regions where the order is destroyed, ranging from points to lines [10]. The identification and understanding of defects and their interactions plays an important role both in liquid crystal studies and applications. For example, phase recognition and elastic properties can be indirectly obtained by observing defect interactions [11]. If a liquid crystal phase is

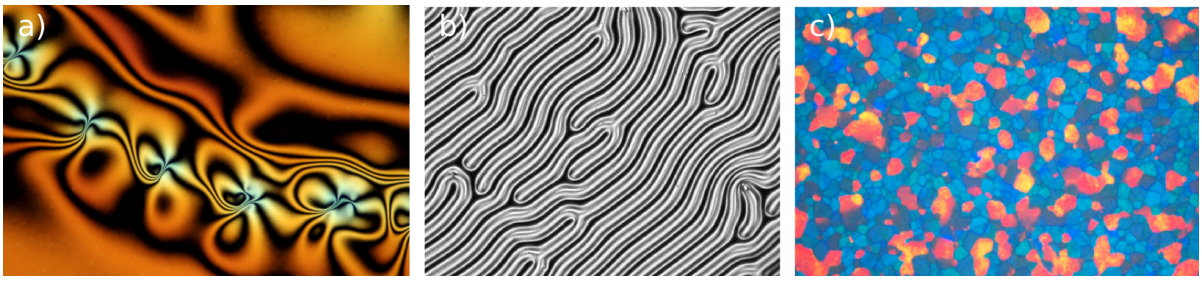

Fig. 1.2: Polarizing microscope texture of: a) nematic liquid crystal with defects [16]; b) cholesteric liquid crystal with defects [17]; c) blue phase [17].

one with a defect lattice, as is the case of blue phases [12], or if defects condition an interface texture [13], then understanding their nature is of considerable relevance for the interpretation of such systems. Furthermore, while some applications require that defects are eliminated, others actually require their presence [14, 15], so again understanding and controlling them has practical importance, specially when dealing with LC free surfaces.

Interfaces in liquid crystals occur at coexistence between different phases, that may occur in a typical discontinuous LC phase transition of one component [7, 8, 18–20] or in LC mixtures [21–23]. Either way, what characterizes liquid crystals stationary interfaces is the competition between the phases features, orientational order, elasticity and symmetry. At equilibrium, each phase is organized in the most symmetric way, in which the free energy is minimized. The organization is extended into the interface, where it conflicts with the other phase orientational order, elasticity and symmetry, which endows this region with a surface tension, i.e, an excess free energy of the surface. Free surfaces between normal liquids, where both phases have translational symmetry, are generally planar if no external constraints are present. If one of the phases has homogeneous orientation, as is the case in the nematic-isotropic (N-I) coexistence system, specific molecular arrangements of the orientation at the surface are expected, i.e, anchoring, while preserving the flatness caused by the broken translational-rotational symmetry [24]. If the ordered phase orientational order is non homogeneous, as is the case for the cholesteric-isotropic (C-I) coexistence system due to the presence of a twist axis, this symmetry is also broken and the competition between the properties of the two phases may manifest itself through the creation of undulated interfaces and topological defects at the free surface [13, 25].

Apart from its conceptual interest, the study of liquid crystal interfaces is of great importance both because it presents a viable way to create a variety of applications, as for example liquid crystal colloidal systems, and because it is a necessary ingredient to interpret other applications, as for example substrate confined LC systems where wetting properties emerge. The use of interfaces for the study of surface-induced ordering of liquid crystals has a major advantage by contrast to surface-induced ordering of LCs on solid substrates, as the behaviour of molecules at the interface can be coupled and manipulated with the orientational order and elastic properties of the sample [26]. The phenomenology associated with interfaces and wetting is very rich and the unique features of liquid crystals, such as elasticity and the presence of topological defects are promising routes to new microfluidic devices, where interfacial properties play a critical role [27]. In wetting systems, the balance between the elastic properties, the interfacial properties and the substrate anchoring may be used to create novel applications, for example, the creation of a nematic wetting layer and its interfacial properties can be used for example to mimic naturally occurring biological fibrous composites [28].

In liquid crystal colloidal systems, nematic-isotropic interfaces can be used, to control the motion and morphology of a colloid through a moving free surface with a given speed and surface anchoring

[29]. N-I interfaces can also be used for particle selection, depending on the free surface anchoring and particles size [30]. Cholesteric-isotropic interfaces can be used to select the distribution of particles at the free surface and to create chains of particles parallel to the cholesteric layers [21], or to create a template of particles at the interface [22, 23] through the control of the ratio between the particles size the cholesteric pitch and ratio between the anchoring strength and the elastic contributions. Nematic colloids can also be explored through substrate-induced properties, either jointly with interface-induced properties or solely [31].

In substrate confined liquid crystal systems, when a disordered phase is in contact with a substrate that imposes order, wetting phenomena may occur, followed by the creation of LC-isotropic interfaces. This may happen in a variety of substrate geometries, either flat, sawtooth, sinusoidal or crenellated surfaces. If an isotropic phase of a nematic sample is in contact with a flat surface, a nematic-isotropic interface will be observed at a distance from the substrate that depends on the energetic balance between the substrate and the interface anchoring strength and orientation, [32]. If the substrate is structured, more complex relations between the substrate and nematic-isotropic interface anchoring strength and orientation emerge depending on the geometry [32–37]. For example, in the case of a sawtooth substrate, the substrate roughness imposes deformations in the nematic phase and increases the elastic deformations, enhancing the repulsion between the substrate and the interface. This behaviour depends on the relations between the amount of elastic deformations, the length and aperture of the wedges and the presence of topological defects [32, 34, 35].

Cholesterics near surfaces have only more recently started to be studied, but rich phenomena were expected from the beginning since analogously to the nematics, in which distortions are imposed by patterned surfaces, cholesterics have an intrinsic twist that endows them with similarly exotic properties even for the most trivial surface configurations. It was observed that when an isotropic phase is confined by a flat substrate with parallel anchoring, a pattern is induced at the cholesteric-isotropic interface, with a distance to between the interface and the substrate that grows with the cholesteric pitch and decreases with temperature [28]. The properties of the cholesteric-isotropic free surface were then explored with respect to the surface tension and surface undulation. It was observed that, when homeotropic anchoring is present at the surface, the undulations amplitude depends linearly on the twist of the elastic constant and on the square root of the pitch. For smaller pitch values and for higher twist deformations, the surface tension departed from that of the nematic. Preliminary results were obtained for the cholesteric phase transition to the blue phase, as a result of the properties of the interface [13]. These results were then used to study cholesteric wetting phenomena at flat substrate with planar anchoring. They were also used to explore how the anchoring strength of the substrate is related with the cholesteric pitch in the creation of an array of defects near the same substrate when the cholesteric-isotropic interface has homeotropic anchoring [27, 38].

As for blue phases, regarding applications very little has been explored so far. However due to their exotic properties, for instance the orientational periodicity and defect lattice, and motivated by recent developments in colloidal and substrate confined liquid crystal applications, some new methods to control the blue-phase systems have been developed. The blue phases narrow temperature range of stability was seen to be broadened through the introduction of colloids in the system [39]. The presence of colloids was also observed to cause localized melting of the blue phase to the isotropic at temperatures below the BP-isotropic transition into regions whose shapes were influenced by the surface-tension [40].

Given the recent advances in chiral nematic liquid crystals at interfaces and substrates, we dedicate this thesis to develop the subject further, by exploring the blue phase-isotropic and blue phase-cholesteric interfaces. We also present some preliminary results on cholesterics confined by a sawthooth substrate.

In Chapter 2 the concepts of this chapter are developed both conceptually and analytically. The notions of orientational field, uniaxial and biaxial symmetry are first developed. The influence of chirality on these compounds and how the nematic can be interpreted as a limit of the cholesteric, is then added. From the presence of chirality the way in which it relates with orientational field frustrations and how the blue phase emerges through the nucleation of topological defects, is explored. To explain the stability and the orientational profile of the chiral nematic phases the first continuum model of liquid crystals, the Frank-Oseen model, it is developed. This model allows to see how the system free energy is related to the orientational field distortions through the *splay*, *twist*, *bend* e *saddle-splay*. It is also shown how the model contemplates the presence of *double-twist*. Next, the model is explored under the presence of topological defects and typical form of their energetic penalties. With this, the bridge between these penalties and the order is established, in which the different blue phase phases emerge with respect to the intrinsic frustrations of the orientational field. Given the failure of the model in explaining the systems in the presence of interfaces, the concept of order parameter, the base for the Landau model of phase transitions, is introduced. The difference between first and second order phase transitions is then explored to connect this model with liquid crystals leading to the Landau-de Gennes model that uses a scalar and a tensor order parameter. As a consequence and in a way that allows this model to have an intuitive interpretation, the connection between the Landau-de Gennes and the Frank-Oseen is established and different approximations are considered with respect to the elastic constants degeneracy. In order to obtain a transversal model suitable to describe any chiral nematic liquid crystal compound, the free energy of the Landau-de Gennes functional is rescaled. Lastly, a brief extension of this model is done to consider situations where substrates that impose order are present.

In Chapter 3 the Euler-Lagrange equation is developed and applied to the Landau-de Gennes free energy functional, in order to obtain the equilibrium state, from which it is then possible to read the surface tension for different parameters of the system. This state is given in function of profile of the tensor order parameter in all the system, which expresses the orientational field, thus allowing to study the structure of the different interfaces. Then a brief introduction is done on the ideas behind the computational method that we use, the Finite Element Method, and on how the numerical solutions of the Euler-Lagrange equations are obtained for the different terms of the tensor order parameter.

With all the necessary concepts and tools developed, Chapter 4 is dedicated to the revision of previous results for the C-I interface. This interface was studied with respect to the surface tension and surface undulations profile which emerge due to the presence of the pitch. It was observed that when the anchoring is homeotropic the interface equilibrium configuration occurs when the cholesteric layers are oriented perpendicular to the surface and that the undulations amplitude scales sub-linearly with the square root of the pitch. When the anchoring is planar, however, the interface equilibrium configuration occurs when the cholesteric layers are oriented parallel to the interface and there are no undulations. For the homeotropic case it was additionally observed that for low pitch values the nucleation of *double-twist* cells occurred at the interface, i.e, that a phase transition from the cholesteric to the blue phase occurred.

Lastly, in Chapters 5 and 6 new results are presented. A triple phase diagram is first obtained to understand at what pitch and rescaled elastic constant values the three phases, isotropic, cholesteric and blue phase, coexist. This way it is then possible to study separately each interface over the triple line. The interfaces BP-I and BP-C are studied for each of its two configurations with respect to the surface tension and undulations profile. To conclude, the behaviour of a rough substrate confined cholesteric is explored.

Chapter 2

Theoretical concepts

This chapter is dedicated to the ideas and mathematical tools required to understand the developed work. Sec.2.1, Sec.2.2 and Sec.2.3 are dedicated to the conceptual description of the different chiral nematic phases, the nematic, the cholesteric and the blue phase. Based on these ideas, in Sec.2.4 the cornerstone of liquid crystals models is constructed, the Frank-Oseen model. Associated to this model, the description of topological defects is constructed in Sec.2.5, providing insight on crucial phenomena through the rest of this work. Sec.2.6 is dedicated to make the bridge between the Frank-Oseen classic model and the LdG model, introducing the notion of order parameter and how it relates to physical parameters. Sec.2.7 briefly introduces the concepts of phase transitions, around which the LdG model is constructed. In Sec.2.8 the LdG model is constructed and the approximations in which this work will be presented. Finally, Sec.2.9 connects all the previous concepts in the presence of substrates.

2.1 Nematic

As in liquids, the nematic phase possesses no positional order, meaning that molecules are randomly distributed throughout the sample. However, the nematic phase differs from ordinary liquids in one fundamental aspect, it has orientational anisotropy. From this anisotropy a unique axis emerges, along which molecules tend to align parallel to their neighbours and the phase exhibits a particular set of physical properties. This parallel alignment tendency is attributed to molecular cylindrical symmetry and a practical example is how it manifests through the optical properties, in which rays polarized parallel to the symmetry axis have a different index of refraction from those polarized perpendicular to it [1].

In order to describe the phenomenology of a nematic phase with respect to the geometry and dynamics around the preferred axis, given that physical properties along this axis do not change on a local scale, i.e, are locally invariant, a continuous vector field **n(r)** is assumed to describe the phase, also known as director, which gives the orientation profile of the cylindrical axis throughout the nematic. The director magnitude has no meaning and for simplicity it is simply defined as unity. Furthermore, physical properties along the director are invariant under π rotations of the system, meaning that nematic molecules do not exhibit polar features. Thus, the director is defined as $\mathbf{n} = -\mathbf{n}$, also referred to as head-tail symmetry. Even if molecules do possess any polar feature, this symmetry implies that there is an even proportion between head and tail polarities.

When uniaxial systems are exposed to certain constraints, such as interfaces or substrates, due to frustrations imposed by the constraints, there may occur a break of cylindrical and head-tail symmetry and polar and biaxial features may emerge, even though the molecules might not have any polar or biaxial features [30]. Nevertheless, biaxial phases may also occur naturally, even in the absence of

constraints. Biaxiality is characterized by two axis of symmetry, one main axis of symmetry, **n**, and a second symmetry axis, **m**, locally invariant and with head-tail symmetry. Thus, the parallel alignment tendency can be attributed to molecular brick-like, or rod-like and disc-like mixtures or boomerang-like symmetries, where all the molecules tend to align along both the long and short axes [41].

2.2 Cholesteric (Chiral nematic)

The cholesteric phase differs from the nematic in that it incorporates chiral centres which can be either a natural feature of the material or an artificial result, achieved through doping a nematic phase with some chiral component. The density of chiral centres, or simply put, chiralilty, induces a macroscopic helical twist distortion of the sample along an axis perpendicular to the director plane. By doing so, the director precesses along the twist direction, with a typical 2π precession distance, called the pitch length, P, as shown Fig. 2.1.

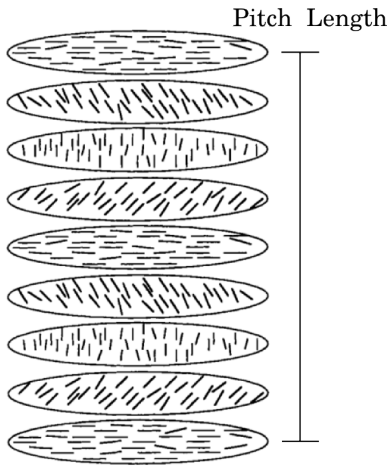

Fig. 2.1: Schematic representation of the orientational order precession of a cholesteric phase. The distance between two planes with the same orientation is half the pitch distance, $P/2$ due to head-tail symmetry (Figure from [42]).

Typically the cholesteric pitch length is of the order of a few micrometers, comparable with the wavelength of visible light, $400-750$nm, while chiral nematic molecules have a typical length of $1-5$nm along their long axis. The pitch is generally quite sensitive to temperature, chemical composition and applied magnetic or electric fields [6]. When the density of chiral centres is close to zero, the full precession length goes to infinity ($P \sim \infty$) . Thus, on the low chirality limit one can interpret the cholesteric just as a regular nematic, where the director doesnt precess at all. Typically, the relation between the degree of chirality, q, and the pitch is established as $P = 2\pi/q$.

Analogously to nematics, a degree of biaxiality can emerge in cholesterics if the sample is confined by surfaces or interfaces. However, in contrast to nematics, in cholesterics biaxiality emerges even in unconstrained systems. This is due to the natural helical feature of cholesterics. Given that the orientation of the director twists along the pitch axis, a cholesteric can be imagined as a set of layers that, depending on the distance between them, impose their orientation order on their neighbours and induce elastic frustrations between them. As the distance between layers is reduced, both natural frustrations and orientational order between planes are enhanced and biaxial order is created. Thus, for systems with low chilarity the inter plane phenomena can be neglected, but when dealing with systems of high chirality, biaxiality plays an important role that cannot be ignored [7].

2.3 Blue Phase (Double twist phase)

The blue phases are mesophases observed in the transition from the low temperature cholesteric phase to the high temperature isotropic liquid. They only exist in systems with high chirality, with pitch typically less than 500nm [7] and are due to a delicate balance between the increased degree of twist and the expense of forming defect lines. They exist in a narrow temperature range of typically one degree [40]. They exhibit bright coloured texture of individual, micron size platelets with a periodic structure typical of crystals, as shown in Fig. 1.2 (c). But still, they are liquids since no positional order is present, meaning their crystalline properties are related to the long range orientational order.

The distance between the centers of the platelets, that we defined here as $\tilde{P}/2$, is typically of the order of half the cholesteric pitch. Thus, due to this dependence this phase is characterized by the pitch, and as will be seen ahead, also by elastic properties. Although both the pitch [6] and elastic properties [43] are temperature dependent, since the blue phases are only stable in a narrow temperature range, they are usually considered temperature independent [7]. This assumption is, nevertheless, invalidated when the blue phase stability temperature range is broadened, for example due to the presence of colloids [39], since the blue phase periodicity suffers some changes [12]. Like cholesterics, blue phases are optically active and therefore rotate the direction of polarization of linearly polarized light, although orders of magnitude weaker than those of cholesterics. Their viscosity has been found to be about 10^6 times larger than the viscosity of their cholesteric phase, due to the stability that topological defects grant to the phase [7].

Up to three distinct thermodynamically stable blue phases can be distinguished in a great variety of chiral nematic compounds, separated by first order transitions, which occur in the order blue phase-I, blue phase-II and blue-phase III, for increasing temperatures [8, 44]. The two lower temperature phases, the blue phase I and II exhibit body-centered cubic and simple cubic defect lattice structures, respectively. The higher temperature phase, the blue phase III, appears to be amorphous, with isotropic symmetry.

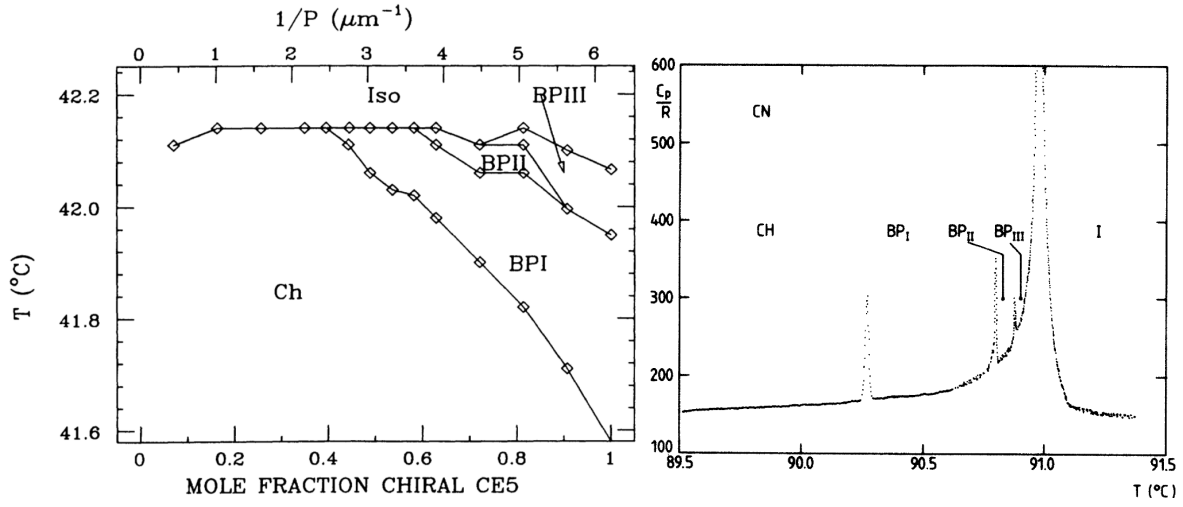

Fig. 2.2: (left) Phase diagram of the blue phases as a function of the inverse of the pitch for the CE5 chiral-racemic mixture (Figure from [8]). (right) Heat capacity measurements for the blue phase. The latent heat measured at the transitions decreases for growing temperatures (figure from [44]).

Following a symmetry argument it is possible to see that in the narrow temperature range of the transition from the cholesteric to the isotropic, where the blue phase is observed, the system goes from a low symmetry phase, the cholesteric, to a high symmetry phase, the isotropic. In this region, the low pitch values induce rotational frustrations between cholesteric planes and eventually stability is only

achieved when the twist axis is endowed with another rotation plane [45]. This leads to the nucleation of defect lines. When the creation of defect lines is favourable, a phase transition from the cholesteric to a higher symmetry phase occurs, the blue phase I, followed by the creation of *double twist* cylinders and a lattice of defects [46]. As temperature approaches the isotropic phase, frustrations are enhanced and the defect lattice is forced to change, into a phase with higher symmetry, the blue phase II. Finally the blue-phase III presents an amorphous defect structure, the most symmetric of the three. Thus, this symmetry argument states that the blue-phase symmetry increases with temperature. This is supported by the fact that first-order phase transitions are observed between the different blue phases, a typical feature of symmetry breaking, as can be seen in Fig.2.2.

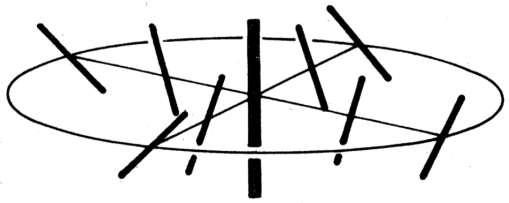

Fig. 2.3: Schematic representation of the director double-twist on a xy plane with the director pointing along z at the center of the figure. (figure from [7]).

A pictorial image of a blue phase projection on a plane comes from considering overlapped single helical pieces of cholesteric. If three pieces are separated by an angle of $\pi/3$, a *double-twist* cell with hexagonal symmetry bounded by corner defects is produced, like in Fig.2.4 [12]. A system composed of such cells produces a honeycomb lattice of defects. If alternatively, two pieces are separated by an angle of $\pi/2$, they will produce a *double-twist* cell with square symmetry and a square lattice of defects. The details of the defects will be presented in Sec. 2.5, but it is worth mentioning that, the defects of the honeycomb lattice are more stable than those of the square lattice, meaning that an honeycomb defect lattice is expected to show up before a square defect lattice. Even though blue phases are 3D phases, by following this pictorial construction some insight can be obtained by associating the 2D honeycomb symmetry with blue-phase I and the 2D square symmetry with blue-phase II.

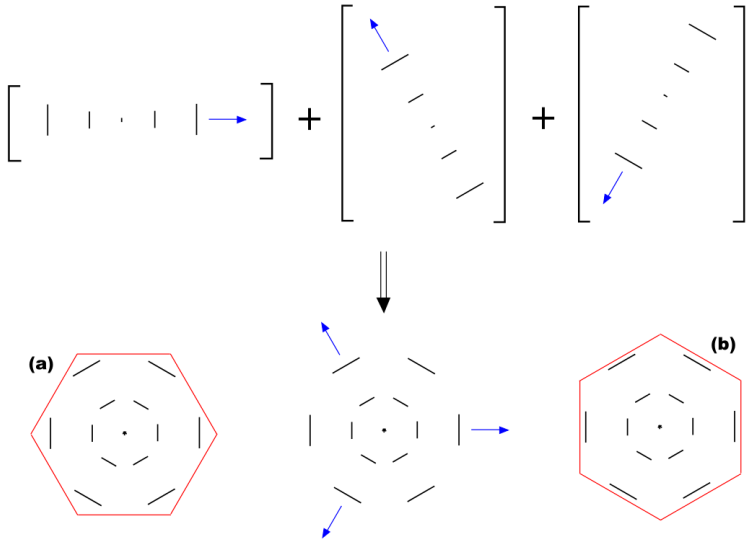

Fig. 2.4: Schematic representation of the superposition of cholesteric helices forming a region of local double twist that can be seen as unit cells of a two dimensional hexagonal lattice (Figure from [12]).

2.4 Frank-Oseen Model

In the nematic phase, molecules prefer to be aligned parallel to each other, along the director **n**. This does not mean the director orientation is not changed throughout the sample, it means that it only does so on a scale much larger then the molecule size. Thus, in the equilibrium configuration, locally the director does not exhibit any kind of distortion and $\partial n_i/\partial x_j = 0$, where the indices $i, j = 1, 2, 3$ denote the components of a three dimensional orthogonal axis of the system.

However, if the system is perturbed, either by forced orientation on surfaces, application of external fields, or changing temperatures, deformations will be imposed on the nematic equilibrium configuration and the director will be locally distorted, $\partial n_i/\partial x_j \neq 0$. Such distortions increase the free energy of the system. The local free energy density can thus be described in terms of energetic penalties of possible distortions, relative to a reference free energy density that corresponds to the equilibrium configuration [1, 47],

$$f = f_{eq} + f_{dist}. \tag{2.1}$$

To describe the free energy density based on the nature of the different director distortions, as those shown in Fig.2.5, the Frank-Oseen classical approach was proposed [47]. By definition the undistorted director of a nematic phase is chosen to be oriented along the z, direction in which, by imposition, there are no variations of the director. The director is defined in terms of its components as $\mathbf{n} = (n_x, n_y, n_z)$ and upon any distortion, they may change separately in different directions. There are three main bulk distortions [11]: if $\partial n_x/\partial x \neq 0$ and $\partial n_y/\partial y \neq 0$, they are *splay* distortions, Fig.2.5 (a); if $\partial n_x/\partial y \neq 0$ and $\partial n_y/\partial x \neq 0$, they are called *twist* distortions, Fig.2.5 (b); if $\partial n_x/\partial z \neq 0$ and $\partial n_y/\partial z \neq 0$, they are called *bend* distortions, Fig.2.5 (c).

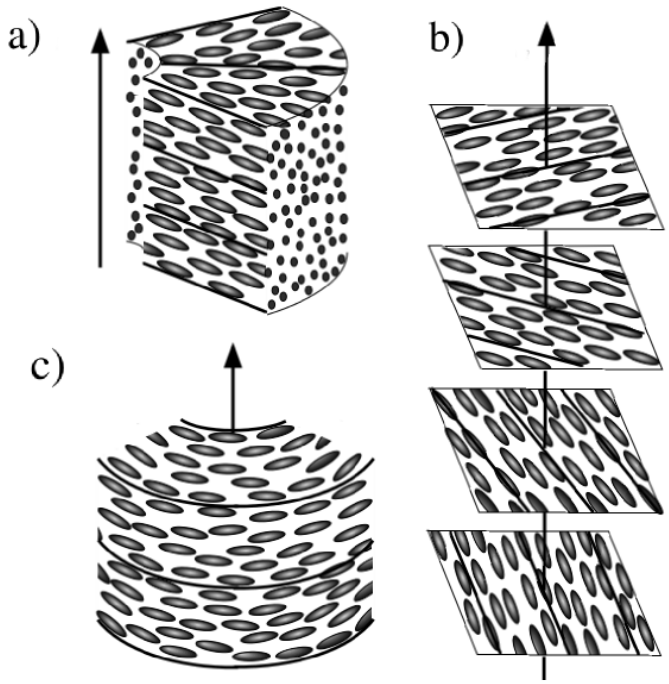

Fig. 2.5: Schematic representation of the elementary distortions of the director field: (a) splay; (b) twist; (c) bend (Figure from [45]).

Associated with each particular distortion, relative to the equilibrium orientation of the director, there is an energetic penalty that contributes to the distortion free energy density f_{dist}. Thus, the free energy density can be written in the general form as,

$$f_{dist} = K_{ij}^{lin}\frac{\partial n_i}{\partial x_j} + \frac{1}{2}K_{ijlm}^{quad}\frac{\partial n_i}{\partial x_j}\cdot\frac{\partial n_l}{\partial x_m}, \tag{2.2}$$

with K_{ij}^{lin} the energetic penalties associated with linear distortions and K_{ijlm}^{quad} associated with quadratic distortions. This expression can be developed for uniaxial chiral nematics, considering that along the z direction there are no variations of the director, i.e, $n_z \approx 1$ everywhere, with $\frac{\partial n_z}{\partial x} = 0$ $\frac{\partial n_z}{\partial y} = 0$ and $\frac{\partial n_z}{\partial z} = 0$, yielding the Frank-Oseen formula [11, 43, 47] (Appendix A), in which all the K terms correspond to quadratic terms,

$$\begin{aligned} f_{dist} = \frac{1}{2}K_{11}(\nabla\cdot\mathbf{n})^2 + \frac{1}{2}K_{22}(\mathbf{n}\cdot(\nabla\times\mathbf{n}) - q_0)^2 + \frac{1}{2}K_{33}(\mathbf{n}\times\nabla\times\mathbf{n})^2 \\ +\frac{1}{2}(K_{22}+K_{24})\nabla\cdot[(\mathbf{n}\cdot\nabla)\mathbf{n} - \mathbf{n}(\nabla\cdot\mathbf{n})]. \end{aligned} \tag{2.3}$$

The energetic elastic contributions K_{11}, K_{22}, K_{33} and K_{24} are associated with the splay, twist, bend and saddle-splay distortions, respectively. q_0 is the natural chirality of the material and is associated to the natural twist. The elastic constants values (J/m) depend on the sample considered, but a general feature is that the energetic elastic penalties always decrease when temperature is increased [43]. There is, nevertheless, a common feature of all substances, that $K_{22} \leq K_{11} \leq K_{33}$ [48]. The term associated with $(K_{22}+K_{24})$ has the form of a divergence, so the total free energy contribution of this term can be transformed into a surface integral. Thus, energetic contributions associated to such term should only be considered when surfaces are present, either bounding regions of the topological defect core's, interfaces, or substrates, due the arise of polar features.

The Frank-Oseen approach can also be used to model other phases as long as they preserve the properties of chiral nematics. Thus, let us consider the blue phase, that has a stable structure of the *double-twist* cylinders filling a lattice of defects at the temperature transition from the cholesteric to the isotropic phase. For simplicity let us consider a 2D blue phase structure, say with a honeycomb geometry as presented in Fig.2.4, where defects have $s = -1/2$. In the xy plane with translational invariance along z and with molecules rotating helically in all directions perpendicular to the cylinder orientation, the director field can be written in cylindrical coordinates as, $n_r = 0$, $n_\phi = \sin(\psi(r))$, $n_z = \cos(\psi(r))$, with $\psi(r) = qr$ and q the periodicity between the center of the different cylinders. Replacing this vector field in Eq.2.3 results,

$$f_{dist} = \frac{1}{2}K_{22}\left(q - q_0 + \frac{1}{r}\sin(qr)\cos(qr)\right)^2 + \frac{1}{2}K_{33}\left(\frac{\sin^2(qr)}{r}\right)^2 - \frac{q(K_{22}+K_{24})}{r}\sin(qr)\cos(qr). \tag{2.4}$$

Thus, the stability of the blue phase does not depend on *splay* contributions. It does however strongly depend on *saddle-splay*. If the bounding regions of defects are considered this elastic penalty must be also considered and when its contribution is strong enough it results that the free energy is negative, i.e, lower than that of the cholesteric at the transition. This construction stresses out that, on one hand a lattice of defects stabilizes the blue phases and on the other hand that this stabilization is mediated by the presence of strong polar and biaxial [45, 46].

2.5 Topological Defects

Generally, unconstrained liquid crystal samples do not exhibit a global smooth behaviour of their orientational field. Instead, they exhibit local homogeneous domains with arbitrary orientation, incoherent with other domains orientations, as can for example be seen in Fig.1.2 (a) and (b). The regions in which these domains contact have a locally undefined orientational field, called topological defects or disclinations [10].

In the spirit of the Frank-Oseen model, the way to describe defects is by associating them with some free energy, since the creation of such regions involves, on one hand, the orientational distortions around a core region and, on the other hand, orientational disorder inside the core region. Thus, these regions must be associated with a higher free energy than the unconstrained remaining sample [49]. Let us consider, as an illustrative example, that there is a disclination in a nematic layer confined to the xy plane, in which the director has no natural twist, at least in the xy plane. The free energy counts only with splay and bend contributions and the free energy density takes the form,

$$f_{disc} = \frac{1}{2}\left[K_{11}(\nabla \cdot \mathbf{n})^2 + K_{33}(\mathbf{n} \times \nabla \times \mathbf{n})^2\right]. \tag{2.5}$$

Assuming that there is an arbitrary angular function centred at $x = 0$ and $y = 0$, $\phi(x, y)$, that defines the director orientation on the plane around the core, its components can be written in terms of $\phi(x, y)$ as $n_x = \cos(\phi(x, y))$ and $n_y = \sin(\phi(x, y))$, ensuring a unitary director [6]. For simplicity let us consider the one-constant approximation, with $K_{11} = K_{33} = K$. Expanding the splay and bend terms,

$$\begin{aligned}
(\nabla \cdot \mathbf{n})^2 &= \left(-\sin(\phi)\frac{\partial \phi}{\partial x} + \cos(\phi)\frac{\partial \phi}{\partial y}\right)^2 \\
&= \sin^2(\phi)\left(\frac{\partial \phi}{\partial x}\right)^2 - 2\sin(\phi)\cos(\phi)\frac{\partial \phi}{\partial x}\frac{\partial \phi}{\partial y} + \cos^2(\phi)\left(\frac{\partial \phi}{\partial y}\right)^2 \\
(\mathbf{n} \times \nabla \times \mathbf{n})^2 &= \left(\left(\sin(\phi)\cos(\phi)\frac{\partial \phi}{\partial x} + \sin^2(\phi)\frac{\partial \phi}{\partial y}\right)\overrightarrow{e}_x - \left(\cos^2(\phi)\frac{\partial \phi}{\partial x} + \sin(\phi)\cos(\phi)\frac{\partial \phi}{\partial y}\right)\overrightarrow{e}_y\right)^2 \\
&= \cos^2(\phi)\left(\frac{\partial \phi}{\partial x}\right)^2 + 2\sin(\phi)\cos(\phi)\frac{\partial \phi}{\partial x}\frac{\partial \phi}{\partial y} + \sin^2(\phi)\left(\frac{\partial \phi}{\partial y}\right)^2
\end{aligned} \tag{2.6}$$

Adding the two terms, the free energy density is written in terms of the angular function as,

$$f_{disc} = \frac{1}{2}K\left[\left(\frac{\partial \phi}{\partial x}\right)^2 + \left(\frac{\partial \phi}{\partial y}\right)^2\right] = \frac{1}{2}K(\nabla \phi)^2 \tag{2.7}$$

Now, due to the presence of the disclination, the function $\phi(x, y)$ that defines the director everywhere in the plane is given as the sum of, $\phi_0(x, y)$, associated with the angular function when no defects are present, and of, $\eta(x, y)$, a first order perturbation term associated with the presence of the defect that perturbs the undistorted system described by $\phi_0(x, y)$, with magnitude α, that is assumed to be small, $\alpha << 1$. The total free energy around a disclination core is given by the integration of f_{disc}, with $\phi(x, y) = \phi_0(x, y) + \alpha\eta(x, y)$, inside a region centered at the defect and with boundaries far enough so that the director field is unperturbed, such that,

$$F_{disc} = \frac{1}{2}K\int_A \left[\left(\frac{\partial \phi_0}{\partial x}\right)^2 + \left(\frac{\partial \phi_0}{\partial y}\right)^2\right] + 2\alpha\left[\frac{\partial \phi_0}{\partial x}\frac{\partial \eta}{\partial x} + \frac{\partial \phi_0}{\partial y}\frac{\partial \eta}{\partial y}\right] + \alpha^2\left[\left(\frac{\partial \eta}{\partial x}\right)^2 + \left(\frac{\partial \eta}{\partial y}\right)^2\right]dA \tag{2.8}$$

The first term of the integral corresponds to the defect free undistorted system. The third term depends solely on the induced perturbations and can be neglected since perturbations are considered to be of very small magnitude. As for the second term, it can be integrated by parts as,

$$F_{disc} = 2\alpha K \left(\frac{\partial \phi_0}{\partial x} + \frac{\partial \phi_0}{\partial y} \right) \eta(x,y) \Bigg|_x \Bigg|_y - 2\alpha K \int \int \eta(x,y) \left[\frac{\partial^2 \phi_0}{\partial x^2} + \frac{\partial^2 \phi_0}{\partial y^2} \right] dxdy \tag{2.9}$$

Since in the integration limits the system is unperturbed, there $\eta(x,y)$ is zero and the first term of Eq.2.9 is zero. Considering that the perturbation decays from the core to the outer regions, in a region close to the core, it may be assumed constant. Thus, the free energy minimum can be obtained differentiating f_{disc} with respect to η, resulting in the two-dimensional Laplace equation,

$$\frac{\partial^2 \phi_0}{\partial x^2} + \frac{\partial^2 \phi_0}{\partial y^2} = 0 \tag{2.10}$$

For simplicity, lets regard ϕ_0 simply as ϕ. In polar coordinates, with $x = r\cos(\psi)$, $y = r\sin(\psi)$, $\tan(\psi) = \frac{y}{x}$ and with r measured from the center of the disclination, the Laplace equation yields,

$$\frac{1}{r} \frac{\partial}{\partial r} \left(r \frac{\partial \phi}{\partial r} \right) + \frac{1}{r^2} \left(\frac{\partial^2 \phi}{\partial \psi^2} \right) = 0 \tag{2.11}$$

For disclinations with translational invariance along the z axis, i.e, for axial disclinations along z, ϕ is axially symmetric and independent of the distance to the core. Thus, the above Laplace equation has the trivial solution of $\phi(\psi) = s\psi + \tilde{\phi}$, where s is a constant, called defect strength, and $\tilde{\phi}$ is a reference angle for ϕ. Due to the head-tail symmetry of the director, when ψ increases by 2π, ϕ must change by an integral multiple of π so that the director keeps the same orientation as before. Thus, the defect strength is $s = n/2$, with $n = \pm 1, \pm 2, ..$ the winding number, with positive value if, disregarding head-tail symmetry, the director keeps its orientation through a full ψ rotation and with negative value otherwise [50].

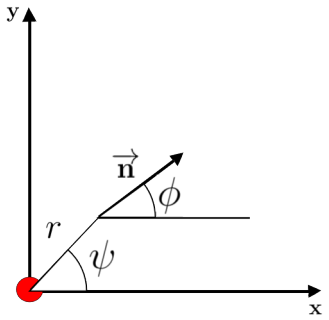

Fig. 2.6: Schematic representation of the angular function ϕ and the angle ψ around a topological defect.

This leads to the total distortion free energy associated with a disclination, F_{disc}, by integrating the distortion free energy density of Eq.2.7, from a core region of radius r_0, to an outer region with dimension of the defect driven orientational distortions R, such that with $\phi = s\psi + \tilde{\phi}$,

$$F_{disc} = \frac{1}{2} K \int_0^{2\pi} d\psi \int_{r_0}^{R} r(\nabla \phi)^2 dr \tag{2.12}$$

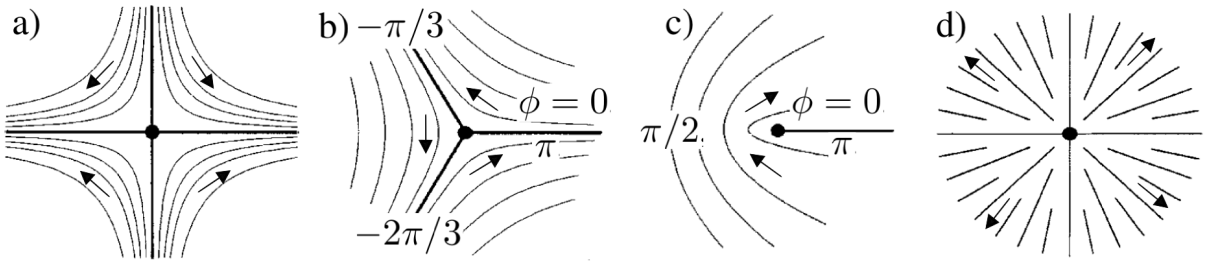

Fig. 2.7: Examples of topological defects on a plane. The black lines represent the director orientation around the line disclinations and the dots represent the core regions. The defects have charges: a) $s = -1$; b) $s = -1/2$; c) $s = +1/2$; d) $s = +1$ (schematic representations from [50] and arrow display from [11].

Solving the above integral yields,

$$F_{disc} = \pi K s^2 \ln\left(\frac{R}{r_0}\right), R > r_0 \tag{2.13}$$

which diverges if $R \to \infty$. This limit implies that a line disclination affects all the system and that the distortions observed around it are projected throughout the system. Such a limit is, however, not real, since the distorted regions are locally confined in a typical radius of $R \sim 10 - 100\ \mu m$ [11], either due to the existence of other disclinations or due to the elasticity of the liquid crystal itself, that gradually smooths the imposed distortions. The core radius, typically $r_0 \sim 10nm$, corresponds to a region with dimensions in which the Frank-Oseen theory does not apply. It requires going beyond the Frank-Oseen treatment, and is for simplicity associated with an energy F_{core} proportional to the core's volume that depends on the charge [10, 46, 51].

From Eq.2.13, it is now clear what was stated about the different blue phases stability in Sec.2.3. The blue-phase I has a honeycomb lattice of defects with charge $s = -1/2$, while blue-phase II has a square lattice of defects, with charge $s = -1$. Thus, their free energy contribution is $F_{disc} = \pi K \ln(R/r_0)/4$ and $F_{disc} = \pi K \ln(R/r_0)$ respectively, meaning that the amount of *double-twist* frustration is much higher in blue-phase II to overcome the formation of defects.

When two defects are present, each one is defined by its own particular angular function $\phi(x, y)$ and the total free energy of the system comes from the linear combination of energetic contributions of two distinct angular functions, as in Eq.2.7, yielding, [10, 11, 45, 52],

$$\begin{aligned}
F_{disc} &= \frac{1}{2}K\int_0^{2\pi} d\psi \int_{r_0}^{R} r\left(\nabla(\phi_1+\phi_2)\right)^2 dr \\
&= \frac{1}{2}K\int_0^{2\pi} d\psi \int_{r_0}^{R} r\left((\nabla\phi_1)^2+(\nabla\phi_2)^2\right)dr + K\int_0^{2\pi} d\psi\left(\int_{r_0}^{r} r\nabla\phi_1\nabla\phi_2 dr + \int_{r}^{R} r\nabla\phi_1\nabla\phi_2 dr\right) \\
&= \frac{1}{2}K\int_0^{2\pi} d\psi \int_{r_0}^{R} r\left((\nabla\phi_1)^2+(\nabla\phi_2)^2\right)dr + K\int_0^{2\pi} d\psi\left(\int_{r}^{R} r\nabla\phi_1\nabla\phi_2 dr\right) \\
F_{disc} &= \pi K(s_1+s_2)^2 \ln\left(\frac{R}{r_0}\right) - 2\pi K s_1 s_2 \ln\left(\frac{r}{r_0}\right), r \geq r_0
\end{aligned} \tag{2.14}$$

with the second term being the interaction energy, that vanishes when the distance between defects is the same as the limit of the defect driven orientational distortions. From this result we see that the interaction free energy between defects is proportional to the charges product $s_1 s_2$. The interaction is repulsive when the defects have the same sign, and attractive otherwise [10].

2.6 Order parameter

The Frank-Oseen continuum model is successful in describing chiral nematics through the construction of a director field, that allows the description of the phase orientational configuration and the identification of defects. This construction is, nevertheless, limited in that it cannot consider a system with two distinct symmetries, which makes it inappropriate to describe phase transitions or mixtures, where different symmetries coexist. Thus, to properly describe such a scenario, something that accommodates both the ideas of symmetry and director field must be constructed, the order parameter.

Let us consider a microscopic region, small enough so that the director field is unchanged, but large enough so that it contains multiple molecules that are allowed not to be perfectly aligned and the director field defined as the average molecular orientation. The distribution of the molecules orientation around this average can thus be related with the macroscopic properties, which change throughout the system. Thus, a quantity that relates the director properties , the amount of order around this director and the way it changes throughout the system is created, suitable to contemplate symmetry breaking. This quantity is the tensor order parameter.

2.6.1 Microscopic approach

The idea of a local preferred orientation given by the director **n** is maintained, and to it, is locally associated a distribution of the orientation of the molecules long axes. The average over this distribution gives the local scalar order parameter, that is maximum when all molecules are perfectly aligned along the director and minimum when their orientation is isotropically distributed [53]. One way of constructing an order parameter for uniaxial nematics can be easily obtained through a simple heuristic approach. Another way, a more formal one, is achieved using the Legendre Polynomials.

Heuristic approach on nematic uniaxial parameter

At finite temperatures, the thermal motion of the molecules prevents perfect alignment and the molecular orientation is distributed around a most populated orientation, the director. With respect to the director a single molecule can be described with the three Euler angles, ψ (rotation of the long molecular axis), ϕ (rotation in the azimuthal direction) and θ (departure from the director orientation), as in Fig.2.8. For molecules with uniaxial symmetry the first two angles can be omitted, since they do not affect the projection of alignment along the director. Thus, the remaining angle, θ is the one for which a degree of uniaxial order can exist. If molecules have biaxial symmetry, i.e, they also possess a short axes, angles ψ or ϕ have to be considered, for which a degree of biaxial order can exist. There are cases, in the presence of particular constraints, as for example the presence of surfaces, in which these angles may also have to be considered even for systems with uniaxial symmetry. Regardless, there is a balance between the two types of symmetry so that the scalar order parameter is kept constant and when biaxial order is increased, uniaxial order is decreased in the same proportion [30, 54, 55]. When the preference for any set of θ, ψ and ϕ angles is equally probable, complete isotropy is obtained, hence, the isotropic phase [1, 53, 56].

Since through the polar angle θ of Fig.2.8 it is possible to distinguish between the uniaxial nematic and the isotropic phase, an order parameter of the form $\cos(\theta)$ would seem like a suitable candidate. However, nematics have head-tail symmetry and such order parameter allows for sign changes. Thus, to prevent the order parameter from describing situations where the nematic phase is polarized, $\cos^2(\theta)$ is used instead. But still, the order parameter should not be described by $\cos^2(\theta)$, since it corresponds to a single molecule, but instead it should be $< \cos^2(\theta) >$, the average over all molecules in the liquid. Thus,

when all the molecules are fully aligned with **n**, $\theta = 0$ and $< \cos^2(\theta) >= 1$ and when all molecules are randomly distributed, all values of θ are equally likely and $< \cos^2(\theta) >= \frac{1}{3}$ [1]. By definition, the ordered nematic phase is said to have unit order parameter, while the disordered isotropic phase is said to have order parameter zero. Thus, the scalar order parameter for uniaxial nematics can be written as,

$$S = \frac{3}{2} < \cos^2(\theta) - \frac{1}{3} > \tag{2.15}$$

with $S = 1$ in the ordered phase, when the average molecule orientation is parallel to the director, with $S = 0$ in the disordered phase when molecules are isotropically distributed and with $S = -\frac{1}{2}$ when molecules are oriented perpendicular to the director, which happens for example, with disk-like molecules [53].

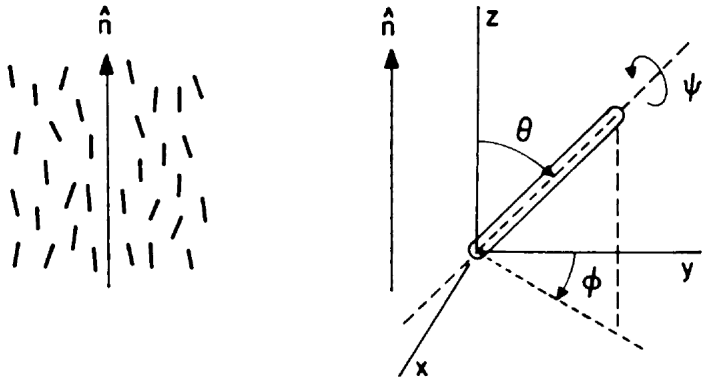

Fig. 2.8: (a) Schematic representation of the structure at a uniaxial nematic liquid crystal. Molecules are represented by black bars and point on average parallel to the director. (b) The Euler angles required to describe the orientation of a molecule in a nematic liquid. [1].

Formal approach - uniaxial nematic

Another route to obtain the order parameter is to definite a molecular orientation distribution function, which depends on the set of angles shown in Fig.2.8, θ, ϕ, ψ and is radially limited by a distance r. For this purpose, a general function exists such that given a set of imposed constraints, suitably describes how rod-like molecules are distributed. For this purpose it is proposed that the distribution is a solution of the Laplace Equation,

$$\nabla^2 f(r, \theta, \phi, \psi) = 0 \tag{2.16}$$

Considering that the distribution is not affected by the rotation of the molecules by an angle ψ, the Laplace equation is rewritten is spherical coordinates, with θ the azimuthal angle, ϕ the radial angle and r the distance of a certain chosen point to the spatial center of the region where the distribution is well defined. For nematics with uniaxial symmetry, then the only angle of interest to define an order degree along the director is θ, such that $f(r, \theta, \phi, \psi) = f(r, \theta)$ and the Laplace equation can thus be written in spherical coordinates as,

$$\nabla^2 f(r, \theta) = \frac{1}{r^2}\frac{\partial}{\partial r}\left(r^2 \frac{\partial f}{\partial r}\right) + \frac{1}{r^2 \sin(\theta)}\frac{\partial}{\partial \theta}\left(\sin(\theta)\frac{\partial f}{\partial \theta}\right) = 0 \tag{2.17}$$

The detailed calculation of the solutions for this equation, the Legendre Polynomials, is shown in Appendix B [53, 57, 58]. The resulting form of the distribution is,

$$f(\theta) = \sum_{n=0}^{\infty} \frac{4n+1}{2} < P_{2n}(\cos(\theta)) > P_{2n}(\cos(\theta)) \tag{2.18}$$

The first non trivial Legendre polynomial that satisfies all the symmetry conditions of the system is,

$$< P_2(\cos(\theta)) >= \frac{3}{2} < \cos(\theta)^2 - \frac{1}{3} >, \quad \theta \in [-\pi, \pi] \tag{2.19}$$

which is exactly the same as the scalar order parameter obtained in the so called "heuristic approach". Furthermore, since the objective is to recreate the overall behaviour of the molecules around the director, the third (singular) term is also unimportant. This leaves only the second term, the scalar order parameter. The first order approximation of the Legendre Polynomials will be the one used throughout the work. It should be pointed out, however, that in some special cases higher orders of approximation of the scalar order parameter are required. All the symmetry arguments used throughout the formal approach are referred to the reference alignment direction, the director **n**, and to an angle θ that the molecules average orientation, **a**, makes relative to the director. Thus, the general assumption can be made in that $\langle P_2(\cos(\theta))\rangle = \langle P_2(\mathbf{a}\cdot\mathbf{n})\rangle = S$ [56].

This construction is indeed able to locally describe features which regard the orientational order of a simple nematic. However, it is not adapted to systems that have twist features, or in systems with director deformations due to external fields or due to boundary constraints, like substrates and interfaces. In this sense, in order to accommodate all the above possibilities, a global order parameter must be constructed that is spatial dependent, whilst keeping the information about the molecular orientational distribution.

2.6.2 Macroscopic approach

Since the director field is directly related to the macroscopic physical properties of the LC, then, to describe these properties is to indirectly describe the director field orientation and its spatial dependence throughout the bulk. Thus, a coherent and compact order parameter will contain not only information about the microscopic landscape, but will also contain information on how it manifests macroscopically, which is indeed what is measured.

For an aligned uniaxial nematic ordered phase, the total response to such measurements (magnetic or dielectric susceptibilities), may be written as a diagonal tensor [1, 50],

$$\boldsymbol{\chi} = \begin{bmatrix} \chi_\perp & 0 & 0 \\ 0 & \chi_\perp & 0 \\ 0 & 0 & \chi_\parallel \end{bmatrix} \tag{2.20}$$

with $\chi_\perp$ and $\chi_\parallel$ referring to the susceptibility perpendicular and parallel to the director, respectively. In the isotropic phase, the response will be a combination of all these perpendicular and parallel components, since molecules are isotropically distributed, such that,

$$\chi_{iso} = \frac{1}{3} Tr[\boldsymbol{\chi}] \tag{2.21}$$

In order to have a vanishing order parameter in the isotropic phase, one can simply redefine the total susceptibility tensor by subtracting the isotropic response. This leaves out the anisotropic response, which is non zero in the ordered phase and zero in the disordered phase,

$$\boldsymbol{\chi}_{ani} = \boldsymbol{\chi} - \chi_{iso}\delta_{\alpha\beta} = \Delta\chi \begin{bmatrix} -\frac{1}{3} & 0 & 0 \\ 0 & -\frac{1}{3} & 0 \\ 0 & 0 & \frac{2}{3} \end{bmatrix}, \Delta\chi = (\chi_\parallel - \chi_\perp) \tag{2.22}$$

Thus, the anisotropic response is bounded from below, with zero value in the disordered phase. It is not, however, bounded from above, in the ordered phase. Normalizing the response in terms of the maximum

amplitude $\Delta\chi_{max}$, i.e, the maximum difference between the parallel and perpendicular responses, yields a tensor order parameter with zero value in the isotropic phase and unity along the parallel orientation of the ordered phase,

$$\boldsymbol{Q} = \frac{3}{2}\frac{\boldsymbol{\chi}_{ani}}{\Delta\chi_{max}} = \frac{3}{2}\frac{\Delta\chi}{\Delta\chi_{max}}\begin{bmatrix} -\frac{1}{3} & 0 & 0 \\ 0 & -\frac{1}{3} & 0 \\ 0 & 0 & \frac{2}{3} \end{bmatrix} \tag{2.23}$$

The factor $\frac{\Delta\chi}{\Delta\chi_{max}}$ is bounded between 0 and 1 and its value depends on the deviation of $\Delta\chi$ from $\Delta\chi_{max}$, which is a result of the deviation θ of the molecules orientation from the director orientation. Thus, such factor can be substituted by the scalar order parameter of the microscopic approach, resulting in an order parameter that combines both microscopic and macroscopic approaches,

$$\boldsymbol{Q} = \frac{3}{2}\langle P_2(cos(\theta)\rangle \begin{bmatrix} -\frac{1}{3} & 0 & 0 \\ 0 & -\frac{1}{3} & 0 \\ 0 & 0 & \frac{2}{3} \end{bmatrix} = \frac{3}{2}S\begin{bmatrix} -\frac{1}{3} & 0 & 0 \\ 0 & -\frac{1}{3} & 0 \\ 0 & 0 & \frac{2}{3} \end{bmatrix} \tag{2.24}$$

The above order parameter corresponds to a state oriented along the reference axis, z. For an arbitrary reference frame, the tensor order parameter can be expressed as a traceless symmetric tensor,

$$\boldsymbol{Q}(\mathbf{r}) = \frac{3}{2}S(\mathbf{r})\begin{bmatrix} n_x n_x - \frac{1}{3} & n_x n_y & n_x n_z \\ n_y n_x & n_y n_y - \frac{1}{3} & n_y n_z \\ n_z n_x & n_z n_y & n_z n_z - \frac{1}{3} \end{bmatrix} \tag{2.25}$$

or in a compact form, as

$$Q_{\alpha\beta}(\mathbf{r}) = \frac{3}{2}S(\mathbf{r})\left[n_\alpha(\mathbf{r})n_\beta(\mathbf{r}) - \frac{1}{3}\delta_{\alpha\beta}\right], \tag{2.26}$$

with $\alpha, \beta = x, y, z$. For the director oriented along z, $\mathbf{n} = (0, 0, 1)$, it is clear that Eq. 2.24 is recovered. The advantage of using an order parameter is clear, since it is a quantity defined everywhere in the system, that at the same time accounts for the director field variations and magnitude, and thus includes the description of systems with defects and/or interfaces between ordered and disordered phases.

The tensor order parameter also allows the description of different order symmetries. For biaxial systems, where both a long axis and a small axis are present, it is possible to define the degree of biaxial order by including a second scalar order parameter in the tensor,

$$Q_{\alpha\beta}(\mathbf{r}) = \frac{3}{2}S(\mathbf{r})\left[n_\alpha(\mathbf{r})n_\beta(\mathbf{r}) - \frac{1}{3}\delta_{\alpha\beta}\right] + \frac{B(\mathbf{r})}{2}\left[l_\alpha(\mathbf{r})l_\beta(\mathbf{r}) - m_\alpha(\mathbf{r})m_\beta(\mathbf{r})\right] \tag{2.27}$$

where $\mathbf{n}(\mathbf{r})$ is the long axis, $\mathbf{l}(\mathbf{r})$ is the non polar small axis, orthogonal to $\mathbf{n}(\mathbf{r})$ and $m_\alpha(\mathbf{r}) = (\mathbf{n}(\mathbf{r}) \times \mathbf{l}(\mathbf{r}))_\alpha$ is a polar small axis [10, 30, 54, 55].

2.7 Phase transitions

The description of LC phase transitions may be accomplished via the mean field Landau-de Gennes (LdG) phenomenological theory [54], which is used in this work to explore chiral nematic thermal phase transitions. The key idea of this model lays in using the free energy as a function of the temperature, the order parameter and its spatial variations to describe the stability of each phase. The equilibrium configuration corresponds to one in which the order parameter and its spatial variations correspond to the minimal free energy. Thus, for different temperatures, the system always reconfigures in a way that satisfies this condition and the order parameter must necessarily change to one that characterizes the equilibrium state of the system [1]. As a phenomenological mean field theory, its results are only valid if the scale in which the order parameter spatial fluctuations occurs is higher then the system typical scale.

A phase transition occurs when the symmetry of a phase, expressed by an order parameter, changes in the presence of external constraints. These constraints may be changes of temperature, pressure, external fields or dopant concentration. For a temperature dependent system, when the order parameter changes continuously with temperature from the low symmetry phase with non zero value below the transition temperature, T_c, to the high symmetry phase with zero value above it, the phase transition is called second order [10]. Such systems are characterized by the typical length scale at which the system properties are correlated, called correlation length ξ. This length scale is finite bellow and above T_c and diverges as the temperature approaches T_c according to some power law, reason why the phase transition is observed in all the system.

If the order parameter of the low symmetry phase changes discontinuously with the temperature from a non zero value below the transition temperature to zero above the phase transition is called first order [10]. Such systems are characterized by a typical length scale at which the system properties are coherent, called the coherence length scale ξ_0 (Appendix C) characteristic of systems with non polar features. This length scale is of the order of the intermolecular distance [59] and grows as the temperature approaches T_c up to a finite value, reason why the phase transition is associated to phase nucleation. These discontinuous phase transition can range from one in which the order parameter goes from its maximum value to its lowest when temperature exceeds the coexistence temperature, to one in which the order parameter decreases up to the transition and then falls to zero above coexistence temperature, called a weakly first order phase transition. This is the case for thermotropic chiral nematics [54, 56].

An interface is observed at conditions that make the low and high symmetry phases equality stable, i.e, with equal free energy. This leads to an equilibrium profile of the order parameter and its spatial fluctuations [6], that ultimately dictate the structure of the interface. The interface is associated with a surface tension, or free energy per unit area, that arises from the contact between the molecules of the two phases with distinct symmetries but equally stable [60].

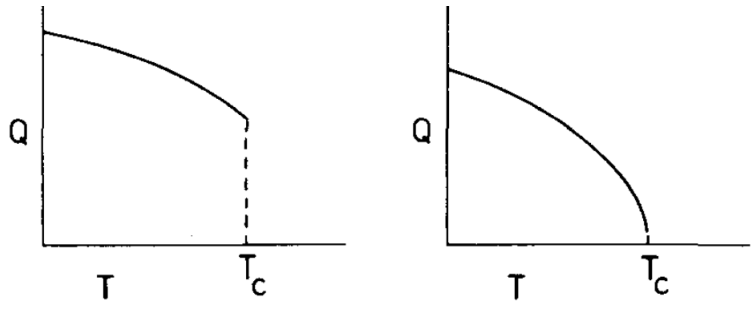

Fig. 2.9: (a) Weakly discontinuous phase transition. (b) continuous first order transition. (image from [4]).

2.8 Landau - de Gennes Model

It was proposed by Landau, for second order phase transitions that near the transition temperature, considering that the order parameter has a small value and is uniform [10], i.e, in the low symmetry phase, it is possible to expand the free energy density functional in a Taylor series (about the high symmetry phase) in terms of the order parameter with non-vanishing leading terms,

$$f_{lsym}(T,S) = f_{hsym}(T,0) + \lambda(T)S + \frac{1}{2}A(T)S^2 + \frac{1}{3}B(T)S^3 + \frac{1}{4}C(T)S^4 + .. \tag{2.28}$$

with $\lambda(T)$, $A(T)$, $B(T)$ and $C(T)$ the temperature dependent free energy derivatives with respect to the order parameter S and with f_{lsym} and f_{hsym} corresponding to the low symmetry and high symmetry phases free energy, respectively. The coefficients $\frac{1}{2}$,$\frac{1}{3}$,$\frac{1}{4}$ are kept for convenience [4]. The equilibrium configuration of the system corresponds to a minimum of the free energy density, which is ensured by the stability conditions,

$$\frac{\partial f_{lsym}}{\partial S} = 0 \quad , \quad \frac{\partial^2 f_{lsym}}{\partial S^2} > 0 \tag{2.29}$$

In order to satisfy the first stability condition it is necessary that $\lambda(T) = 0$, or else, the condition would not be fulfilled in the high symmetry phase ($S = 0$). However, when a field is applied it is expected for the system to have a linear response, either towards the ordered or the disordered phase. In this sense the coefficient λ is assumed to be field dependent. To satisfy the second stability condition, the coefficient $A(T)$ must be positive in the high symmetry phase ($S = 0$). However, when temperature is decreased and the low symmetry phase ($S \neq 0$) is preferred over the high symmetry phase ($S = 0$), the system must have a new free energy minimum, which is ensured if $A(T)$ is allowed to change sign. Thus, it is assumed that the coefficient $A(T)$ changes sign from temperatures above to temperatures below a certain temperature, the supercolling temperature, T_c^*, where the ordered phase becomes stable and the disordered phase from metastable to unstable, slightly below the coexistence temperature [54]. The quadratic coefficient may then be Taylor expanded for temperatures around T_c^* as,

$$A(T) = A(T_c^*) + \frac{dA}{dT}|_{T_c^*}(T - T_c^*) = a(T - T_c^*) \tag{2.30}$$

where a is a characteristic constant of the system. Since the coefficient $A(T)$ is associated to the dominant term of the free energy expansion and since it is temperature dependent, the coefficients B and C are assumed to be temperature independent. Having these features in consideration, when looking for the equilibrium state,

$$\frac{\partial f_{lsym}}{\partial S}(T,S) = a(T - T_c^*)S + BS^2 + CS^3 = 0 \tag{2.31}$$

the solutions are,

$$S = 0 \quad , \quad S = \frac{-B + [B^2 - 4aC(T - T_c^*)]^{1/2}}{2C} \quad , \quad S = \frac{-B - [B^2 - 4aC(T - T_c^*)]^{1/2}}{2C} \tag{2.32}$$

The first solution corresponds to the high symmetry phase while the other two solutions correspond to low symmetry phase. By looking at Eq.2.32 it is possible to see that for vanishing B the order parameter behaves continuously with temperature around T_c^*, while for non-vanishing B, it has a gap. So, by manipulating the value of the B coefficient it is possible to describe different systems, with first or second-order phase transitions, corresponding to $B \neq 0$ or $B = 0$, respectively. In order to ensure a minimum of the free energy, the highest term of the functional expansion must be positive, such that developing the expansion up to the fourth order requires C to positive.

For a vanishing B, the solutions are,

$$S = 0 \quad , \quad S = +[a(T_c - T)/C]^{1/2} \quad , \quad S = -[a(T_c - T)/C]^{1/2} \tag{2.33}$$

Since the free energy functional must be a scalar, the coefficient B and all coefficients associated to odd powers of S are excluded in systems in which the order parameter is sign sensitive, like systems with vector order parameter with polar features. From temperatures below the supercooling temperature, $T \leq T_c^*$, where the only possible (real) solution is $S \neq 0$, to temperatures above the superheating temperature, $T_c^{**} < T$, where the only possible solution is $S = 0$, it is possible to see that the order parameter decreases smoothly with temperature. Thus, there are no metastable states and the only temperature at which both phases are equally stable is $T = T_c^{**} = T_c = T_c^*$. For a vanishing B, the coefficient C must be positive in order to bound the free energy from below. If this is the case, such a system has a second-order phase transition.

For a non-vanishing B, the solutions are those of Eq.2.32 and below the supercooling temperature, $T < T_c^*$, under the condition that $B^2 > 4aC(T - T_c^*)$, the only possible (real) solution is $S \neq 0$, corresponding to an ordered stable state. For low intermediate temperatures, $T_c^* < T \leq T_c$ the order parameter goes from $S \simeq -B/C$, right above T_c^*, down to $S = (-B + [B^2 + 4aC(T - T_c^*)]^{1/2})/2C$, right below T_c, and the disordered phase goes from unstable to metastable. To ensure a positive scalar order parameter, B is set as a negative value. At $T = T_c$, the free energy of both phases is the same indicating a phase coexistence, in which both phases are equality stable [11]. For temperatures, between the coexistence temperature and the superheating temperature, $T_c < T < T_c^{**}$, the disordered phase goes from mestastable to stable and the ordered phase from stable to metastable and for $T_c^{**} \leq T$ the ordered phase becomes unstable. Thus, it is possible to state that the introduction of odd terms in the expansion destroys the metastability degeneracy in temperature observed in second-order phase transitions.

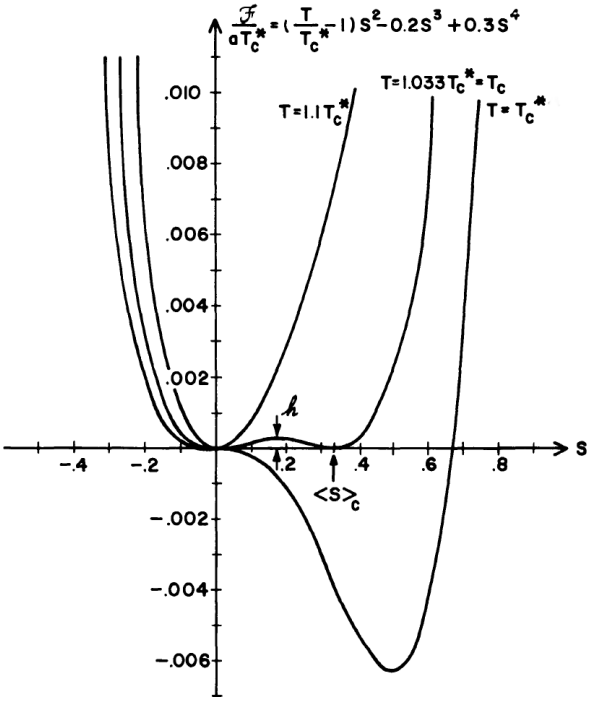

Fig. 2.10: Landau free energy density for a non-vanishing B coefficient. For $T > (T_c^{**} = 1.1T_c^*)$ the global minimum is at $S = 0$. For $T_c^{**} > T > T_c$, the global minimum is at $S = 0$ and the local minimum is at some value $S \neq 0$. For $T = T_c$ the two phases coexist. For $T_c > T > T_c^*$ the global minimum is at some value $S \neq 0$ and the local minimum is at $S = 0$. For $T_c^* > T$ the global minimum is at $S \neq 0$ (Figure from [1]).

Considering the limiting cases of $S = 0$ and $S = 1$ ($B = -C$) for the disordered and ordered phases, respectively, if at $T = T_c^*$, the order parameter is somewhere in the middle of these limiting values then there is a weakly first order phase transition. However, this does not agree with the initial statement of the expansion in powers of S, that S should be small around the transition, both above and below. Thus, by considering such an approximation, even though the free energy is expanded in the high symmetry phase, this approach is bounded to be a qualitative description of a phase transition [53]. Furthermore, it is also required that the order parameter fluctuations amplitude is small, so that thermally activated fluctuations that lead to the transition from one phase to the other, in either direction, occur with negligible probability [59].

The ideas developed so far point towards the Landau-de Gennes model. On one hand, there is a spatial dependent tensor order parameter, Eq.2.27, from which it is possible to extract all the information of the system regarding symmetry. On the other hand, there is a suitable free energy treatment, from which it is possible to extract the equilibrium configuration of the tensor order parameter throughout the system (Eq.2.28). The combination of these ideas takes form in the phenomenological Landau - de Gennes (LdG) model for the uniaxial nematic-isotropic phase transition (N-I) where free energy density is expanded in powers of invariant combinations of the uniaxial form of the tensor order parameter of Eq.2.27, yielding (Appendix C),

$$\begin{aligned} f_{nem}(T,\boldsymbol{Q}) - f_{iso}(T,0) &= \frac{1}{2}a(T-T_c^*)Q_{ij}Q_{ji} + \frac{1}{3}BQ_{ij}Q_{jk}Q_{ki} + \frac{1}{4}C[Q_{ij}Q_{ji}]^2 \\ &= \frac{1}{2}a(T-T_c^*)Tr[\boldsymbol{Q}^2] + \frac{1}{3}BTr[\boldsymbol{Q}^3] + \frac{1}{4}C(Tr[\boldsymbol{Q}^2])^2 \\ &= \frac{3}{4}a(T-T_c^*)S^2 + \frac{1}{4}BS^3 + \frac{9}{16}CS^4 \end{aligned} \tag{2.34}$$

with sum over indices implied, and with f_{nem} and f_{iso} corresponding to the nematic and isotropic phases free energy density. The linear dependence on $\boldsymbol{Q}$ is omitted unless an external field is applied. The energy density reference is that of the isotropic phase and all coefficients a, B and C are constants, with B the only coefficient with negative value. The high symmetry phase free energy density is purposely placed in left side of the equation simply to stress that for temperatures below $T_{NI} = T_c$ the free energy density difference in the left side is negative, and the nematic becomes stable and the isotropic metastable. In order to have a transversal qualitative description of such phase transition regardless of the sample, the above expression is usually rescaled as,

$$\tilde{f}_{nem}(T,\boldsymbol{Q}) = \tau\tilde{S}^2 - 2\tilde{S}^3 + \tilde{S}^4 \tag{2.35}$$

with the relations,

$$f = \frac{B^4}{9^3C^3}\tilde{f} \quad , \quad S = \frac{2B}{9C}\tilde{S} \quad , \quad \tau = \frac{27AC}{B^2} \tag{2.36}$$

and assuming that $f_{iso} = 0$ as the reference energy , and that the minus sign of the third term comes from $B < 0$. For $\tau > 1$ the isotropic phase is preferred ($f_{nem} < 0$), for $\tau = 1$ both phases are at coexistence ($f_{nem} = f_0$) and for $\tau < 1$ the nematic phase is preferred ($f_{nem} < f_0$).

So far, uniformity of the order parameter has been implied to describe the system free energy. However, when the system has natural frustrations, or when some orientational order is imposed via external agents, spatial variations of the order parameter may arise. In the continuum limit, when spatial variations of the order parameter occur in a scale much larger than the correlation length, the dominant contribution to the free energy, similarly to the contributions of the order parameter for the bulk free energy density in Eq. 2.28, may be expressed as a Taylor expansion in terms of the gradient of the tensor order parameter

up to leading order [10]. The order of the expansion must be carefully chosen since it provides the model different approximations of a physical system. For example, in systems with a temperature dependent pitch the free energy associated with spatial variations of the order parameter is expanded up the third order [12], resulting in,

$$\begin{aligned} f_{sym}(T,Q,\partial_k Q_{ij}) &= f_{iso}(T,0,0) + \lambda Q + L_{ijk}\partial_k Q_{ij} \\ &+ \frac{1}{2}A(T)Q_{ij}Q_{ji} + L_{ijk,mn}\partial_k Q_{ij}Q_{mn} + \frac{1}{2}L_{ijk,mnl}\partial_k Q_{ij}\partial_l Q_{mn} + \frac{1}{3}BQ_{ij}Q_{jk}Q_{ki} \\ &+ \frac{1}{2}L_{ijk,mnl,op}\partial_k Q_{ij}\partial_l Q_{mn}Q_{op} + \frac{1}{2}L_{ijk,mn,op}\partial_k Q_{ij}Q_{mn}Q_{op} + \frac{1}{3}L_{ijk,mnl,opt}\partial_k Q_{ij}\partial_l Q_{mn}\partial_t Q_{op} \\ &+ \frac{1}{4}C[Q_{ij}Q_{ji}]^2 + ... \end{aligned} \tag{2.37}$$

which, as long as it respects translational and rotational invariance, can be expressed as a bulk term, constrained by symmetry in the absence of external fields (Eq.2.29), and a distortion term, related to spatial variations of the order parameter.

As stated by the Frank-Oseen model, in the continuum limit the director spatial variations take place in a distance much larger than the scale of the system. Thus, introducing derivative terms of the order parameter in the free energy density functional, allows the model to be related to the classic Frank-Oseen model of Eq.ref2.3. However, this relation requires the gradient expansion of the order parameter to be of second order to limit the LdG model to the power of the derivatives of the director field in the Frank-Oseen model, such that the third order terms of the expansion are neglected, associated with $L_{ijk,mnl,op}$ and $L_{ijk,mnl,opt}$. Furthermore, the pitch is considered to be temperature independent, which is ensured only if the LdG gradient expansion is of second order. This manifests the usefulness of the Landau-de Gennes model on how it can be used to go beyond the classic Frank-Oseen model [61]. The free energy can thus be written in a sum of bulk and gradient terms as,

$$\begin{aligned} f_{bulk} &= f_{iso}(T,0) + \frac{1}{2}a(T-T_c^*)Q_{ij}Q_{ji} + \frac{1}{3}BQ_{ij}Q_{jk}Q_{ki} + \frac{1}{4}C[Q_{ij}Q_{ji}]^2 \\ f_{dist} &= L_{ijk}\partial_k Q_{ij} + L_{ijk,mn}\partial_k Q_{ij}Q_{mn} + \frac{1}{2}L_{ijk,mnl}\partial_k Q_{ij}\partial_l Q_{mn} \end{aligned} \tag{2.38}$$

with L_{ijk}, $L_{ijk,mn}$, $L_{ijk,mnl}$ the coefficients associated with the linear, mixed and quadratic terms of the free energy density expansion, respectively.

For the nematic phase, the equilibrium configuration is obtained when the molecules align parallel to each other throughout the system, with no intrinsic spontaneous orientational frustrations. Thus, symmetry breaking can only be imposed in the presence of external fields, a case that is not considered here, and non symmetric terms of the free energy are not allowed, such that $L_{ijk,mn} = 0$. Also, the nematic equilibrium configuration must obey the stability conditions,

$$\frac{\partial f_{sym}}{\partial(\partial_k Q_{ij})} = 0 \quad , \quad \frac{\partial^2 f_{sym}}{\partial(\partial_k Q_{ij})^2} > 0 \tag{2.39}$$

In order to satisfy these conditions it is required that $L_{ijk} = 0$, or else, for the isotropic phase with $\partial_k Q_{ij} = 0$ and $Q_{ij} = 0$ they won't be fulfilled. With the summation of the gradient quadratic terms over all independent invariants of distortion free energy contributions, the LdG free energy density for nematics can be written as [54, 61, 62],

$$\begin{aligned} f_{nem}(T,\mathbf{Q}) - f_{iso}(T,0) = &\frac{1}{2}a(T-T_c^*)Q_{ij}Q_{ji} + \frac{1}{3}BQ_{ij}Q_{jk}Q_{ki} + \frac{1}{4}C[Q_{ij}Q_{ji}]^2 \\ &+ \frac{1}{2}L_1\partial_k Q_{ij}\partial_k Q_{ij} + \frac{1}{2}L_2\partial_j Q_{ij}\partial_k Q_{jk} \end{aligned} \tag{2.40}$$

For chiral nematic phases, the equilibrium configuration is obtained when molecules align parallel to each other in planes with the same director orientation that rotate along an axis perpendicular to planes. Thus, even in the absence of external fields, there are constant intrinsic frustrations that mimic the action of an external field and introduce orientational symmetry breaking that imposes constant variations of the order parameter along some axis, such that the mixed term is allowed, $L_{ijk,mn} \neq 0$. Even though mixed and quadratic terms are allowed, both contributions must balance each other out in order to fulfil the stability conditions. Therefore, with the summation of the gradient mixed and quadratic terms over all independent invariants in the chiral nematics distortion free energy contributions can be written as [54],

$$\begin{aligned} f_{dist} &= \frac{1}{2}L_1\partial_k Q_{ij}\partial_k Q_{ij} + \frac{1}{2}L_2\partial_j Q_{ij}\partial_k Q_{jk} + L_1'\epsilon_{ijk}Q_{il}\partial_k Q_{jl} \\ &= \frac{1}{2}L_1\Big(\epsilon_{ijk}\partial_k Q_{jl} + 2q_0 Q_{il}\Big)^2 + \frac{1}{2}L_2\partial_j Q_{ij}\partial_k Q_{jk} - 2q_0^2 L_1 Q_{il}Q_{li} \end{aligned} \tag{2.41}$$

with $q_0 = L_1'/L_1 = 2\pi/P$ the natural intrinsic chirality, P the pitch of the chiral nematic and ϵ_{ijk} the Levi-Civita symbol such that $\epsilon_{ijk} = 1$ for even permutations, $\epsilon_{ijk} = -1$ for odd permutations and $\epsilon_{ijk} = 0$ if any index is repeated. The last term of f_{dist} is quadratic in $\mathbf{Q}$ and will be included in the bulk temperature term.

Applying the derivative operations of Eq.2.41 on the order parameter tensor in terms of director components of Eq.2.27, it is possible to extract a relation between the Landau-de Gennes coefficients, L_1 and L_2, and the Frank-Oseen elastic constants, K_1, K_2 and K_3, which gives a physically interpretable notion of the LdG constants, such that [63],

$$L_1 = \frac{K_3 + 2K_2 - K_1}{9S^2} \quad , \quad L_2 = \frac{4(K_1 - K_2)}{9S^2} \tag{2.42}$$

The effects of the elastic constants can be evaluated through three different approximations. For nematics, typically but not always, it is used the one-constant approximation, with,

$$K = K_1 = K_2 = K_3 \quad , \quad L = L_1 = \frac{2K}{9S^2} \quad , \quad L_2 = 0 \tag{2.43}$$

corresponding to elastic isotropy. For cholesterics, typically, elastic anisotropy can be considered, and the two-constant approximation is used,

$$K_1 = K_3 \quad , \quad L_1 = \frac{2K_2}{9S^2} \quad , \quad L_2 = \frac{4(K_1 - K_2)}{9S^2} \tag{2.44}$$

which allows to describe the twist deformation on the overall deformation profile, suited to chiral nematic phases. Nevertheless, elastic isotropy is considered in some cases. Thus, the one-constant approximation is but a particular case of the two-constant approximation. Removing degeneracies between the elastic constants into the three-constant approximation, also called anisotropic approximation in which $K_1 \neq K_2 \neq K_3$ [64], is not simply a matter of choice, like the two previous approximations. Removing the degeneracy between K_1 and K_3 is only possible with the introduction of further invariant gradient terms in the expansion of Eq.2.41, that necessarily imply the consideration of different physical properties [65]. The approximations are thus limited by the order of the gradient expansion.

In order to generalize the results of the LdG model to any system, it is important to set it with dimensionless quantities by rescaling the free energy density, the tensor order parameter, temperature, elastic constants and spatial coordinates [30],

$$f = \tilde{f}\frac{\xi_0^3 B^4}{3^6 C^3} \quad , \quad Q_{ij} = \tilde{Q}_{ij}\frac{2B}{9C} \quad , \quad A(T) = \frac{\tau_{col}B^2}{27C} \quad , \quad r = \xi_0\tilde{r} \quad , \quad \kappa = \frac{L_2}{L_1} \quad , \quad \tau_{col} = \tau - \frac{3q_0^2}{6+4\kappa} \tag{2.45}$$

where $\tilde{f}, \tilde{Q}_{ij}, \tau_{col}, \kappa$ and $\tilde{r}$ are the reduced quantities, with $\xi_0^2 = 18C(3L_1 + 2L_2)/B^2$ being the microscopic length scale, or the coherence length [54], set by the relation between bulk and distortion contributions (Appendix C). For the two-constant approximation, the rescaled free energy density LdG functional, with omitted overbars and a (-) sign on the second bulk term coming from $B < 0$, is,

$$\begin{aligned} f_{sym}(T, Q(\mathbf{r}), \partial_k Q_{ij}(\mathbf{r})) &= f_{bulk} + f_{dist} \\ f_{bulk} &= \frac{2}{3}\tau_{col} Q_{ij}Q_{ji} - \frac{8}{3}Q_{ij}Q_{jk}Q_{ki} + \frac{4}{9}(Q_{ij}Q_{ji})^2 \\ f_{dist} &= \frac{1}{3+2\kappa}\left[\left(\partial_k Q_{ij}\partial_k Q_{ij} + 4q_0\epsilon_{ijk}Q_{il}\partial_k Q_{jl} + 4q_0^2 Q_{ij}Q_{ji}\right) + \kappa\partial_j Q_{ij}\partial_k Q_{jk}\right] \end{aligned} \tag{2.46}$$

2.9 Surface Anchoring

The common ground for LC surface systems is that surfaces impose a specific director orientation, called the anchoring direction [24].

For phase coexisting systems, in the absence of external fields, the anchoring direction at the interface is defined solely by the LC elastic features [54] and may have parallel, perpendicular or any other orientation with respect to the free surface [51, 66]. Given that LC rodlike molecules tend to align parallel, the bulk preferred orientation will always be that imposed by the surface anchoring, at least in case of a flat surface. When this surface is an interface, the anchoring is defined by the elastic constants and is associated with some surface tension that results from the orientational deformations through the interface between the distinct phases. When the surface is a substrate, the anchoring is imposed through different alignment techniques [67] and is not affected by the system elastic properties.

The effect of surface anchoring on the system may be described by a localized orientational field. Whenever the bulk director is moved away from its equilibrium configuration, a free energy elastic penalty must be considered, proportional to some particular elastic constant for an interface and proportional to the anchoring strength and the deviation from the equilibrium preferred orientation. Thus, to consider energetic penalties, assuming that perturbations of the equilibrium configuration at the surface are small on a macroscopic scale, the free energy can be Taylor expanded around the equilibrium director orientation. Under the Frank-Oseen model, this corresponds to the Rapini-Papoular form [68]. Under the LdG model, the expansion is done over the tensor order parameter, around the preferred tensor order parameter, with derivatives of the free energy representing the anchoring strength [69], such that,

$$\begin{aligned} f_{surf} &= W'(Q_{ij} - Q_{ij}^0) + \frac{1}{2}W(Q_{ij} - Q_{ij}^0)^2 \\ &= \frac{1}{2}W(Q_{ij} - Q_{ij}^0)^2 \end{aligned} \tag{2.47}$$

To ensure that the surface free energy is bounded from below the linear term W' must be a vanishing term and W must be positive. This form of f_{surf} suffices to take into account the free energy contributions of the deviation of $\boldsymbol{Q}$ from $\boldsymbol{Q}^0$ in the simpler cases of anchoring considered above. Rescaling the surface energy using to the rescaling relations of the previous section, it results,

$$\tilde{f}_{surf} = \tilde{W}(Q_{ij} - Q_{ij}^0)^2 \quad , \quad W = \frac{B^2\xi}{27C}\tilde{W} \tag{2.48}$$

Chapter 3

Computational Method

To understand the structure of chiral nematic liquid crystals with the Landau-de Gennes model, a method that allows the system to relax into thermodynamic equilibrium is required, which implies that the system free energy is minimized. The free energy is described in terms of the integration of the LdG free energy density functional $f_{LdG}(T, \mathbf{Q}(\mathbf{r}), \nabla\mathbf{Q}(\mathbf{r}))$ that uses the κ, P parameters, so the equilibrium state is obtained when all the variables behave in such a way that the value of this integral, F, is minimum. Thus, it is in the functional variables that we are interested, in order to observe the behaviour of the director profile/tensor order parameter throughout the system and therefore, the structure of the chiral nematic interfaces.

For the system of interest, let us assume the system temperature is constant, in particular at the coexistence temperature between two phases. The functions inside the functional are considered as being the sum of the functions $\mathbf{Q}_0(\mathbf{r}), \nabla\mathbf{Q}_0(\mathbf{r})$ that minimize the integral plus some perturbation term, $\alpha\eta$, with α a small constant value that represents the magnitude of the perturbation and $\eta(\mathbf{r})$ a function that dictates the behaviour of the perturbation throughout the system. Thus, the free energy is written as,

$$F(\alpha) = \int_V f_{LdG}(\mathbf{Q}(\mathbf{r}), \nabla\mathbf{Q}(\mathbf{r}))dV = \int_V f_{LdG}(\mathbf{Q}_0(\mathbf{r}) + \alpha\eta(\mathbf{r}), \nabla\mathbf{Q}_0(\mathbf{r}) + \alpha\nabla\eta(\mathbf{r}))dV \tag{3.1}$$

The minimum of the integral will of course be achieved when it reaches the minimum with respect to the perturbation at some state where the magnitude is so small that it can be neglected ($\alpha = 0$), regardless of the perturbation, that vanishes at the systems frontiers, such that,

$$\begin{aligned}
\frac{dF}{d\alpha} &= \int_V \left(\frac{\partial f_{LdG}}{\partial \mathbf{Q}}\eta + \frac{\partial f_{LdG}}{\partial(\nabla\mathbf{Q})}\nabla\eta \right) dV \\
&= \int_V \frac{\partial f_{LdG}}{\partial \mathbf{Q}}\eta dV + \frac{\partial f_{LdG}}{\partial(\nabla\mathbf{Q})}\eta\bigg|_V - \int \partial_k \frac{\partial f_{LdG}}{\partial(\nabla\mathbf{Q})}\eta(\mathbf{r}))dV \\
&= \int_V \eta(\mathbf{r}) \left[\frac{\partial f_{LdG}}{\partial \mathbf{Q}} - \nabla\left(\frac{\partial f_{LdG}}{\partial(\nabla\mathbf{Q})} \right) \right] dV = 0
\end{aligned} \tag{3.2}$$

This leads to the Euler-Lagrange equations of the system, for which the LdG functional corresponds to the minimum total free energy, when the system is at equilibrium. Writing the tensor order parameter in the expanded form it becomes,

$$\partial_k \left[\frac{\partial f}{\partial_k Q_{ij}} \right] - \frac{\partial f}{\partial Q_{ij}} = 0 \tag{3.3}$$

with $f = f_{bulk} + f_{dist}$ the rescaled free energy density, $\mathbf{Q}$ the rescaled tensor order parameter, $\partial_k = \frac{\partial}{\partial x_k}$

and $x_k = x, y, z$. Writing the tensor order parameter as the traceless symmetric tensor,

$$\boldsymbol{Q} = \begin{bmatrix} q_1 & q_2 & q_3 \\ q_2 & q_4 & q_5 \\ q_3 & q_5 & -(q_1+q_4) \end{bmatrix} \tag{3.4}$$

with Eq.2.46, solving the Euler-Lagrange equation yields a set of non analytically solvable partial differential equations (PDEs), one for each independent component of the tensor order parameter **Q** (Appendix C),

$$\begin{aligned} &\bullet\ \nabla^2 q_1 + \frac{\kappa}{3}\Big(2\partial_{xx}q_1 + \partial_{zz}q_1 + \partial_{xz}q_3 - \partial_{yy}q_4 + \partial_{zz}q_4 - 2\partial_{yz}q_5\Big) - 4q_0\Big(\partial_y q_3 - \partial_z q_2\Big) \\ &= \frac{2}{3}(3+2\kappa)q_1\Sigma - \frac{4}{3}(3+2\kappa)\Big(q_1^2 + q_2^2 + q_3^2 - 2q_4^2 - 2q_5^2 - 2q_1q_4\Big) \end{aligned} \tag{3.5}$$

$$\begin{aligned} &\bullet\ \nabla^2 q_2 + \frac{\kappa}{2}\Big(\partial_{xy}q_1 + \partial_{xx}q_2 + \partial_{yy}q_2 + \partial_{yz}q_3 + \partial_{yz}q_4 + \partial_{xz}q_5\Big) - 2q_0\Big(\partial_x q_5 - 2\partial_y q_3 + \partial_z q_2\Big) \\ &= \frac{(3+2\kappa)}{6}q_2\Sigma - 4(3+2\kappa)\Big(q_1q_2 + q_2q_4 + q_3q_5\Big) \end{aligned} \tag{3.6}$$

$$\begin{aligned} &\bullet\ \nabla^2 q_3 + \frac{\kappa}{2}\Big(\partial_{yz}q_2 + \partial_{xx}q_3 + \partial_{zz}q_3 - \partial_{zx}q_4 + \partial_{yx}q_5\Big) - 2q_0\Big(-\partial_y q_1 + \partial_x q_2 - \partial_y q_4 - \partial_z q_5\Big) \\ &= \frac{(3+2\kappa)}{6}q_3\Sigma - 4(3+2\kappa)\Big(q_2q_5 + q_3q_4\Big) \end{aligned} \tag{3.7}$$

$$\begin{aligned} &\bullet\ \nabla^2 q_4 + \frac{\kappa}{3}\Big(-\partial_{xx}q_1 + \partial_{zz}q_1 - 2\partial_{xz}q_3 + 2\partial_{yy}q_4 + \partial_{zz}q_4 + \partial_{yz}q_5\Big) - 4q_0\Big(\partial_y q_3 - \partial_z q_2\Big) \\ &= \frac{2}{3}(3+2\kappa)q_4\Sigma - \frac{4}{3}(3+2\kappa)\Big(2q_1^2 - q_2^2 + 2q_3^2 - q_4^2 - q_5^2 + 2q_1q_4\Big) \end{aligned} \tag{3.8}$$

$$\begin{aligned} &\bullet\ \nabla^2 q_5 + \frac{\kappa}{2}\Big(-\partial_{zy}q_1 + \partial_{xy}q_3 - \partial_{zy}q_4 + \partial_{yy}q_5\Big) - 2q_0\Big(2\partial_x q_1 - \partial_y q_2 + \partial_z q_3 + \partial_x q_4\Big) \\ &= \frac{(3+2\kappa)}{6}q_3\Sigma + 4(3+2\kappa)\Big(q_2q_5 + q_3q_4\Big) \end{aligned} \tag{3.9}$$

with $\Sigma = \Big(\tau + \frac{4}{3}(2Tr\boldsymbol{Q}^2) + \frac{6q_0^2}{3+2\kappa})\Big)$.

The solutions of the set of Euler-Lagrange equations are obtained with the finite element method (FEM), a numerical technique that obtains approximate solutions of boundary-value problems, using the commercial software COMSOL Multiphysics 3.5a. The basic idea behind FEM is to divide a continuous domain into a controlled number of subdomains in which the unknown subdomain solution is approximated to a trial function with a selected number of unknown coefficients, thus reducing the entire solution to a finite number of unknown coefficients. This approximation is constructed is four steps [70].

The first step, also called triangulation step, consists in discretizing the domain into smaller subdomains, creating a mesh of finite non-overlapping elements. The number of elements that follows from this discretization depends on the system dimension, element size and element geometry, that can all be separately customized, both globally and locally. In 2D systems, elements can be triangular, square or rectangular. To the elements vertices are associated nodes with a local number, the ith node position out of the n nodes in the element to which is associated some interpolation function v_i, and a global number, the node position in the total M nodes of the system. After the discretization is complete all of the system's information is cut from the continuous surface excluding only the nodes and the boundaries of the domain and therefore the continuous system governing equations will only be defined on the nodes. The simulations in this work are run with triangular elements and there is no further customization apart from reducing the element size and thus increasing their number. The number of elements/nodes is proportional to the degree of approximation of the discrete system to the continuous system.

The second step consists in selecting an interpolation function that, according to some numerical method (Ritz or Galerkin's method), provides an approximation to the unknown solution at each node, from which it is possible to interpolate the solution within an element by making an average weighting of the nodes approximate solutions. The interpolation function is usually selected to be a polynomial of order k, also referred to as the order of the element. The expression of the unknown element solution has the form,

$$\tilde{\phi}^e = \sum_{i=1}^{n} v_i^e \phi_i^e = \{v^e\}^T \{\phi^e\} \tag{3.10}$$

with $\tilde{\phi}_i^e$ the value of the approximated node solution, zero valued outside the respective element, and v_i^e the interpolation function of the ith from the n nodes of the element e. The above $\{.\}$ and $\{.\}^T$ denote a line and a column vector, respectively, with dimension n. The name of interpolation function comes from the fact that each node belongs to different elements and thus can relate the information of the different elements to which it is connected and by associating such function to them allows to interpolate the solutions in neighbour elements. The above expression, Eq.3.10 simply states that the solution inside each element is a weighted average of the nodes solutions, with v_i the weight function.

The third step consists in formulating a system of equations that characterize the system by computing them with the weighted solution within each element in the previous step, $\tilde{\phi}^e$. One possible method to do this, is to apply Galerkin's method, used in COMSOL Multiphysics 3.5a [71], which measures the residual of the differential equations using the weighted solution. For the LdG model this means having a set of 5 Euler-Lagrange equations with 5 distinct weighted solutions, but for illustrative purposes let us neglect this and assume the system obeys only one differential equation. Considering the differential operator $\mathcal{L}$, the excitation function f and the solution of the continuous domain ϕ, the system can be described by the differential equation,

$$\mathcal{L}\phi - f = 0. \tag{3.11}$$

For a discretized domain, the above differential equation is applied to the weighted solution within an element, resulting in the residual of the element e,

$$r^e = \mathcal{L}\tilde{\phi}^e - f \neq 0. \tag{3.12}$$

The best approximation between $\tilde{\phi}^e$ and ϕ, i.e, between the solution of an element of the discretized domain and the solution of the continuous domain, will be one that minimizes the residual value in that element. For each of the element nodes, the weighted residual is considered the residual of the element e weighted by the interpolation function of the nodes,

$$R_i^e = \sum_i^n v_i^e r^e = \sum_i^n v_i^e (\mathcal{L}\tilde{\phi}^e - f) \tag{3.13}$$

and substituting Eq.3.10 into Eq.3.12 yields,

$$R_i^e = \sum_i^n \{v^e\}\mathcal{L}\{v^e\}^T\{\phi^e\} - \{v^e\}f \tag{3.14}$$

which can be written in matrix form as,

$$\{R^e\} = [K^e]\{\phi^e\} - \{b^e\} \tag{3.15}$$

in which $[K^e]$ is a $n \times n$ matrix with n being the total number of nodes in element e, $\{\phi^e\}$ an $n \times 1$ vector in whose elements are the unknown node solutions and $\{b^e\}$ an $n \times 1$ vector whose elements are known, since f is known and v_i is selected. Since the weighted residual R_i is weighted over all the neighbour elements residuals, then R_i is a summation over the elements directly connected to i. Thus, the global node weighted residual can be seen as the sum over all of the M system nodes,

$$\{R\} = \sum_{e=1}^{M}\{R^e\} = \sum_{e=1}^{M}([K^e]\{\phi^e\} - \{b^e\}) = [K]\{\phi\} - \{b\} \tag{3.16}$$

and the system of equations can be obtained by making $\{R\} = \{0\}$. But now the question is what is the initial solution at the nodes in which all this approximation and weighting process is based. The nodal solutions are initialized both by the initial condition over the domain and by the boundary conditions. There are two types of boundary conditions, the Dirichlet boundary condition that imposes some value on the solution at the boundaries, and the Neumann boundary condition that imposes the continuity of the solution, i.e, a vanishing derivative of the solution.

The fourth and final step consists of course in solving the system of equations numerically in order to obtained the desired quantities, in our case the tensor order parameter elements with respect to the system's coordinates. With these quantities and with the constants, T, κ, P it is possible to describe the system structural properties and any other quantity, such as bulk, elastic and surface energy.

Chapter 4

Previous results for Interfaces

4.1 Nematic - Isotropic interface

At the nematic-isotropic interface, the LC goes from the nematic phase to the isotropic phase with an order parameter that changes through the interface, which is of the order of the microscopic length scale, ξ_0 [54]. The system can be described by three regions, the isotropic phase in which molecules have no preferred orientation, the nematic phase in which molecules tend to align parallel to each other and the interface itself, in which the molecular arrangement is in a transition state between the two distinct symmetries. At the interface, no symmetry rules over the other since both phases coexist and the scalar other parameter is simply assumed to be described by a smooth symmetric function that goes from $S = 1$ at the nematic phase to $S = 0$ at the isotropic phase, passing through $S = 1/2$ at the middle of the interface. For the nematic, the scalar order parameter can thus be described by the ansatz,

$$S(z) = \frac{1}{2}\left[1 - \tanh\left(\frac{z}{z_0}\right)\right] \quad , \quad B(z) = 0 \tag{4.1}$$

which describes an interface parallel to the $x - y$ plane centered at $z = 0$, with translational invariance under the z direction and thickness z_0 [13, 30, 32, 54].

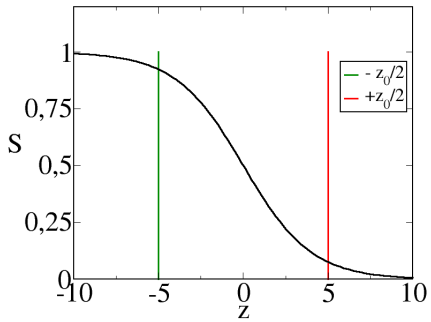

Fig. 4.1: Schematic representation of an interface, with scalar order parameter going from $S = 1$ at $z = -\infty$ to $S = 0$ at $z = \infty$.

Using the LdG model, it is imposed that the director orientation is fixed everywhere over the interface thickness z_0, either with parallel or homeotropic orientation, depending on the relation between L_1 and L_2. If $L_2 > 0$, parallel anchoring is preferred, while for $L_2 < 0$, homeotropic anchoring is preferred [54], or according to the rescaled elastic constants, if $\kappa > 0$ and $\kappa < 0$, respectively. Since the nematic equilibrium configuration has the same director orientation throughout the bulk, in order to minimize elastic penalties the bulk equilibrium configuration will correspond to one in which the director has the

same orientation of that imposed by the free surface. It should be stated that the director orientation at the surface will always keep its orientation with respect to the surface normal, regardless if the surface is flat or not. If the bulk initial director orientation is perpendicular to that of the interface, a transition from that state to one where the bulk and the surface director have the same orientation is smooth and continuous, meaning that no metastable state is found in between, as shown in Fig.4.2.

Although the LdG model is suited to describe interfaces with homeotropic and planar anchoring, it must be pointed out that the NI interface is often found with tilted anchoring [18]. For the LdG model to contemplate such cases, higher order terms of the expansion must be considered [30]. Both Parsons, for the nematic free surface [72], and Mada, for the free surface and substrate [73] proposed phenomenological theories that take into account tilted director orientations at the surface, with a free energy description based on the relation between the director field and the vector normal to the free surface and between the director and the preferred surface orientation vector, respectively.

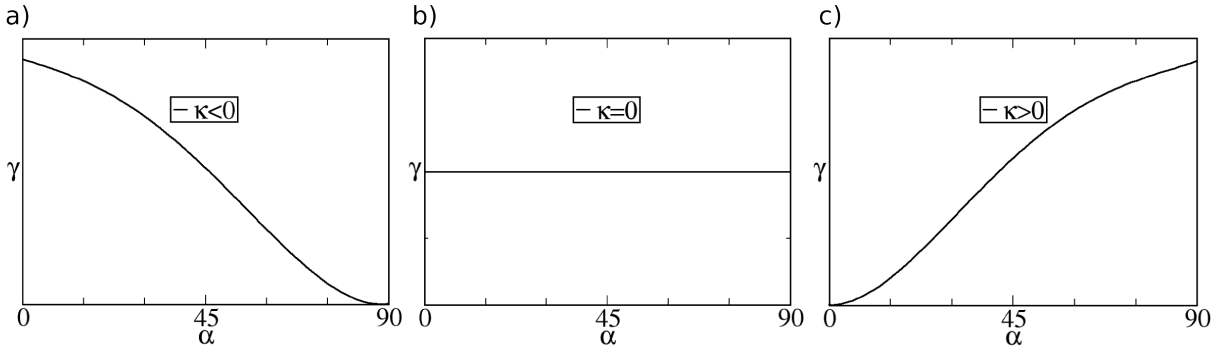

Fig. 4.2: With γ the surface tension and α the nematic angle with respect to the interface plane: a) for $\kappa < 0$ the anchoring is homeotropic and the nematic bulk orientation chooses the lowest energy and more stable state, to be perpendicular to the interface; b) for $\kappa = 0$ there is no preferential anchoring direction and there is no preferential orientation for the nematic bulk; c) For $\kappa > 0$ the anchoring is planar and the nematic bulk orientation chooses the lowest energy and more stable state, to be perpendicular to the interface. There are no intermediate orientation states, since the surface tension has a global minimum for both anchorings (the figures correspond to a schematic representation).

Substituting the ansatz of Eq.4.1 in the tensor order parameter of Eq.2.41 and assuming a fixed director over the interface, either perpendicular ($\perp$) or parallel ($\parallel$) to the interface, minimizing $F/(L_x L_y) = \int_z f_{LdG} dz$ with respect to z_0 and integrating over the z axis, gives $z_0 = \sqrt{2}$. Calculating the integral with the value obtained for z_0 gives the surface tension γ, as a function of κ (Appendix C). Neglecting biaxial symmetry, with the two-constant-approximation and with the proposed ansatz, it results that the surface tension for homeotropic and planar anchoring can be described as [13, 32],

$$\gamma_\perp = \frac{\sqrt{2}}{6} \quad , \quad \kappa \leq 0 \quad , \qquad \gamma_\parallel = \frac{\sqrt{2}}{6}\sqrt{\frac{6+\kappa}{6+4\kappa}} \quad , \quad \kappa \geq 0 \tag{4.2}$$

It may also occur that $\kappa = 0$, which corresponds to the one-constant approximation and means that all distortions are equally preferred. The interface structural profile is simply obtained by measuring $S = 1/2$ over the interface, which for the nematic-isotropic interface gives a flat line.

Through the interface induced orientation, at equilibrium, the bulk orientation is the same as that of the interface, so, there is no orientational symmetry breaking between the bulk and the surface. Thus, biaxiality is not expected in the ordered phase close to the interface. It is just at the interface region that biaxial features may arise, since there is symmetry breaking. This is demonstrated through numerical results for the NI interface with parallel anchoring, in which biaxial order emerges at the interface, but only with a negligible magnitude [30, 55].

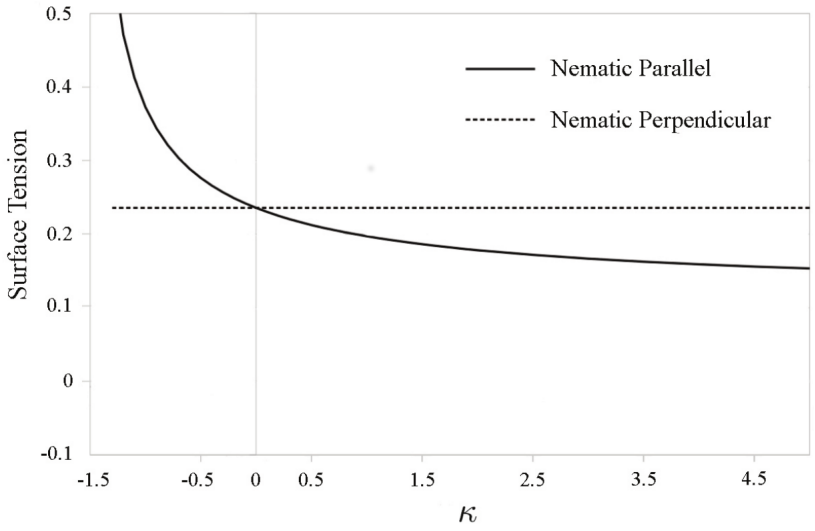

Fig. 4.3: Surface tension of the nematic-isotropic interface depending on the elastic constant κ. The surface tension is measured for the bulk nematic with the same orientation as the anchoring. For $\kappa < 0$ the surface tension for planar anchoring is greater than for homeotropic anchoring, so the latter is preferred. For $\kappa > 0$ the surface tension for planar anchoring is greater than for homeotropic anchoring, so the first is preferred (figure from [38]).

4.2 Cholesteric - Isotropic interface

The bulk orientational profile of nematics is homogeneous and, in the absence of external fields, regardless of the interface anchoring orientation, the system adopts the minimum distortion configuration simply by aligning with the free surface director orientation, which provides the interface a flat profile. For cholesterics, given the spatial periodicity of the director orientation, the bulk orientational profile at the interface may be significantly different from that of a nematic, depending on the direction and scale that the periodicity has regarding the interface in the equilibrium state. As a consequence, in a situation where the pitch axis is parallel to the free surface, as in Fig.4.4, the periodic alignment of the bulk will not correspond to the uniform anchoring orientation, thus creating elastic frustrations. In this scenario the minimum distortion configuration can only be achieved by deformations of the free surface, leading to a rough profile, set by the predominant elastic contributions. Thus, the shape of cholesteric-isotropic interface depends on a combination between the cholesteric layer orientation and spatial periodicity and the anchoring orientation, given by the elastic properties [74].

When cholesteric layers are perpendicular to an initially fixed flat surface with large but finite homeotropic anchoring strength and translational invariance, there are regions, with the cholesteric spatial periodicity, where the surface director orientation is incompatible with that of the cholesteric, called χ disclination lines (invariant in the out of the plane direction), as in Fig.4.4 (left). To minimize the elastic energetic penalties associated with these regions, deformations are introduced around the χ disclinations which induce the dissociation of the χ disclination lines into a pair of τ^- and λ^+ line defects [11,25], as in Fig.4.4 (right). Around the λ^+ defects the system is allowed to rearrange in a way that elastic penalties are minimized. Around, τ^- defects, however, such is not the case. Since the anchoring strength is large but finite, the surface is allowed to deform if necessary and in this case, it does so by removing the τ^- defects, given that undulations are energetically favourable to the presence of these defects. These undulations do nevertheless increase the surface area and one might say that surface deformations increase the surface tension. Below a certain pitch value, the geometry of the surface undulations with homeotropic anchoring, induces the creation of $s = -1/2$ defects on the edges of the undulations, in

order to minimize elastic frustrations.

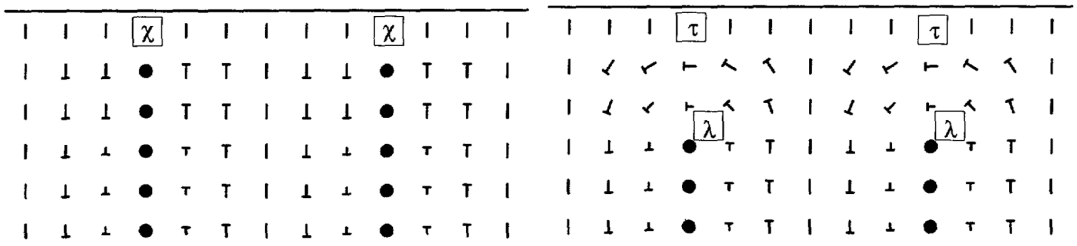

Fig. 4.4: Cholesteric layers perpendicular to a fixed flat surface with homeotropic anchoring. On the left, the system is in a pre χ disclination line dissociation, while on the right, χ defects have dissociated into τ^- and λ^+ defects, at the surface and below the surface, respectively (figures from [25]).

When cholesteric layers are parallel to the surface, assuming the same anchoring conditions as in the previous example, the system induces the creation of $s = +1/2$ and $s = -1/2$ disclination lines (invariant in the out of the plane direction) along the surface, as shown in Fig.4.5 (left) [75]. However, unlike the previous case, where it is always energetically favourable to eliminate defects and induce surface undulations, here, such process is limited by defect interactions, which depend solely on the distance between defects. Systems in which the cholesteric has lower pitch values will have layers with the same orientation closer together and, as a consequence, defects will be closer together. This increases their interaction energy making surface undulations energetically favourable to the presence of defects and their interactions. Defects are then removed and replaced by surface undulations and *double-twist* cells near the surface, with an orientational periodicity larger than that of the cholesteric, as shown in Fig.4.5 (right) [25]. For pitch values small enough, the creation of $s = -1/2$ defects is induced on the edges of the undulations, in order to minimize elastic frustrations. Thus, regardless of the cholesteric layers orientation, for homeotropic anchoring, surface undulations can always be created.

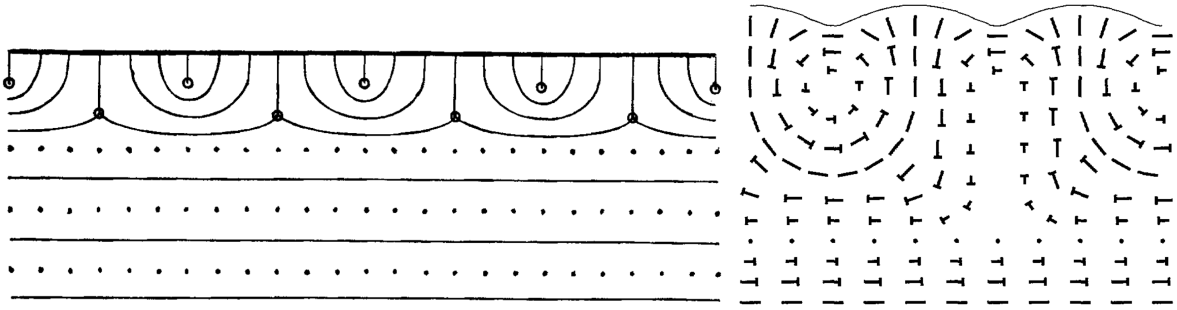

Fig. 4.5: Cholesteric layers parallel to a surface with homeotropic anchoring. On the left, for high pitch values, no surface undulations are observed and the surface is marked by an array of $s = -1/2$ and $s = +1/2$ defects. On the right, for low pitch values, the array of defects gives place to surface undulations and *double-twist* cells near the surface, with periodicity larger then the cholesteric (figure (left) from [75] and (right) from [25]).

In systems with cholesteric layers perpendicular to a surface with planar anchoring, the surface director orientation is incompatible with that of the cholesteric and the system induces the creation of disclination lines along the surface, λ^+ at the interface and $s = -1/2$ between layers below the surface, the opposite of the defect disposition on a system with layers parallel and homeotropic anchoring. This gives rise to an energetic balance between the elastic energy contributions associated with the $s = -1/2$ defects and the surface energy. When the pitch value decreases, layers with the same orientation are closer together and so are the defects. However, in this scenario defect interaction is not forced to increase like in the previous examples, but instead they are kept at its minimum value because λ^+ defects

are allowed to move away from the surface. In turn this also makes the $s = -1/2$ defects near the surface stable for every pitch value. Thus, this interface is not expected to have any kind of undulation regardless of the pitch value, since the presence of defects is always energetically favourable. If instead, the cholesteric layers are parallel to a surface with planar anchoring, then the layers orientation coincides with the orientation of the surface and no frustrations emerge. This results in a flat free interface with the same behaviour as a nematic interface. Thus, regardless of the cholesteric layers orientations, for planar anchoring, surface deformations are never created.

Even though this heuristic argumentation allows to understand the behaviour of chiral nematic interfaces, with respect to the anchoring orientation, the layer's orientation and the pitch, it lacks the quantitative description to confirm it. Thus, to capture all the above situations the LdG model can be used and a quantitative description of the surface tension and the surface undulation profile can be obtained. Recalling from Eq.2.46, a quadratic term in $\mathbf{Q}$ from the gradient terms is included in the bulk terms redefining the coexistence temperature as,

$$\tau_{col} = \tau - \frac{3}{2}\frac{q_0^2}{3+2\kappa}. \tag{4.3}$$

This indicates that, unlike nematics, the cholesteric natural distortions coming from chirality affect the coexistence conditions. As can be observed in the experimental results of Fig.2.2 (left), for low chirality values, the coexistence temperature between the cholesteric and the isotropic phase is practically constant and decreases for higher chirality only, in agreement with Eq.4.4. The equilibrium configuration of a cholesteric with homeotropic or planar anchoring at the interface corresponds to bulk free energy minimum redefining the scalar order parameter as,

$$\frac{\partial}{\partial S}\left(\tau_{col}S^2 - 2S^3 + S^4\right) = 0 \Rightarrow S = \frac{3}{4} + \frac{1}{4}\left[9 - 8\tau_{col}\right]^{1/2} \tag{4.4}$$

As stated in Sec.2.2, biaxial symmetry is expected to grow in system with high chirality. Thus, the coexistence temperature is expected to be affected not only by chirality but also by biaxial features. Considering that two scalar order parameters are now considered in the tensor order parameter, S and B, developing the LdG model, relatively to the simple uniaxial case, results in extra bulk and gradient free energy density terms. Analogous to the effect on on the coexistence temperature of adding a uniaxial quadratic term of the gradient free energy into the bulk free energy, including biaxial gradient terms into the bulk free energy leads to further increments in the coexistence temperature resulting in [7, 12],

$$\tau_{col} = \frac{1}{2} - \frac{3q_0^2}{3+2\kappa} + \frac{1}{2}\left(1 + \frac{2q_0^2}{3+2\kappa}\right)^{3/2} \tag{4.5}$$

which leads to the redefinition of the equilibrium value of the scalar order parameter in the chiral nematic phase as [13],

$$S = \frac{A}{3} + \frac{3B}{4} \tag{4.6}$$

$$A = \frac{3}{4} - \frac{1}{2}\frac{q_0^2}{3+2\kappa} + \frac{1}{4}\left[9 - 8\tau_{col} - \frac{12q_0^2}{3+2\kappa} + 4\left(\frac{q_0^2}{3+2\kappa}\right)^2\right]^{1/2} \tag{4.7}$$

$$B^2 = \frac{9}{8} - \frac{\tau_{col}}{2} + \left(\frac{3}{8} + \frac{1}{12}\frac{q_0^2}{3+2\kappa}\right)\left[9 - 8\tau_{col} - \frac{12q_0^2}{3+2\kappa} + 4\left(\frac{q_0^2}{3+2\kappa}\right)^2\right]^{1/2} - \frac{1}{2}\frac{q_0^2}{3+2\kappa} - \frac{1}{6}\left(\frac{q_0^2}{3+2\kappa}\right)^2 \tag{4.8}$$

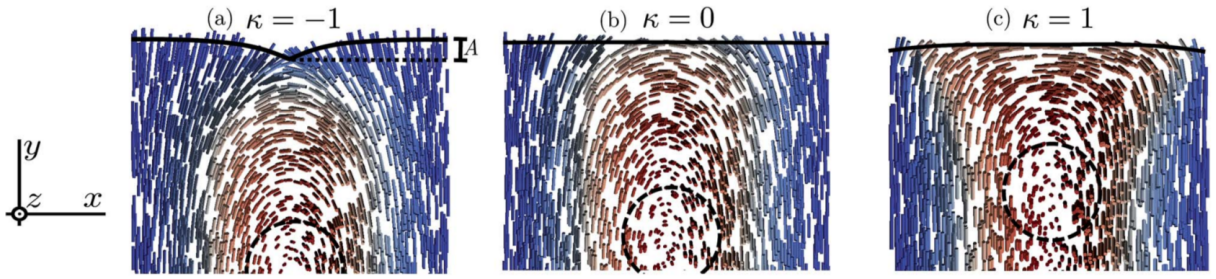

Fig. 4.6: Cholesteric-isotropic interface configurations for $P = 1000\xi$ and: (a) homeotropic anchoring with surface undulations and surface tension greater then the NI interface (stable); (b) no anchoring; (c) planar anchoring with no surface undulations and surface tension equal to the NI interface (unstable). The undulations amplitude A of the interface corresponds to the difference between the maximum and minimum heights of $S \approx 1/2$. Red represents molecules with out-of-plane alignment and blue represents molecules with in-plane alignment (figure from [13]).

The interfacial configurations of Fig.4.6 were simulated using the rescaled version of the LdG model in Eq.2.46. The surface tension is given by the total system free energy divided by the total surface area, and the interfacial structure profile was measured over the surface along the line of value $S(x) = 1/2$, with undulations amplitude given by the difference between the higher and lower y values on that line. With respect to the surface tension, for the nematic limit where $P \to \infty$, the surface tension has the same behaviour as in the nematic-isotropic interface, as shown in Fig.4.7. This happens regardless of the anchoring orientation, with an anchoring transition point occurring at $\kappa = \kappa_c = 0$ between homeotropic and planar anchoring.

For intermediate pitch values, the C-I deviation from the nematic-isotropic interfacial behaviour is manifested through a deviation of the surface tension and κ_c. Regarding the transition point, at $P = 1000\xi$ it was found to be $\kappa_c = 0.14$ and the transition point is a function of P. As for the surface tension, above κ_c, planar anchoring is preferred and the surface tension is minimal when cholesteric layers are aligned parallel to the interface, with roughly the same surface tension values as in the nematic as shown in Fig.4.7, as would be expected since no frustrations are present near the surface in this alignment. Below κ_c homeotropic anchoring is preferred and the surface tension is minimal when cholesteric layers are aligned perpendicular to the interface, although, with higher surface tension than those that would be found in the nematic, increasing proportionally to $|\kappa - \kappa_c|$. This increase is due to the creation of surface undulations that increase the surface area, which happens when surface undulations are energetically favourable to the presence of surface elastic frustrations and τ^- defects. Thus, regardless of the layers orientation, interfacial roughness only emerges for homeotropic anchoring in agreement with the previous qualitative argument.

For low pitch values, the deviation between the surface tension and κ_c of the C-I and the N-I is further increased. Regarding the transition point, at $P = 100\xi$ it is observed that $\kappa_c = 2.1$. Above κ_c, since planar anchoring is preferred, the surface tension is minimal when cholesteric layers are aligned parallel to the interface. However, even though no interface deformations are expected to emerge, the surface tension no longer follows that of the nematic indicating that something must happen to the orientational profile close to the interface. Nevertheless, this was not explored. Below κ_c, again, homeotropic anchoring is preferred and the surface tension is minimal when cholesteric layers are aligned perpendicular to the interface. However, in this regime, instead of increasing, the surface tension decreases with increasing $|\kappa - \kappa_c|$. In fact, from a certain $\kappa_{tp}(P)$, the surface tension goes from positive to negative values. The negative surface tension is a manifestation that, near the transition temperature between the cholesteric and isotropic phases, the free energy of a new phase is lower then the energy of the cholesteric phase [46]. Looking at the orientational profile of the system, it is possible to see that the surface tension

positive-negative transitions is followed by the nucleation of *double-twist* cylinders near the C-I interface that propagate through the cholesteric bulk, forming a lattice of defects, characteristic of blue phases, in agreement with experimental observations of cholesterics with high chirality at the C-I transition temperature [7]. In the $x-y$ plane, the defect lattice is hexagonal, with the cylinders projection into the cell cores, and thus a blue phase I.

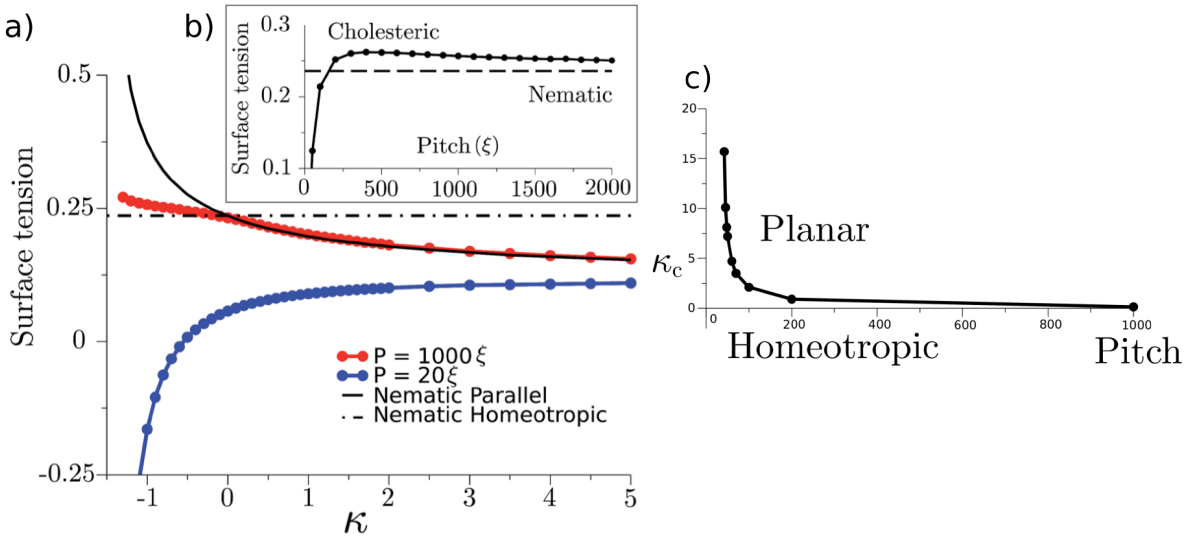

Fig. 4.7: (a) C-I surface tension dependence on κ for fixed P. The surface tension is measured for the bulk cholesteric layers perpendicular to the interface. The surface tension of the N-I interface is represented in the black-full line for planar anchoring and in black-dashed line for homeotropic anchoring. The red line is the surface tension for $P = 1000\xi$ and the blue line for $P = 20\xi$. (b) C-I surface tension dependence on P for $\kappa = -1$. N-I interface is the black-dashed line and the C-I is the black-full line (figures from [13]). (c) Anchoring transition κ_c dependence on the pitch, between homeotropic and planar anchoring. For $\kappa > \kappa_c(P)$ the anchoring is planar while for $\kappa < \kappa_c(P)$ the anchoring is homeotropic (figure from [13]).

Above the transition to the blue phase, for $\kappa < \kappa_c$, the undulations amplitude scales as $A \sim \sqrt{P}$ and $A \sim -k$, and the relative amplitude, $\sim A/P$ scales as $r \sim 1/\sqrt{P}$, and is zero in the nematic limit [13], as can be seen in Fig.4.8. Experimental results on cholesteric droplets with controlled chirality indicate, however, that the interface undulations amplitude goes as $A \sim P$ [76], in contrast to the numerical results. The value of κ_c grows inversily with the pitch and so, planar anchoring behaviour is progressively ruled out as pitch is decreased, indicating that homeotropic anchoring should be more often expected for cholesterics then for nematics [13, 18].

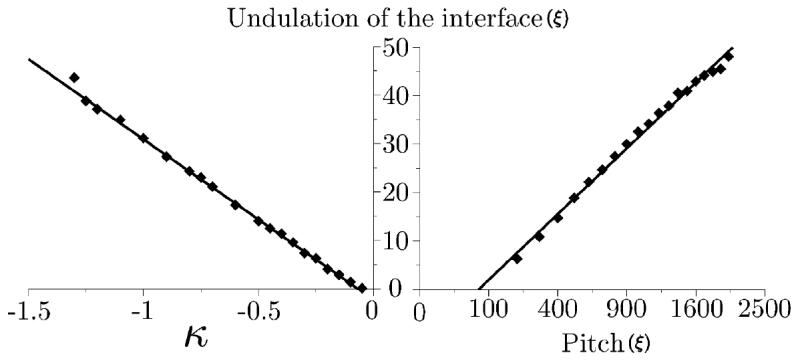

Fig. 4.8: C-I interface undulations amplitude with respect to the rescaled elastic constant for $P = 1000\xi$, $A = -33.1\kappa - 2.2$ (left) and with respect to the pitch for $\kappa = -1$, with $A = 1.359\sqrt{P} - 11.6$ (right) [13]).

Chapter 5

New Results and Discussion for Interfaces

The central goal of this thesis is to understand the behaviour of chiral nematic interfaces over the triple coexistence between the isotropic, cholesteric and blue phase. So far, it is known that the cholesteric-isotropic interface surface tension and undulations amplitude depend strongly on the elastic features, κ, and P. Furthermore, at the coexistence temperature, $\tau(\kappa, P)$, between these two phases, it was observed that the cholesteric phase becomes unstable with respect to the blue phase, for some combinations of these two parameters. This phenomenon opens the way for the study of two distinct interfaces, the BP-I and the BP-C interfaces.

The equilibrium interfaces are obtained for the profile of the tensor order parameter and its spatial fluctuations that for a given set of κ, P and τ parameters minimize the system free energy. Thus, the first step towards the comprehension of interfacial properties of both interfaces is to set the relation between κ and P that at coexistence give the 2D profile of blue phase with minimum free energy. From this results a blue phase with a regular honeycomb lattice of defects filled with *double-twist* cells that exhibits an orientational periodicity of the *double-twist* cells linear with the orientational periodicity of the cholesteric layers of the phase it coexists with. An hyperbolic relation between κ and P is observed that defines the triple line between the isotropic, the cholesteric and the blue phase, above which the cholesteric-isotropic coexistence is preferred and below which the blue phase-isotropic is preferred and over which the three phases coexist.

The BP-I interface is explored for different pitch values, regarding both the surface tension and the undulation profile. Two interface configurations are obtained, named literally after their *double-twist* cell arrangement towards the interface, the *zig-zag* and the *linear* configurations, that respectively correspond to an initial perpendicular and parallel orientation of the cholesteric layers at the surface. The *zig-zag* configuration has higher undulations amplitude and lower surface tension values while the *linear* configuration has lower undulations amplitude and higher surface tension. To explain the difference between the two configurations undulations amplitude we develop a simple geometric argument in which surface cells are considered to be undistorted that gives qualitative agreement with the numerical results. One common feature between the two configurations is that the surface tension has an approximate logarithmic grow with P. These results agree with those of the C-I system in that the equilibrium C-I interface has higher undulations amplitude when the layers are perpendicular at the interface and is also the most stable. Another common feature is that both configurations have distinct roughness behaviours with pitch, with high roughness for small pitch, below P_u and with low roughness for large pitch, above P_u. Although not completely understood, the different roughness regions is a manifestation of an anchoring transition that occurs at P_u, with planar anchoring below and homeotropic anchoring above P_u. These results agree with those of the C-I system in that the equilibrium C-I interface has

homeotropic anchoring and the roughness decreases for high pitch values. Remarkably an interception between the roughness profiles of the BP-I and the C-I over the triple line is also observed.

The BP-C interface is also explored for different pitch values regarding both the surface tension and the undulation profile. There is, however, one further parameter to have in consideration. Due to the different orientational periodicities of the phases the amount of deformations of each phase close to the interface will depend on the cholesteric layers angle α and thus, it is considered as a new parameter. Indeed both interface configurations have minimum surface tension when the cholesteric layers are oriented at an angle $\alpha \simeq \pi/4$ at the surface, angle at which where both the cholesteric and the blue phase are not distorted near the interface. To understand why we develop a geometric argument in which the projection of the two phases periodicities is considered the same and observe that such situation corresponds to cholesteric layers angle of $\pi/4$. However this argument only holds for the *linear* configuration. Contrary to the previous equilibrium interface, the *zig-zag* configuration has higher surface tension than the *linear* configuration. It is observed that, for low pitch values, the surface tension is negative. Even though not completely understood, this might be due to elastic penalties associated with periodic mismatches between the cholesteric and blue phase periodicities and the system dimension, or it might indicate that a new ordered and more symmetric phase is the new free energy minimum of the system over the triple phase coexistence line. As for the surface undulations, the method of following the line $S = 1/2$ is ruled out since $S = 1$ in all the system. Since at $\alpha = \pi/4$ the equilibrium interface is one where the BP is not distorted, the undulations amplitude is simply be measured following the same geometric approach used in the BP-I section in the understanding of the difference between the two configurations undulations amplitude.

5.1 Phase Diagram

Cholesterics heated to temperatures just below the isotropic phase can become either, energetically equivalent to the isotropic phase, if chirality and twist elastic penalties are low, or energetically equivalent to the blue phase otherwise. For C-I coexistence, changes of chirality or twist elastic penalties can enhance orientational frustrations and, to counterbalance them, the creation of topological defects is induced. Thus, the cholesteric becomes unstable with respect to the blue phase and the BP-I coexistence emerges. Also there is the case in which the cholesteric and the blue phase are energetically equivalent (BP-C), while in coexistence with the isotropic phase, thus in a triple phase coexistence. Looking at Fig.2.2 (left), such point corresponds to the interception of the cholesteric, blue phase I and isotropic phases [7, 8]. Nevertheless, such states corresponds to a very particular combination of chirality, twist elastic penalties and temperature. So, to obtain it, the stability limit of each phase needs to be explored. The control of these parameters can be accomplished through doping agents or the effects of external fields. However, in this work we neglect the source of the changes and use the chirality, elastic penalties freely and temperature freely. To recreate infinite systems, simulations were performed in periodic boundary rectangular domains.

What was previously observed in [13] was that for small pitch values, $P < 1000\xi$, and for negative κ values, a phase transition from the cholesteric to the blue phase occurred. So, the problem here is to understand what are the P and κ values that at the coexistence temperature τ result in a blue phase with zero free energy density.

Thus, first, to a bulk domain of cholesteric at τ and with domain dimensions mensurable with P, a quenching of κ is developed, this is, κ it taken into its limit, close to $\kappa \approx -1.5$. From this a phase transition from the cholesteric, Fig.5.1 a), to the blue phase, Fig.5.1 b) is ensured. Thus, the 2D blue

phase structure is has a hexagonal lattice of defects, observed in the corners of the hexagons. However, the resulting BP does not have zero free energy meaning that it is not at coexistence with the cholesteric and with isotropic phases.

Then, a set of κ values is tested and the behaviour of the free energy density observed, where some result in systems with free energy far from zero while others result in energies closer to zero. From the tested κ values the first two that both from negative and positive free energy values are in the interval of $f = 0 \pm 5 \times 10^{-4}$ are selected. For simplicity let us call them κ^- when negative and κ^+ when positive, as can be seen in Fig.5.1 d). For each of the selected κ's, in order to minimize the free energy density, different domain dimensions are also tested and the minimum obtained for the relation $H \simeq L/\sqrt{3}$, with H the side parallel to the direction of the smallest distance between the *double-twist* cores, as in Fig.5.1 b) and c). To this distance we call the the blue phase pitch $\tilde{P}$, with $2H = \tilde{P}$.

This implies that the blue phase stable structure roughly corresponds to a honeycomb lattice of defects. Following the fixed relation $H \simeq L/\sqrt{3}$ the free energy is further minimized for different L values and the minimum obtained for the sets κ^+, L^+ and κ^-, L^-, as can be seen in Fig.5.1 d). Tracing lines for f with respect to κ and f with respect to L between these two points, the set of κ, P and τ obtained when the lines cross the zero free energy density corresponds to the state where the three phases coexist. Repeating this process for different pitch values resulted that $L = \sqrt{3}P/\sqrt{2}$ and $\kappa = -1.42 + 6.59q$. Besides giving the triple coexistence line this also gives a fixed relation between the cholesteric and the blue phase orientational periodicities, $P \approx \sqrt{2}\tilde{P}$. The process was repeated from $P = 10\xi$ to $P = 300\xi$, where the blue phase could no longer be observed.

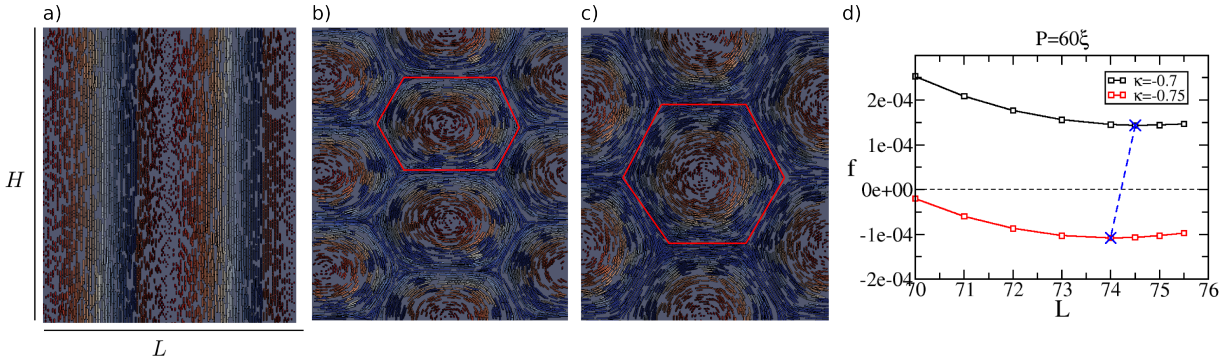

Fig. 5.1: Steps of the triple phase diagram construction: a) Cholesteric with $P = 60$; b) Blue phase with κ close to the one for which $f = 0$, initially obtained from a cholesteric with $\kappa \approx -1.5$; c) Blue phase with minimized free energy following the relation $H \simeq 1/\sqrt{3}L$, that results in regular honeycomb lattice of defects; d) Free energy density of the blue phase for κ's that give an energy close to zero and with changing L following the relation $H \simeq 1/\sqrt{3}L$. From this process the relations $P \approx \sqrt{2}\tilde{P}$ and $\kappa = -1.42 + 6.59q$ are obtained.

Lets consider as an assumption, that defects have $s = -1/2$, as in Fig.2.7 b). This implies that the double twist cores are equidistant. Also given that the cores are separated by a pitch dependent length, then the structure should be a regular honeycomb lattice. As will be seen in the BP-C section, it is possible to obtain quantitative agreement between the numerical results and a geometric approach that is based on the assumption that defects are indeed $s = -1/2$ and that the structure of the blue phase is indeed a regular honeycomb defect lattice. Thus, even though the simulations only give an approximated honeycomb structure at the triple coexistence, let us say from now on that the lattice is indeed regular.

Comparing the values of the triple line $\kappa_{tp}(q) = -1.42 + 6.59q$ with the values of the C-I interface anchoring transition κ_{at}, it is possible to conclude that the BP-I interface has homeotropic anchoring regardless of the P value.

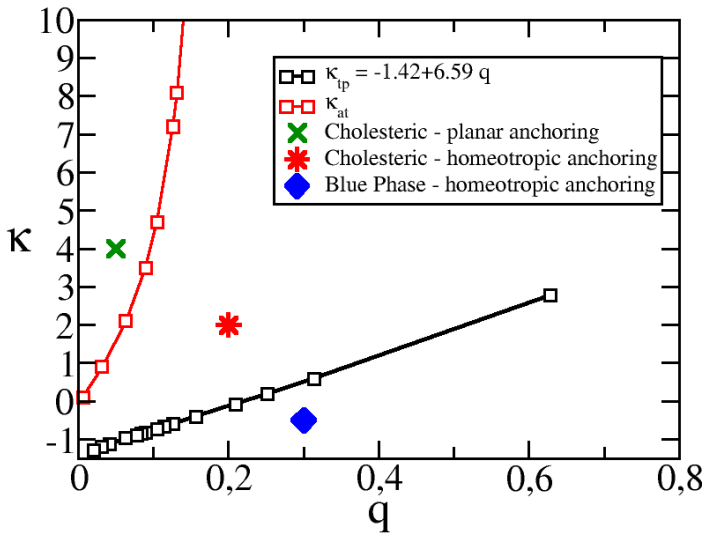

Fig. 5.2: Following the coexistence temperature $\tau(\kappa, P)$: (green cross) C-I interface with planar anchoring, $\kappa > \kappa_c$; (red line) Anchoring transition of between planar and homeotropic anchoring of a C-I interface, $\kappa = \kappa_{at}$; (red star) C-I interface with homeotropic anchoring, $\kappa_c > \kappa > \kappa_{tp}$; (black line) Triple phase coexistence of the isotropic, cholesteric and blue phase with homeotropic anchoring, $\kappa = \kappa_{tp}$; (blue diamond) BP-I interface with homeotropic anchoring $\kappa_{tp} > \kappa$.

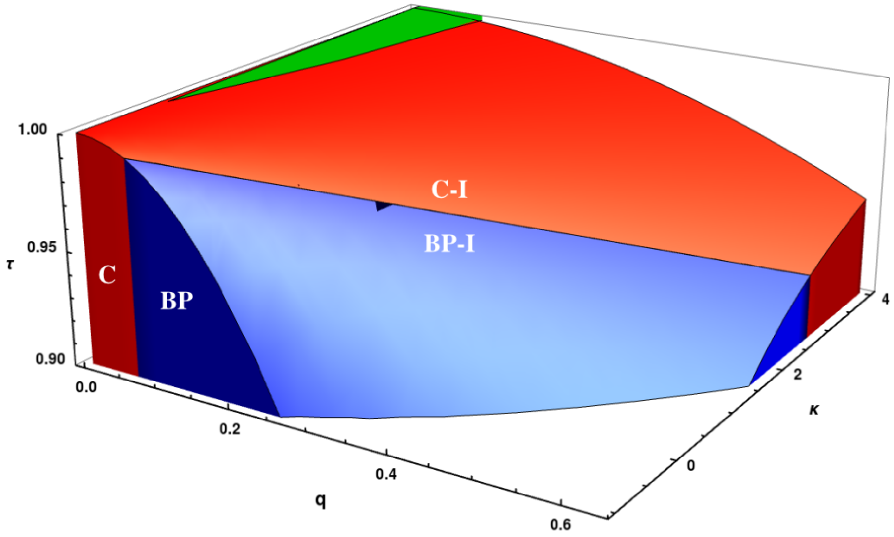

Fig. 5.3: Coexistence is obtained at the diagram surface: (green surface) C-I interface with planar anchoring; (red surface) C-I interface with homeotropic anchoring; (red-blue line surface) BP-C-I coexistence; (blue surface) BP-I interface with homeotropic anchoring; (red-green interior) cholesteric phase; (blue interior) blue phase; (above the surface) isotropic phase. This representation used a coexistence temperature that neglect biaxial symmetry, with τ of Eq.4.3

These results are obtained under the imposition that splay and bend deformations contribute with the same weight to the overall energetic penalties, i.e, the two constant approximation. This imposition manifests in an almost perfect hexagonal defect lattice caused by the balance between bend and splay contributions in the *double-twist* cells, This raises the suspicion that if a three constant approximation was used a different defect lattice would result, given that the equilibrium blue phase would depend on the balance between the three elastic constants. For the same pitch values it would, for example exhibit a distorted honeycomb lattice or even possibly another defect lattice, like the square lattice encountered in the blue phase II with $s = -1$ defects [12]. If this is indeed the case, the phase diagram of Fig.5.2 regarding the elastic properties and chirality will certainly be different, as will the interfacial properties.

5.2 Blue Phase - Isotropic Interface

To obtain the BP-I interface, the quenching process described before is applied to a C-I system in order to observe a phase transition to the BP-I coexistence. The interface is then studies along the κ_{tp} line. Depending on the initial cholesteric orientation at the interface two BP-I are found. For cholesteric layers perpendicular to the free surface the resulting BP configuration has a *zig-zag* arrangement of the *double-twist* cells at the interface, as in Fig.5.4 (a), while for parallel cholesteric layers the resulting configuration has a *linear* arrangement of cells at the interface, as in Fig.5.4 (b).

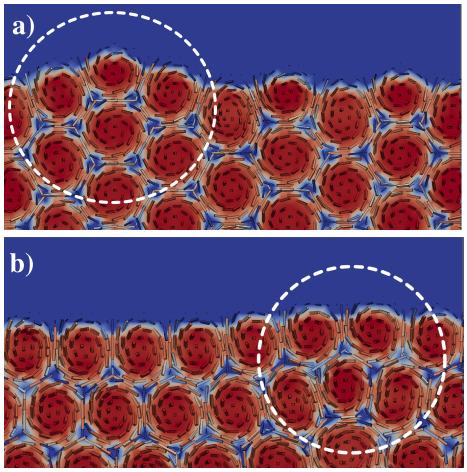

Fig. 5.4: BP-I interface for a BP with $P = 30$ and $\kappa = -0.083$ with: a) zig-zag configuration; b) linear configuration. Red regions correspond to ordered regions with red bars oriented along z and blue bars oriented in the $x - y$ plane, while blue regions correspond to disordered regions. The top region is the isotropic phase and the bottom the BP. Irregularities of the interface double twist cell arrangement can be observed inside the white circles.

Even though the quenching process is a suitable method to locate the phase transition from the cholesteric to the blue phase and to obtain the interfaces, there is a major flaw in the method. As seen in Fig.5.4, both interfacial configurations exhibit irregularities, either dislocated Fig.5.4(a) or deformed *double-twist* cells Fig.5.4(b). These irregularities, or symmetry violations, can only be eliminated by running simulations with very long relaxation times, which of course, for practical purposes is inefficient. To avoid this and to ditch the rather time consuming relaxation and quenching process and to obtain the symmetry of the system, the following ansatz for a BP bulk configuration with a honeycomb defect lattice was proposed for the initial configuration,

$$\begin{aligned}
q_1^{init} &= -\frac{3}{2}\cos(\tilde{q}x) \times \cos(\tilde{q}\sqrt{3}y) \\
q_2^{init} &= -\frac{\sqrt{3}}{2}\sin(\tilde{q}x) \times \sin(\tilde{q}\sqrt{3}y) \\
q_3^{init} &= \sqrt{3}\cos(\tilde{q}x) \times \sin(\tilde{q}\sqrt{3}y) \\
q_4^{init} &= -\cos(\tilde{q}2x) - \frac{1}{2}\cos(\tilde{q}x) \times \cos(\tilde{q}\sqrt{3}y) \\
q_5^{init} &= -\sin(\tilde{q}2x) - \sin(\tilde{q}x) \times \cos(\tilde{q}\sqrt{3}y)
\end{aligned} \tag{5.1}$$

in which $\tilde{q} = 2\pi/\tilde{P}$ is the blue phase effective chirality and $\tilde{P} = \sqrt{2}P$ the distance between neighbouring *double-twist* cell centers, or simply, the effective pitch, since the ansatz corresponds to honeycomb lattice. This ansatz sets the linear configuration parallel to the y direction and the zig-zag configuration parallel to the x direction. The resulting interfaces can be observed in Fig.5.5.

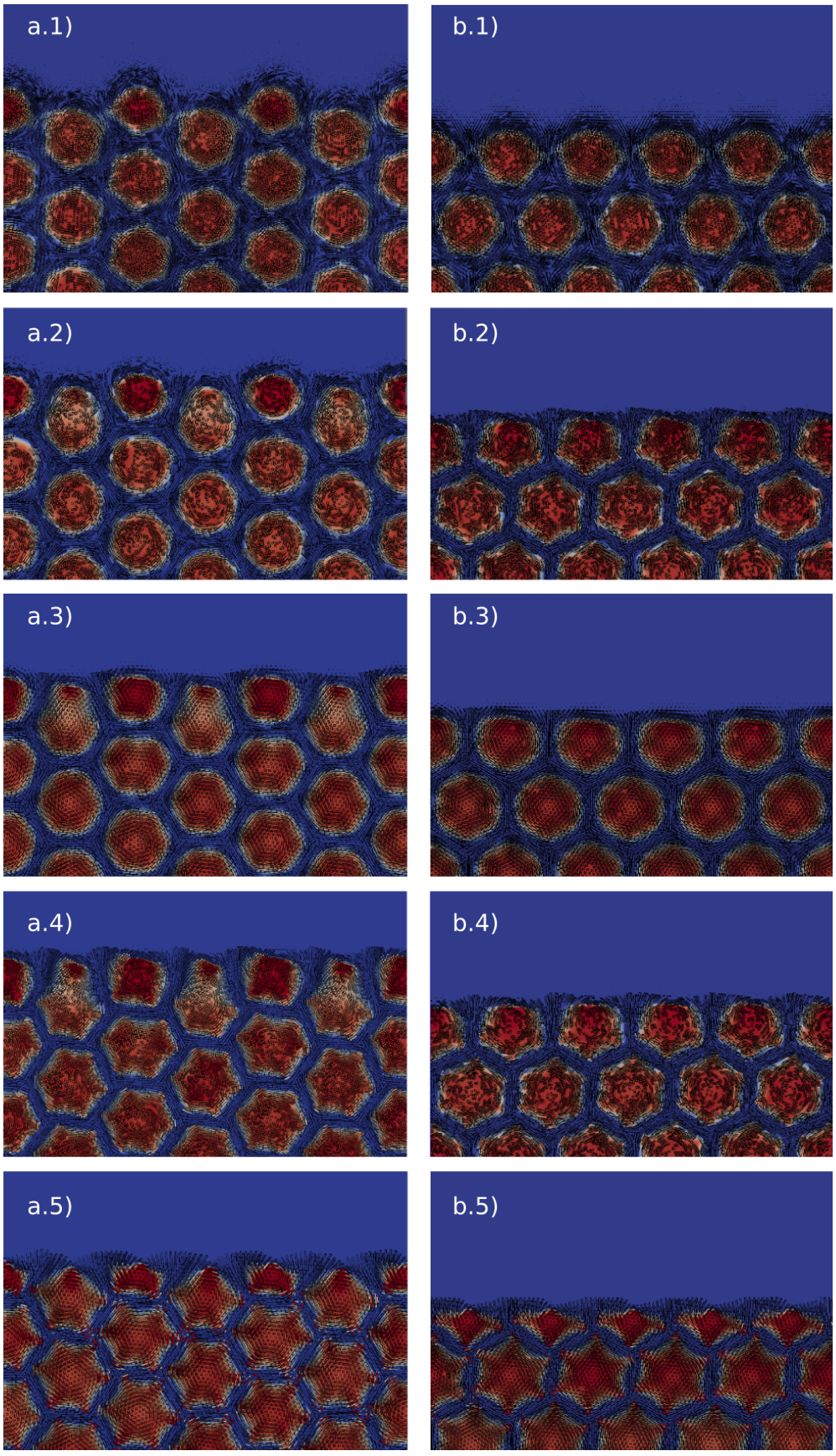

Fig. 5.5: BP-I interface for the zig-zag (a) and the linear (b) configurations for (.1) $P = 10\xi$, (.2) $P = 30\xi$, (.3) $P = 50\xi$, (.4) $P = 100\xi$ and (.5) $P = 300\xi$. For both configurations, the *double-twist* cells at the surface deform until they reach their final equilibrium configuration. In the *zig-zag* configuration the outer cells have in deformations while the inner cells have out deformations while in the *linear* configuration the cells have only in deformations. Furthermore it is possible to see that there is a shift in undulations phases, for (.1), (.2), (.3) elevations occur over the *double-twist* cores and for (.4) and (.5) elevations occur between *double-twist* cores. This shift marks an anchoring transition.

The surface tension, γ, is measured for different pitch values and corresponds to the domain total free energy divided by the length of the interface, since only the interfacial region corresponds to non-zero free energy values. The following values were obtained with a numerical precision of about 2%. It can be seen from Fig.5.6 that the surface tension of the *zig-zag* configuration has lower values than its counterpart, which means that it is the stable BP-I configuration. Nevertheless, in this pitch range, the surface tension has the same (quantitative) dependence on the pitch as the *linear* configuration. Both surface tensions exhibit an approximate logarithmic growth with the pitch. Given that defect interactions follow a logarithmic behaviour with the distance between them and given that in the honeycomb defect lattice the distance between defects scales with pitch, it is suggestive to say that the surface tension behaviour is associated with defect interactions. However, this statement has not been proved. Comparing the BP-I and C-I surface tensions it is possible to see that there is a marked difference over the triple line, with the C-I having much higher values. This is simply the mark of the first order phase transition between the cholesteric and the blue phase.

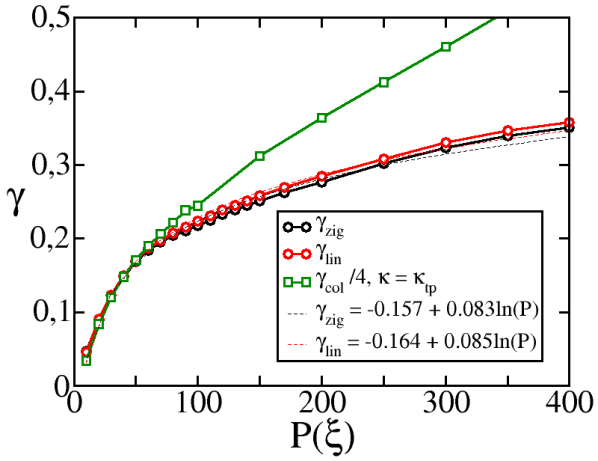

Fig. 5.6: Surface tension of the BP-I *zig-zag* (black line) and *linear* (red line) configurations and of the C-I interface (green line) at the triple line.

The interface undulations amplitude and roughness are measured on the interface line with $S = 0.5$. The undulations amplitude, A, is simply defined as the difference between the highest and lowest points of the surface and the roughness, r is defined as the amplitude divided by distance between high or low peaks, h. For a system with undistorted cells, for the *linear* configuration this corresponds to $A_{lin} = \sqrt{6}P/12$, $h_{lin} = P/\sqrt{2}$ and $r_{lin} = 1/\sqrt{12}$ and for the *zig-zag* configuration corresponds to $A_{zig} = \sqrt{2}P/4$, $h_{zig} = \sqrt{3}P/\sqrt{2}$ and $r_{zig} = 1/\sqrt{12}$, considering that the radius of a non-deformed *double-twist* core is $R = \sqrt{2}P/4$. For the C-I interface the roughness is $r_{col} = 2A/P$.

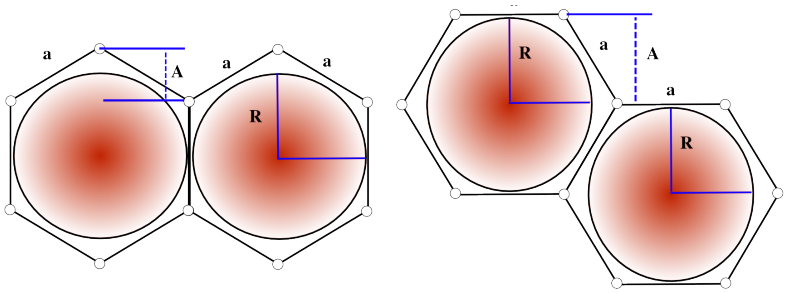

Fig. 5.7: Schematic representation of the BP-I interface for the *linear* (left) and *zig-zag* (right) configurations with non-deformed *double-twist* cores. With $\tilde{P} = \sqrt{2}P$, $a = P/\sqrt{6}$ and $R = \sqrt{2}P/4$ the undulations amplitudes are $A_{lin} = \sqrt{6}P/12$ and $A_{zig} = \sqrt{2}P/4$ for the *linear* and *zig-zag* configurations, respectively.

From the amplitude relation described above, it is possible to understand that regardless of the pitch the undulations amplitude of the *zig-zag* configuration are higher than those of the *linear* configuration. Having in consideration that the mechanisms that induce the cell deformations are equal in the two configurations, allowing the honeycomb lattice to deform, too, the interface undulations amplitude with deformed cells of the *zig-zag* configuration is higher than that of the *linear* configuration. This argument is supported by the numerical values obtained from Fig.5.8 (a). This is also in agreement with the fact the surface tension of the *linear* is higher than its counterpart, considering that the roughness should follow some inverse relation with the surface tension.

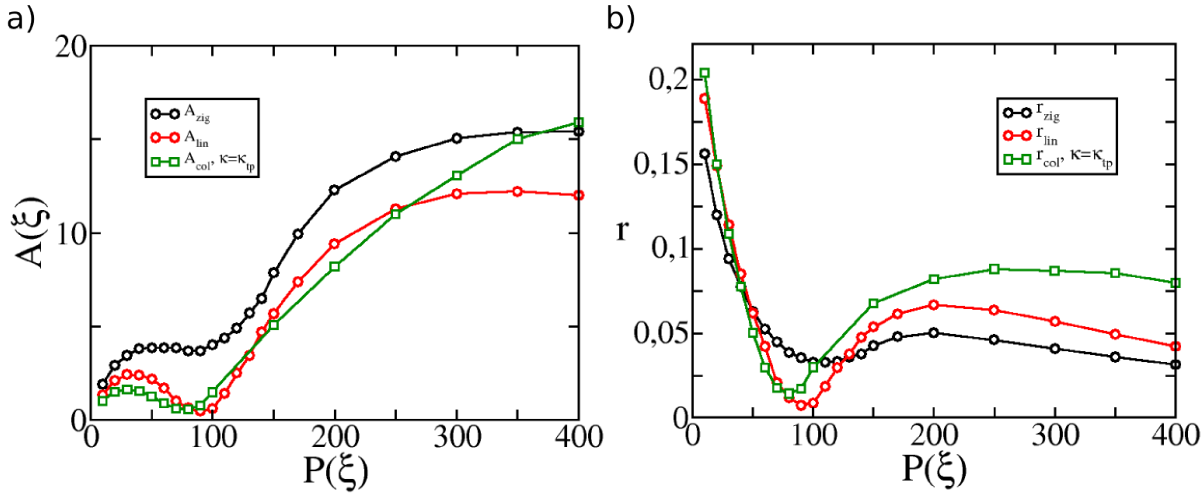

Fig. 5.8: Over the triple phase line: a) Undulations amplitude of the BP-I interfacial *zig-zag* (black line) and *linear* configurations (red line) and of the C-I interface (green line), where two regimes can be distinguished for low and high pitch; b) roughness profile of the BP-I interfacial *zig-zag* (black line) and *linear* (red line) configurations and of the C-I interface (green line), where two regimes can be distinguished for low and high pitch. Both A and r have minimum around $P_u \sim 90\xi$. For low pitch $A_{zig/lin} \sim (P - P_u)^2 P$ and $r_{zig/lin} \sim (P - P_u)^2$ and for high pitch the roughness has a roughly linear decrease with the pitch.

It can be observed in Fig.5.5 that the elevations in the interface undulations shift from being over the *double-twist* cores with the director field parallel to the interface at low pitch, to being between *double-twist* cores, with the director field perpendicular to the interface at high pitch, passing through a pitch where the interface is approximately flat, around $P \sim 100\xi$. Thus, the system goes from a state with planar anchoring to a state with homeotropic anchoring passing through an anchoring transition around $P \sim 100\xi$. The numerics of Fig.5.8, provide a quantitative demonstration of the phenomena observed in Fig.5.5. Both configurations exhibit a roughness transition at a pitch value defined as the *transition point*, P_u, that is clearly somewhere around $P_u \sim 90\xi$, close to the pitch where the interface was approximately flat in Fig.5.5. This is where the anchoring transition occurs. The behaviour with pitch of the amplitude and roughness is $A_{zig/lin} \sim (P - P_u)^2 P$ and $r_{zig/lin} \sim (P - P_u)^2$ for low pitch and for high pitch the roughness has a roughly linear decrease with the pitch. Furthermore, over the triple phase line this roughness transition behaviour is observed not only at the BP-I interface but also at the C-I interface, thus indicating that the mechanisms responsible for the anchoring and the consequent roughness transition are a common feature of chiral nematics. The intefacial behaviour can be understood from our qualitative and quantitative results but it is still unclear why the anchoring transition occurs and why it does so at $P_u \sim 90\xi$.

Even though the cholesteric and the blue phase are distinct phases separated by a first order phase transition, with a marked difference in surface tension when coexisting with the isotropic phase as shown in Fig.5.6, the mechanisms responsible for the creation of surface undulations are the same. The smaller the pitch the higher the orientational frustrations. To eliminate them, defects are nucleated. Near an

interface, these defects can be further eliminated by deforming the surface and creating undulations. The main difference between the two phases is that orientational frustrations in BPs are present not only at surfaces but also in the bulk, manifesting themselves in orientational *double-twist* and in the subsequent honeycomb defect lattice. In cholesterics, orientational frustrations are only present at the interface. Having this in consideration, in the BP-I interface it is also expected to observe a decreasing roughness at higher pitches as in the C-I interface. This statement is supported by the numerical values obtained for the roughness profiles at high pitch in Fig.5.8 (b), where the roughness of the C-I interface over and above the triple phase coexistence line (region around the red star in Fig.5.2) is $r_{C-I}(\kappa = \kappa_{tp}) \sim -P$ while the roughness of the BP-I interface over the triple line is $r_{BP-I}(\kappa_{tp}) \sim -P$, regardless of the configuration. Thus, the C-I and the BP-I roughnesses are decreasing functions of the pitch and go to zero in the nematic limit.

Furthermore, it is possible to see that over the triple line the BP-I interface and the C-I interface roughness lines intercept. So, despite being different phases and despite being separated by a first order phase transition, this interception leads to the staggering result of having a continuous interface undulation profile between different ordered phases of chiral nematics over the triple phase coexistence line. Besides the conceptual insight of this result on chiral nematics rough interfaces, this might represent a major new feature of chiral nematics for application purposes. For example, it can in principle be possible to create a system in which the isotropic and a chiral nematic ordered phase coexist and have an interface with a given fixed roughness an anchoring, that allows to change the ordered phase bulk properties, from those of a layered cholesteric to those of defect honeycomb lattice of a blue phase. Even though a sample that follows the two-constant approximation can in principle exhibit such behaviour according to the LdG model, there is no way to say if the same would be observed for other approximations. Nevertheless, lets us speculate that C-I and the BP-I interfaces roughness profiles did indeed intercept at the triple coexistence for samples that follow relations between the elastic constants other than the two constant approximation. Being able to control the temperature, the pitch and the elastic constants of the sample would provide the control of the set of parameters at which this interception occurs. This means that it would be possible to have a dynamic control of the bulk and roughness and anchoring properties. Once again, this motivates the study of this system with no elastic constant degeneracy.

Still, what was presented so far does not answer why the roughness behaves like it does, or how it is related with the surface tension. In some way, the LdG model ends up telling how the system will be for a certain set of parameters, but not why. As usual, the Frank-Oseen model can be used to obtain further insight, in this case, on the relation between the interface undulated profile and the surface tension.

A first approach is to consider that when a phase is at equilibrium any energetic penalty comes from the perturbation of its equilibrium orientational profile. In a coexistence system such perturbations occur at the interface and therefore, energetic penalties are represented by the surface tension. In the case of the blue-phase, the equilibrium orientational profile corresponds to the honeycomb lattice of defects and *double-twist* cores and any perturbation of this structure corresponds to an energetic penalty. This can be due to the variation of the defect density per cell, *double-twist* cores deformations, or both. Looking at Fig.5.5, it is possible to see that deformations of the honeycomb lattice only occur close to the interface, meaning that only the surface cells will be associated with energetic contributions. Thus, the surface tension is simply the sum of these contributions. To accurately describe the deformations observed in Fig.5.5, an elliptic approximation of the cells deformation close to the surface, with chirality changing accordingly, is presented in Fig.5.9 for the *linear* and *zig-zag* configurations. From this representation it is possible to see that only the top half part of the cells needs to be considered in the *linear* configuration, since the lower part is non-deformed, while one top half and a full cell are deformed in the the *zig-zag*

configuration. The relative cell deformation amplitude is d and the core radius $R = \sqrt{2}P/4$.

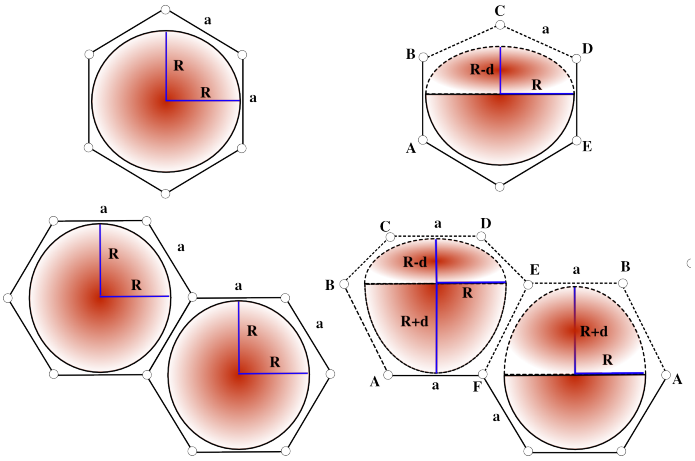

Fig. 5.9: Schematic representation of surface *double-twist* cells of a linear (top) and zig-zag (bottom) configuration at a BP-I interface, with deformations approximated by ellipses. The red regions represent the *double-twist* cores, with $R = \sqrt{2}/4$ the non-deformed core radius, d the relative deformation amplitude, $R(1-d)$ the deformed core radius and $a = \sqrt{6}P/6$ the distance between defects.

Recalling from Sec.2.4, the energy associated with a *double-twist* core can be written with respect to a director field in cylindrical coordinates as [45],

$$F_c = \int_0^{2\pi} d\theta \int_0^R r \left[\frac{1}{2} K_2 \left(q - q_0 + \frac{1}{r} \sin(qr)\cos(qr) \right)^2 + \frac{1}{2} K_3 \left(\frac{\sin^2(qr)}{r} \right)^2 \right] dr \tag{5.2}$$

with translational invariance along z in which molecules rotate helically in all directions perpendicular to the orientation of the core center, $n_r = 0$, $n_\phi = \sin(\psi(r))$, $n_z = \cos(\psi(r))$, $\psi(r) = qr$, q the *double-twist* phase chirality, q_0 the cholesteric chirality, R the radius of the non-deformed core and r the distance from the core centre. Notice that the *saddle-splay* is omitted since non-polarity is always considered, even at the surface.

In order to make a quantitative comparison with the energetic penalties associated with deformations of this *double-twist* core and the surface tension obtained with the two constant-approximation LdG model, this expression needs to be rescaled. To do so the same rescaling factor associated to the distortion term of the LdG free energy (Appendix C) is applied to the Frank-Oseen free energy. Thus, with $\alpha = \xi^3 B^4/3^6 C^3$, $\beta = 2B/9C$, $r = \tilde{r}\xi$, the rescaled Frank-Oseen free energy density reads,

$$\begin{aligned} \frac{\alpha}{\xi^3}\tilde{f}_c &= \frac{\beta^2}{\xi^2}\left[\frac{1}{2} K_2 \left(\tilde{q} - \tilde{q}_0 + \frac{1}{\tilde{r}} \sin(\tilde{q}\tilde{r})\cos(\tilde{q}\tilde{r}) \right)^2 + \frac{1}{2} K_3 \left(\frac{\sin^2(\tilde{q}\tilde{r})}{\tilde{r}} \right)^2 \right] \\ \Leftrightarrow \tilde{f}_c &= \frac{18C}{B^2\xi}\left[K_2 \left(\tilde{q} - \tilde{q}_0 + \frac{1}{\tilde{r}} \sin(\tilde{q}\tilde{r})\cos(\tilde{q}\tilde{r}) \right)^2 + K_3 \left(\frac{\sin^2(\tilde{q}\tilde{r})}{\tilde{r}} \right)^2 \right] \end{aligned} \tag{5.3}$$

With $\xi^2 = \frac{18C(3+2\kappa)L_1}{B^2}$, $L_1 = \frac{2K_2}{9\tilde{S}^2}$ and $\tilde{S} = 1$, it becomes,

$$\tilde{f}_c = \frac{9}{2}\frac{1}{(3+2\kappa)}\left[\left(\tilde{q} - \tilde{q}_0 + \frac{1}{\tilde{r}} \sin(\tilde{q}\tilde{r})\cos(\tilde{q}\tilde{r}) \right)^2 + \frac{1}{2}(\kappa+2) \left(\frac{\sin^2(\tilde{q}\tilde{r})}{\tilde{r}} \right)^2 \right] \tag{5.4}$$

The energetic penalties associated with the deformation of *double-twist* cores can thus be computed by relating the free energy density of a non-deformed cell core, F_c^0, assumed to be the reference free energy, with that of a deformed cell core, $F_c^{\pm}$, with relative chirality deformation equal to the relative

amplitude deformation, $d^{\pm}$, in which $\pm$ denotes if the deformation is out of or in to the *double-twist* core. With $r^{\pm} = r\sqrt{\cos^2(\theta) + (1 \pm d)^2 \sin^2(\theta)}$ the radius of an elliptic *double-twist* core and $q^{\pm} = q/\sqrt{\cos^2(\theta) + (1 \pm d)^2 \sin^2(\theta)}$ the chirality of the an elliptic *double-twist* core, the total free energy of the core deformations in the *linear* configuration, for different relative amplitude deformations and pitch values, is given by,

$$F_c^{lin} = F_c^{-} - F_c^{0} = \int_0^{2\pi} \int_0^{R} r(1-d) f(r^{-}, q^{-}) d\theta dr - \int_0^{2\pi} \int_0^{R} r f(r, q) d\theta dr. \tag{5.5}$$

For simplicity only the calculation for the *linear* configuration is presented, having in consideration that the same qualitative results can be extracted for the *zig-zag* configuration. As for the energetic penalties associated with defects, since at the surface the orientational frustrations that originate them are absent, their contributions are not present.

The surface tension is calculated by dividing the free energy for different sets of P and d by the system length, in the linear configuration $2R$, such that $\gamma_c = \sqrt{2} F_c^{lin}(P, d)/P$. The results are shown in Fig.5.10 (a), where it is clear that regardless of the pitch, small deformations are associated to small energetic penalties while high deformations are associated to high energetic penalties. Nevertheless, with this approach it is only possible to obtain the surface tension that would be expected for a set of P and d, instead of the set that corresponds to the equilibrium interface. Nevertheless, it is possible to extract the set of P and d of the equilibrium interface, from the interception between the curves of the Frank-Oseen model with the surface tension of the LdG model, as in Fig.5.10 (a). Thus, the equilibrium sets of P and d are obtained when $\gamma_{LdG}(P) = \gamma_{FO}(P, d)$. Consequently it is also possible to obtain the roughness profile of the equilibrium interface from undistorted *double-twist* cores, such that $r_{eq} = \frac{\sqrt{6}P(1-d_{eq})}{12}$ as in Fig.5.10 (b).

Even though this is a suggestive approach for the problem it does not add any new information on the relation between the undulations amplitude or roughness and the surface tension. However, the roughness obtained here does have a similar qualitative behaviour with the one obtained previously, with the exception that it leaves out the minimum around $P_u \sim 90\xi$. This minimum was previously attributed to the anchoring transition. In contrast, here we do not consider any anchoring features, nor their influence on the free energy density. Thus, this approach is useful in that it indirectly stated that the minimum observed for the undulations amplitude and roughness are indeed due to anchoring features. So, with further corrections and considerations, following Frank-Ossen approach it might be possible to extract further information on the BP-I interface behaviour.

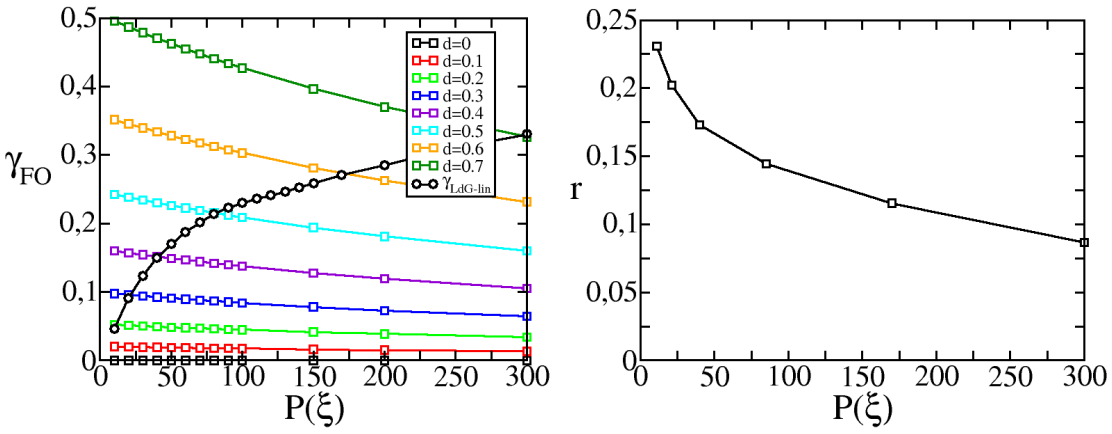

Fig. 5.10: (a) Comparison between the BP-I interface surface tension with the LdG model and the Frank-Oseen approach. The interception between γ_{LdG} and the γ_{FO} curves for the different relative amplitude deformations corresponds to the equilibrium relative amplitude deformation, d_{eq}. (b) Roughness of the BP-I interface with $r = \sqrt{6}P(1 - d_{eq})/12$.

5.3 Blue Phase - Cholesteric Interface

To conclude the study on the triple phase coexistence, the BP-C coexistence is explored, using the same initializing ansatz for the blue phase configuration as in the BP-I coexistence, for P and κ values over the triple phase coexistence line.

Given the relation between the orientational periodicity of the cholesteric and blue phase, $\tilde{P} \simeq \sqrt{2}P$, it is expected that near the free surface both phases exhibit deformations. These deformations can however be minimized when the projection of the periodicity of one phase coincides with the periodicity of the other at the interface. Since a BP interface can only have two configurations, *zig-zag* or *linear*, it is up to the cholesteric to re-arrange to minimize the interfacial deformations. For that purpose one extra parameter is considered, the angle of the cholesteric layers, α. For clarity let us define that, if the cholesteric twist axis is parallel to the interface and the layers are perpendicular to the surface, $\alpha = \pi/2$, and if the twist axis is perpendicular to the interface and the layers are parallel to the interface, $\alpha = 0$.

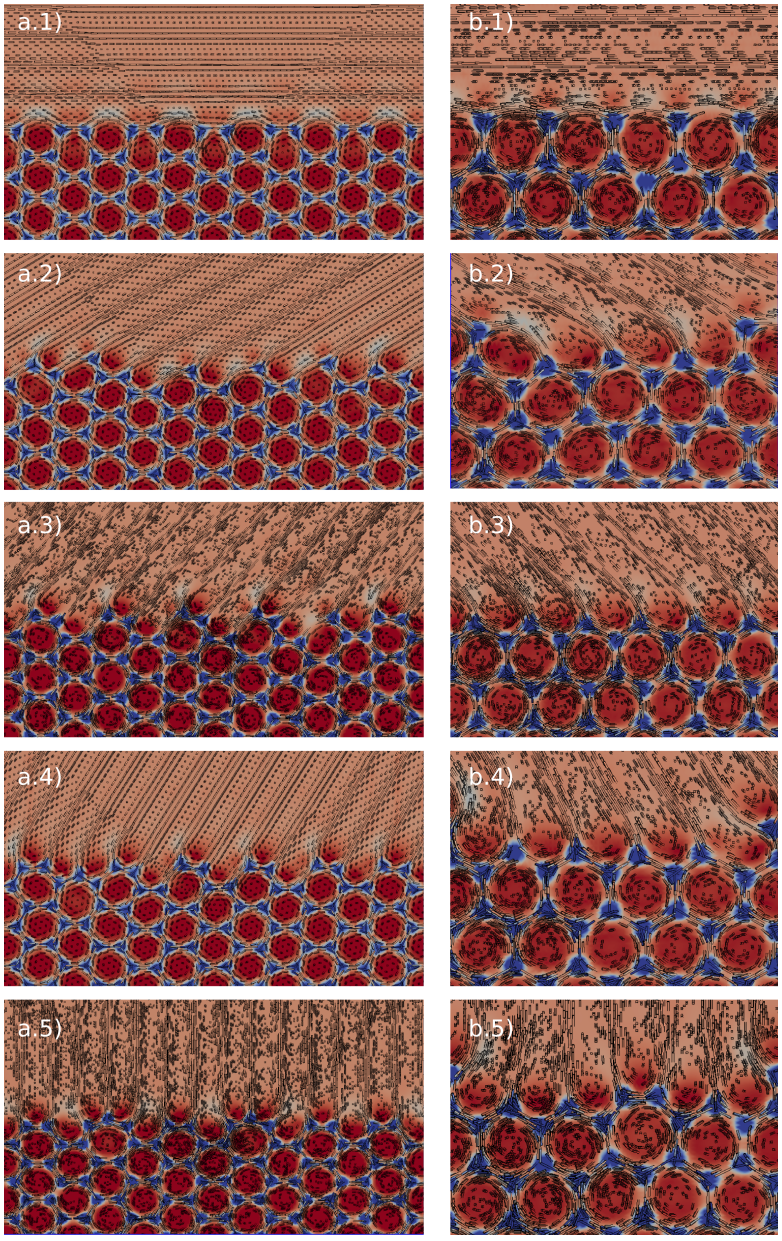

Fig. 5.11: BP-C interface with *zig-zag* (a) and *linear*(b) configurations for $P = 30\xi$ and cholesteric angles of (.1) $\alpha = 0$, (.2) $\alpha = \pi/6$, (.3) $\alpha = \pi/4$, (.4) $\alpha = \pi/3$ and (.5) $\alpha = \pi/2$.

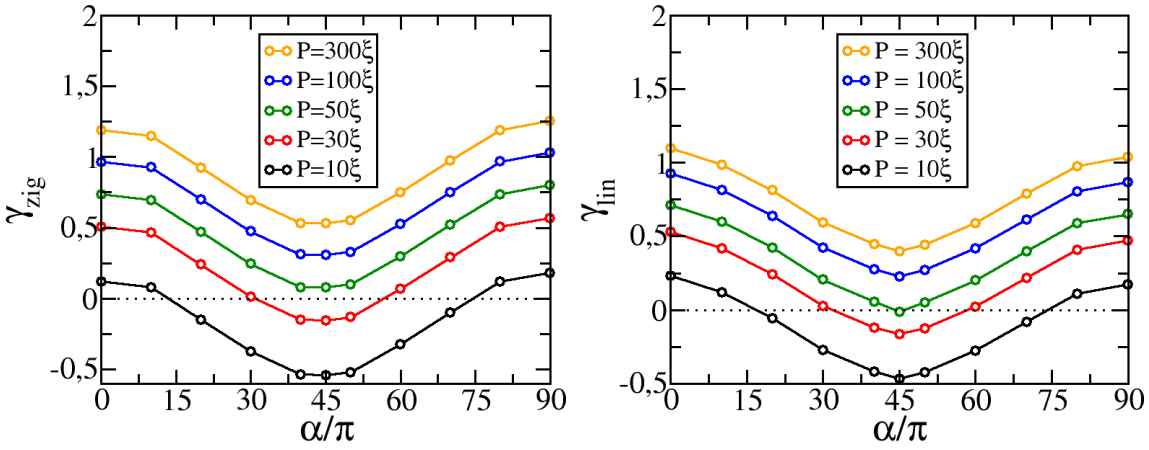

Fig. 5.12: BP-C surface tension as a function of the cholesteric layers angle α of the zig-zag (left) and linear (right) configuration and: $P = 10\xi$ (black), $P = 30\xi$ (red), $P = 50\xi$ (green), $P = 100\xi$ (blue) and $P = 300\xi$ (orange).

As expected, for different cholesteric layer angles, different deformations are observed at the BP-C interface, both in the cholesteric and the blue phase. For angles at which orientational frustrations are high, dislocations of *double-twist* cells near the surface may occur. This can be observed in Fig.5.11 for the *zig-zag* and *linear* configurations, respectively, where the deformations grow as the layer angle drifts away from around $\pi/4$, with the lowest density of defects per *double-twist* surface cell at $\alpha = 0$ and the highest at $\alpha = \pi/2$. These qualitative observations are supported by the surface tension of Fig.5.12, obtained with a numerical precision of about 5% inside a sub-domain of the system. Regardless of the pitch values both configurations have maximal surface tension at $\alpha = 0$ and $\alpha = \pi/2$, where the interface is most deformed, and minimal surface tension at $\alpha \simeq \pi/4$, where the interface is not deformed. Nevertheless, this does not explain why such minimum is observed at $\alpha = \pi/4$ regardless of the pitch value. It must be underlined that regardless of the cholesteric layers, due to the mismatch between the two phases periodicities and the domain size, elastic penalties will always be present at the system boundaries. The weight of such penalties is of course reduced the smaller the dimension of the sub-domain is with respect to the system dimensions and is ideally zero when the system is infinite. But since our systems are finite, residues of these penalties are always projected upon our results given that the system is never really unconstrained, which makes it rather difficult to have a trustworthy interpretation of the numerical results. Nevertheless, such elastic penalties are of course minimized is when at least the cholesteric and the blue phase orientational periodicities projection match, which depends on the layers angle.

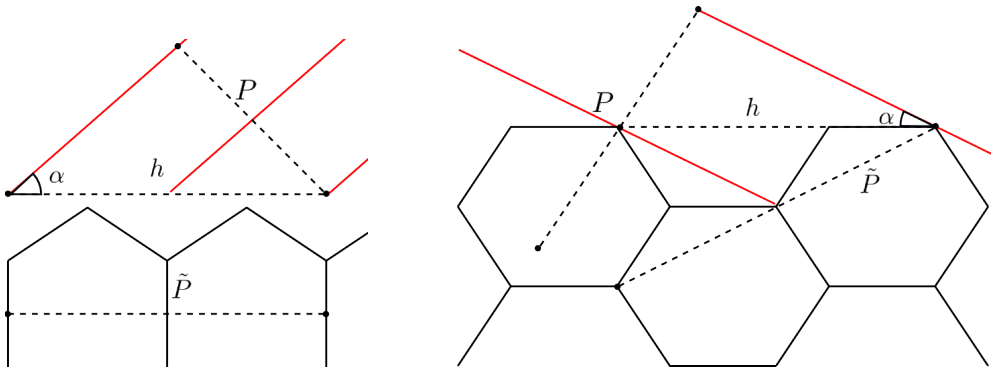

Fig. 5.13: Schematic BP-C interface representation of a linear (left) and a zig-zag (right) configuration. $\tilde{P} = \sqrt{2}P$ is the relation between the two periodicities at which the minimal surface (excess) free energy is observed, with $P/2$ the distance between consecutive cholesteric layers and $\tilde{P}/2$ the distance between nearest core centres.

To understand why $\alpha = \pi/4$ is the angle at which the minimal deformations are observed, let us construct a simple geometric argument based on BP-C representation of Fig.5.13. The idea is that the angle at which the surface tension is minimal corresponds to one in which the projection of the cholesteric periodicity into the surface is equal to that of the blue phase axis projection into the surface. The cholesteric orientational periodicity projection is written as $h_C = P/\sin(\alpha)$, while the the blue phase axis projection is written as $h_{lin} = \tilde{P}$ and $h_{zig} = \sqrt{3}\tilde{P}/2$, for the *linear* and the *zig-zag* configurations, respectively. Thus, considering the case for which $h_C = h_{lin}$ and $h_C = h_{zig}$, it results that $\alpha_{lin} = 45^o$ and $\alpha_{zig} = 54.75^o$ for the *linear* and *zig-zag* configurations, respectively. Using α_{lin} in h_C gives $h_{lin} = \sqrt{2}P$. Recalling from Sec.5.1, for the linear configuration this corresponds to the relation between the cholesteric and the blue phase periodicities at the phase transition, $\tilde{P} \simeq \sqrt{2}P$. However, using α_{zig} in h_C gives $h_{zig} = \sqrt{3}P/\sqrt{2}$, which goes outside the numerical precision of our results and does not correspond to the relation obtained in Sec.5.1. Thus, even though this argument is not fully consistent for the angle at which the surface tension is minimal in Fig.5.12 and the angle at which the projection of the phases periodicity is equal, it nevertheless suggests that the minimal surface tension of the BP-C interface is strongly dependent on the relation between the cholesteric and the blue phase periodicities.

Thus, a generalized form for the equilibrium angle of the cholesteric layers at BP-C interface is proposed to be as $\alpha_0 = \arcsin(\delta)$, with δ the relation between P and $\tilde{P}$. This relation is of course modified if the blue phase does not have a honeycomb deffect lattice, which may occur when the ratio between the splay and bend elastic constants is modified. To explore such scenario, the LdG free energy functional requires a higher order expansion of the tensor order parameter spatial distortion to allow the consideration of a three-constant approximation. This, however, implies that the pitch is temperature dependent [12]. This is not explored in this work, but is left as an open challenge.

At $\alpha = \pi/4$ the two periodicities match and deformations in each of the two phases equilibrium configuration are minimal. The elastic frustrations that require the presence of $s = -1/2$ defects in the honeycomb lattice are present at the interface, which means the the *double-twist* core is not deformed, and the cholesteric layers end up in positions corresponding to the cells of the honeycomb lattice. Thus, the equilibrium surface tension can be measured as a function of the pitch, at $\alpha = \pi/4$, as seen in Fig.5.14.

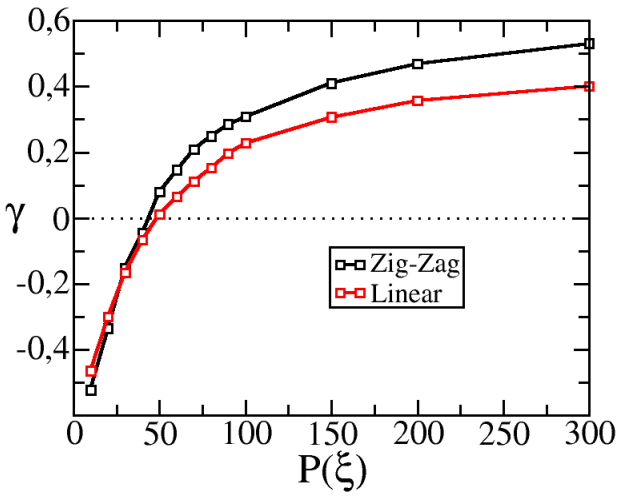

Fig. 5.14: BPI-C surface tension for different pitch values at $\alpha = \pi/4$. For low pitch values the surface tension has negative values, indicating that the system is no longer stable.

As for the surface undulation profile, following Fig.5.6, which corresponds the undistorted honeycomb lattice obtained for $\alpha = \pi/4$, the undulations amplitude can simply be written as $A_{zig} = \sqrt{2}P/4$ and $A_{lin} = \sqrt{6}P/12$ for the *zig-zag* and *linear* configurations, respectively and the roughness as $r_{zig} = 1/\sqrt{12}$ and $r_{lin} = 1/\sqrt{12}$, respectively

There are two major aspects to notice on the surface tension of this interface. The first is that the *linear* configuration has lower values than the *zig-zag* configuration, by contrast to what is observed at the BP-I interface. The main difference between the two interfaces is that in the BP-C orientational frustrations and consequently defects are present at the interface, contrary to what happens in the BP-I. Thus, apart from the fact that at the equilibrium layers' angle there are no deformations of either the *double-twist* cores and cholesteric layers at the interface, the surface tension inversion from the BP-I case should be related with energetic contributions associated with the presence of defects. Indeed the number of surface's defects per h, i.e, the surface defect density n, is higher in the *zig-zag* than in the *linear* configuration, $n_{zig} = \frac{2}{\sqrt{3}} n_{lin}$ and $n_{lin} = \frac{2\sqrt{2}}{P}$ respectively. This is consistent with the initial statement.

The second aspect to notice is that for pitch values below $P \sim 50\xi$ the surface tension is negative. There are two reasons that might explain this. One, as already stated is that the measurement of the surface tension accounts for elastic penalties associated with the periodical mismatches. Another one, considering that these penalties can be neglected and the system is indeed in equilibrium, is that for low pitch the blue phase and the cholesteric can no longer coexist and higher symmetry phase corresponds to the system minimum free energy, i.e, the blue phase II. Following the defect energetic argument introduced in Sec.2.3, this new phase is associated with a square lattice of defects, so an ansatz is proposed considering that the phase pitch is the same as in the blue phase II such that,

$$\begin{aligned}
q_1^{init} &= \frac{3}{2}\sin^2(qy/\sqrt{2}) - \frac{1}{2} \\
q_2^{init} &= \frac{3}{2}\sin(qx/\sqrt{2})\cos(qy/\sqrt{2})\sin(qy/\sqrt{2}) \\
q_3^{init} &= \frac{3}{2}\cos(qx/\sqrt{2})\cos(qy/\sqrt{2})\sin(qy/\sqrt{2}) \\
q_4^{init} &= \frac{3}{2}\sin^2(qx/\sqrt{2})\cos^2(qy/\sqrt{2}) - \frac{1}{2} \\
q_5^{init} &= \frac{3}{2}\cos(qx/\sqrt{2})\sin(qx/\sqrt{2})\cos^2(qy/\sqrt{2})
\end{aligned} \tag{5.6}$$

Still, even from such initial conditions no new stable symmetry was obtained for P and κ over the triple phase line and the honeycomb lattice was obtained again. This result leads to two conclusions. Or the most symmetric state of our system is indeed a honeycomb lattice, which implies that the negative surface tension is originated by the elastic penalties associated with the periodic mismatches of the system. Or, it is the degeneracy between the *splay* and *bend* constants that does not allow a phase transition to a new symmetry, even when elastic penalties so imply, meaning that the negative surface tension is the manifestation of a new free energy minimum that is simply bounded by the model initial conditions. Thus, the reason why the BP-C surface tension is negative for low pitch, when no new symmetry is observed, is left as an open challenge.

Chapter 6

New Results and Discussion for Substrates

Motivated by recent studies of cholesterics confined by flat substrates [38] and by the insight brought to us by the study of BP-I and BP-C interfaces, in which the blue phase acts like a rough substrate, this last chapter is presented as an extension of the work, introducing the new topic of chiral nematics confined by geometric substrates. Here, the attention is focused solely on sawtooth substrates with weak planar anchoring.

6.1 The Cholesteric at a sawtooth substrate

Although a wide range of substrate geometries can be explored, for example crenellated or sinusoidal substrates [35], here the geometry is sawtooth. On one hand because it is similar to the undistorted BP linear interface, which might prove useful in terms of a qualitative comparison between the behaviour of the cholesteric at a substrate and an interface with the same geomeotry. On the other hand, because from all the possible substrate geometries, the sawtooth is one of the simplest, being fully described by two independent parameters, the edge length, L and aperture, θ, thus making it suitable for an introductory study.

At sawtooth substrate confined nematic systems, since there is no intrinsic orientational frustration with an independent length scale, the nematic configuration is controlled entirely by the substrate anchoring orientation, edges aperture θ, length, L and anchoring strength, W. Even though they share the main features of this system, sawtooth substrate confined chiral nematic systems are more complex because there is a natural twist of the director associated to an independent length scale. This implies that there will be a conflict between the two length scales of the system, the dimensions of the substrate and the pitch. Thus, except for the very particular case in which layers are parallel to the surface, orientational frustrations are bound to exist in this system. These frustrations manifest themselves through the creation of topological defects and through the deformation of the cholesteric layers near the surface. Due to these frustrations, the orientational configuration of the cholesteric is not controlled only by the substrate anchoring orientation, aperture θ, length L and anchoring strength W, but also by the cholesteric pitch P and the layers orientation at the surface, α, as can be seen in Fig.6.1 and Fig.6.2. The interest and difficulty of exploring this system lays on how all the parameters relate, which is essential to understand and control the location and frequency at which defects emerge and how cholesteric layers are deformed. Even though confined cholesteric liquid crystal systems are less trivial then confined nematic systems, their wide range of parameters makes them rather versatile, opening the way to more complex and delicate applications.

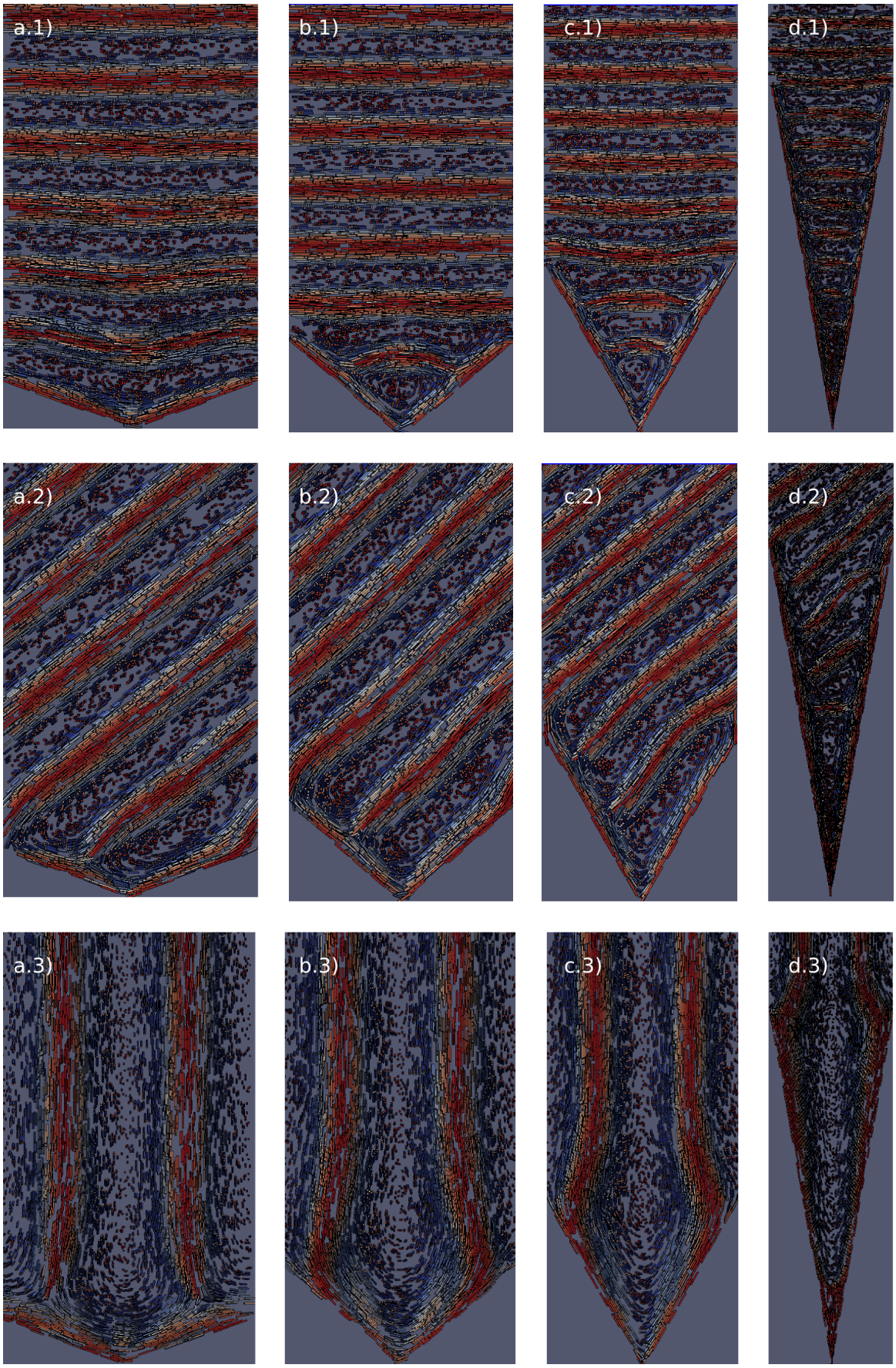

Fig. 6.1: Cholesteric confined by a sawtooth substrate with weak planar anchoring, for cholesteric pitch $P = 100\xi$ with substrate aperture of (a) $\theta = \pi/9$, (b) $\theta = 2\pi/9$, (c) $\theta = 4\pi/9$ and (d) $\theta = \pi/3$ and cholesteric layers angle of (.1) $\alpha = 0$, (.2) $\alpha = 2\pi/9$ and (.3) $\alpha = \pi/2$. The wedge width and length are $T = P/\sin(\alpha)$ and $L = P/2\sin(\alpha)\cos(\theta)$. The red color represents in-plane orientation and blue represents out-of-plane orientation.

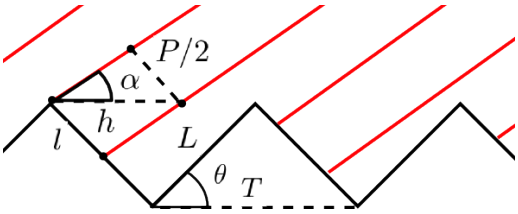

Fig. 6.2: Schematic representation of a cholesteric confined by a sawtooth substrate. α is the cholesteric layers angle, measured from the flat substrate, L is the edge length, θ the edge aperture, $P/2$ the distance between consecutive layers, $T = 2\cos(\theta)/L$ and $l = P\cos(\theta)/2\sin(\alpha)$ the projection of the cholesteric periodicity onto the edge surface.

The system is studied with respect to cholesteric layer angles, α and wedge aperture, θ, with values ranging from 0 to $\pi/2$. The layers angle could effectively be considered for values ranging from 0 and π, but this is redundant since the systems properties are symmetric with respect to $\alpha = \pi/2$. Periodic boundary conditions are imposed along the wedges (one wedge per domain in our simulations), as shown Fig.6.1, and in order to avoid discontinuities regardless of the pitch, layers angle and aperture values, the relation between the cholesteric layers periodicity projection onto the substrate plane, h, and the wedge width, T, are set with the periodic relation $T = 2hc$, with c being an integer. For $c = 1$ the wedge width and length are $T = P/\sin(\alpha)$ and $L = P/2\sin(\alpha)\cos(\theta)$, respectively. Thus, the imposition of the periodic relation $T = 2h$ reduces the system independent parameters to P, α, θ. Defining the substrate roughness as $r = L/T = 1/\cos(\theta)$, means that the roughness is constant for each aperture.

Under these conditions the free energy density is calculated for three pitch values, $P = 50\xi$, $P = 100\xi$ and $P = 200\xi$ with a rescaled elastic constant $\kappa = 2$, surface anchoring strength $W = 10$, and temperature below the coexistence temperature, as shown in Fig.6.3. The excess free energy associated with the presence of defects and cholesteric layer distortions is presented in Fig.6.3 as a function of the layers angle values, for different apertures and pitch values. We found that the free energy behaves as $f \sim P^{-\beta(\alpha,\theta)}$, with $\beta(\alpha,\theta) > 1$ a value that increases with α for $\theta < \pi/4$ and decreases with α for $\theta > \pi/4$.

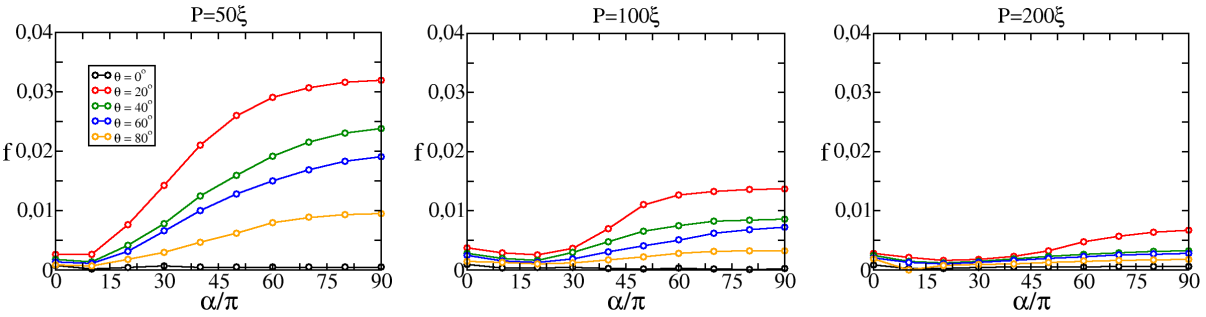

Fig. 6.3: Free energy density of a cholesteric confined by a sawtooth substrate with weak planar anchoring, for pitch values of (left) $P = 50\xi$, (middle) $P = 100\xi$ and (right) $P = 200\xi$, for substrate apertures (black) $\theta = 0$, (red) $\theta = \pi/9$, (green) $\theta = 2\pi/9$, (blue) $\theta = \pi/3$ and (orange) $\theta = 4\pi/9$.

To interpret these results, knowing that the substrate has weak planar anchoring, that the cholesteric preferred anchoring is planar and that a defect is created each time the orientation of the cholesteric does not correspond to that of the surface, a first approach is to follow the basic idea that the the density of defects per wedge surface is proportional to the total free energy density of the system.

At a flat substrate, $\theta = 0$, when the cholesteric layers are perpendicular to the surface, an array of defects separated by a distance equal to the cholesteric layers periodicity, $P/2$ is created near the surface. Tilting the cholesteric layers by an angle α measured from the surface plane, as in Fig. 6.1, increases

the projection of cholesteric periodicity into the surface, h, and the distance between defects increases according to the geometric relation,

$$h = \frac{P}{2}\frac{1}{\sin(\alpha)}. \tag{6.1}$$

This distance diverges as α approaches zero, alongside there is a decrease in the density of defects according to the relation,

$$n = \frac{N}{L} = \frac{1}{h} \tag{6.2}$$

With surface planar anchoring, when the layers are parallel to the surface there are no orientational frustrations and consequently there are no defects. Thus, even though this is a rather basic approach it is clear that these geometric relations are suited to explain the behaviour of the system.

For a sawtooth substrate, $\theta \neq 0$, the overall density of defects can be obtained applying the same relations as in the flat substrate and considering that the periodic conditions impose that a defect at every top corner, the total defect density per wedge is given by,

$$n = \frac{N}{2L}. \tag{6.3}$$

It is also possible to obtain the defect distribution along the edges. With n^- the defect density and l^- the distance between defects in the left edge we find,

$$n^- = \frac{N^-}{L} = \frac{1}{l^-}, \quad l^- = \frac{P}{2}\frac{1}{\sin(\alpha-\theta)}, \tag{6.4}$$

while for the right edge,

$$n^+ = \frac{N^+}{L} = \frac{1}{l^+}, \quad l^+ = \frac{P}{2}\frac{1}{\sin(\alpha+\theta)}. \tag{6.5}$$

Given that the total number of defects per wedge is the sum of the defects, $N = N^- + N^+$, then the total wedge density of defects is,

$$n = \frac{N}{2L} = \frac{1}{P}\big(\sin(\alpha-\theta) + \sin(\alpha+\theta)\big) \propto f_{disc}. \tag{6.6}$$

with free energy density represent in Fig.6.4.

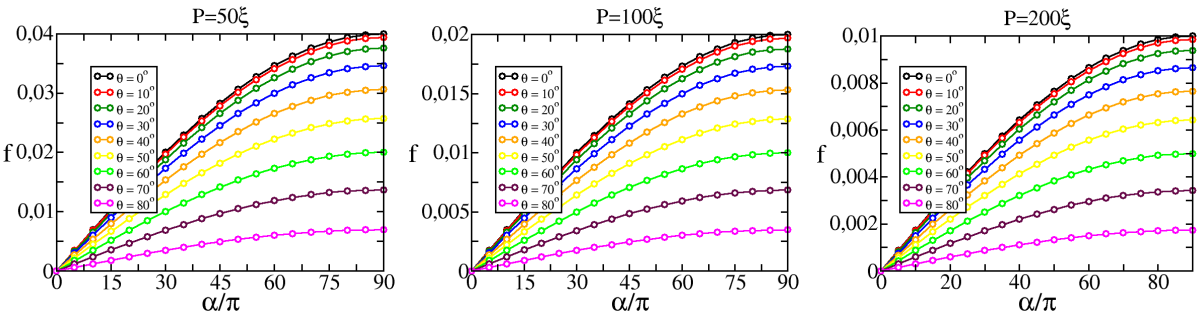

Fig. 6.4: Free energy density of a cholesteric confined by a sawtooth substrate with weak planar anchoring, for cholesteric pitch of (left) $P = 50\xi$, (middle) $P = 100\xi$ and (right) $P = 200\xi$, and substrate apertures represented by the different coloured lines.

From this approach we find that the excess free energy associated with defects has a similar dependence with the layers angle to that observed in the numerical results. Nevertheless the dependency on pitch, it comes that $f_{disc} \sim P^{-1}$, is different from that observed in the numerically. This difference arises from considering the penalties associated to defects only and neglecting those associated with layers deformations.

Considering a BP-C linear interface over the triple line with cholesteric layers angle of $\alpha = \pi/4$, it is possible to observe that the surface *double-twist* cells are undistorted. This means that defects are in their honeycomb equilibrium position, that the radius of the *double-twist* core is proportional to the interface roughness and that around the core, molecules are oriented parallel to the core's center, i.e, are always aligned parallel to the cell's surface. One of the initial assumptions that motivated the study of a sawthooth confined cholesteric with weak planar anchoring was that it would be possible to create an analogy between the behaviour of the cholesteric in this system and the behaviour of the cholesteric in a BP-C linear interface, at least for a substrate aperture of $\theta = \pi/6$. Nevertheless, the results indicate otherwise, since at the BP-C interface for $\theta = \pi/6$ the minimal free energy is observed at $\alpha = \pi/4$, while in a confined cholesteric by substrates aperture with $\theta = \pi/6$ the minimal free energy is observed at $\alpha \simeq \pi/18$. Notice, however, that the chosen set of P and κ values does not correspond to values over the triple phase coexistence line of the BP-C system above $P \sim 50\xi$.

It is possible to see that, even though this is an ultimately simplistic approach to the confined cholesteric behaviour, the results of this geometric construction and those obtained numerically for the rescaled LdG model are in qualitative agreement, with $f \sim 1/P$. This is a good indication that more complex substrates can be qualitatively understood by following a similar geometric approach, providing a simpler and faster method to study the qualitative behaviour of chiral nematics confined by geometric substrates.

Chapter 7

Conclusions

In this work it is observed that at the triple phase coexistence line there is a hyperbolic relation between the two constant approximation LdG rescaled elastic constant and the pitch. Furthermore, it is observed that the 2D blue phase has a honeycomb lattice of defects and that the cholesteric and the blue phase orientational periodicities follow a linear relation, $\tilde{P} \simeq \sqrt{2}P$. An anstaz is proposed for the equilibrium blue phase according to this relation, from which the following results were obtained.

The BP-I interface exhibits two distinct configurations of *double-twist* cell arrangements at the surface, depending on the cholesteric layer's orientation with respect to the interface with the isotropic phase. The configuration can have a *zig-zag* or a *linear* arrangement of the cells, corresponding to a perpendicular and a parallel orientation of the cholesteric layers. Our results agree with previous ones in that the equilibrium BP-I interface corresponds to the *zig-zag* configuration while the equilibrium C-I interface corresponds to one with layers perpendicular to the surface. Both BP-I interface configurations, although with different magnitudes, exhibit two roughness profiles for low and high pitch, with a transition at $P_u \sim 90\xi$, where an anchoring transition occurs. Furthermore, the relation between the amplitude and the surface tension of an interface with deformed *double-twist* cells is consistent since the highest amplitude configuration corresponds to the lowest surface tension and the inverse also applies. Nevertheless, a quantitative relation between γ and A was not obtained. For low pitch, the anchoring is planar, the *double-twist* cells have small deformations and the roughness is high while for high pitch the anchoring is homeotropic as in the C-I, the *double-twist* cells are highly deformed and the roughness is small. A qualitative agreement between the C-I and the BP-I interface's roughness behaviour is also obtained for high pitch over the triple line, where both are decreasing functions of the pitch. An analytical approach via a rescaled Frank-Oseen model is also developed and deformations of the *double-twist* core are considered to have an elliptical form. This is used in order to understand the energetic penalties associated with deformations at the surface cells for different pitch, but apart from underlying that the interface undulations behaviours are due to anchoring features, no new results are obtained. Finally, it was observed that, over the triple line, the roughness of the BP-I and the C-I interface cross at $P \sim 100\xi$, which means that it is possible to have a continuous transition of the interface roughness with homeotropic anchoring for phase transitions between the cholesteric and the blue phase at coexistence with the isotropic phase. This result is a major step in the knowledge involved of blue phase control. It has recently been studied that the blue phase can be stabilized for a wider range of temperatures through the intrusion of colloidal particles in its bulk [40]. Furthermore it has also been studied recently how temperature influences the blue phase pitch [12]. Combining this with the results obtained in this thesis it might be possible to create a system at coexistence that allows a pitch controlled soft structured surface with homeotropic anchoring alongside a bulk orientational profile control, between a cholesteric and a blue phase.

For the BP-C it is again observed that two distinct configurations are exhibited, corresponding to a *zig-zag* and *linear* arrangement of the *double-twist* cells at the surface. For this system the equilibrium interface has a *linear* configuration, unlike the BP-I interface, with cholesteric layers tilted by $\pi/4$ and with undistorted *double-twist* cells and cholesteric layers the surface. This results in undulations with amplitude $A_{lin} = \sqrt{6}P/12$ and roughness $r_{lin} = 1/\sqrt{12}$, regardless of the pitch. It is observed that below $P \sim 50\xi$ the surface tension is negative, however, the reason why is not yet clear. By relating each configuration with its surface defect density it is possible to observe that the surface tension inversion of the two configurations between the BP-I and the BP-C interface is related to the presence of defects, since the *zig-zag* configuration has higher defect density and thus higher surface tension. Considering that the pitch, the elastic constants and the temperature hold a relation such that the triple coexistence is ensured, then a system with three different interfaces may be created in which roughness of the interfaces can be controlled and go from a region where $r_{BP-C} > r_{C-I} > r_{BP-I}$, at $P > P_u$, to a region where $r_{BP-C} > r_{C-I} = r_{BP-I}$, at $P \sim 90\xi$, to a region where $r_{BP-C} > r_{BP-I} > r_{C-I}$ at $P_u > P \gtrsim 50\xi$ and finally into a region where $r_{BP-I} > r_{C-I}$, below $P \sim 50\xi$. Recalling that we are dealing with only one component, the amount of different systems that is possible to create is absolutely staggering. If, even as a very remote hypothesis each of the system variables could be subject to dynamic control, say in a switch like manner, then the number of possibilities in which different surfaces, layers of different phases and phases with different bulk properties could be arranged would certainly deserve further study. If all this wasn't enough, it is even possible to add substrates to the mixture.

Some preliminary results were obtained for a cholesteric confined by a sawtooth substrate with planar weak anchoring. It was observed that regardless of the cholesteric pitch and wedge apertures, the most stable configuration was obtained for cholesteric layers oriented parallel to the substrate. A geometric relation was proposed for the total density of defects and distance between the defects in the wedges in qualitative agreement with the numerical results. This opens the way for further studies of confined cholesterics.

For future work, some of the subtleties of the two previous systems should be clarified. In particular the questions of how the balance between the elastic constants affects the blue phase honeycomb defect lattice, the hyperbolic relation between P and κ in the triple phase coexistence line, the relation between the blue phase and cholesteric orientational periodicities δ and the negative surface tension of the BP-C interface. Answering this will further increase the understating of the previous interfacial systems, not only with respect to pitch but also with respect to the elastic constants, thus increasing the potential of these interfacial systems for applications. Such study would, however, require further gradient terms of the LdG functional expansion to be considered. Furthermore, the use extra terms would bring about the possibility of the model to consider not only the blue phase I but also the blue phase II, opening the way to the study of new interfacial systems. Noting that all the results were obtained for thermodynamic equilibrium, as already stated before, the dynamical study of these systems is of considerable interest too. After a full study of the static and dynamic properties of the chiral nematic interfaces, the logical step would be of course to consider binary systems.

Appendix A

Frank-Oseen functional

The general form of the director distortion free energy density in a continuum medium can be written as a Taylor expansion of the free energy density around the its equilibrium value up to the second order, as a sum of a linear and a quadratic contribution (sum over indices implied) [11, 47],

$$f_{dist} = K_{ij}\frac{\partial n_i}{\partial x_j} + \frac{1}{2}K_{ijlm}\frac{\partial n_i}{\partial x_j}\cdot\frac{\partial n_l}{\partial x_m}, i, j = 1, 2, 3 \tag{7.1}$$

with K_{ij} and K_{ijlm} as constants that correspond to the derivative of the free energy with respect to the coordinates at the equilibrium configuration. For notation simplicity let us consider the linear distortion matrix as,

$$\frac{\partial n_i}{\partial x_j} = \begin{bmatrix} a_1 & a_2 & a_3 \\ -a_4 & a_5 & a_6 \\ a_7 & a_8 & a_9 \end{bmatrix}$$

and the quadratic distortion matrix as,

$$\frac{\partial n_l}{\partial x_m} = \begin{bmatrix} a'_1 & a'_2 & a'_3 \\ -a'_4 & a'_5 & a'_6 \\ a'_7 & a'_8 & a'_9 \end{bmatrix}$$

Developing f_{dist} in terms of the linear and quadratic distortion matrix yields,

$$\begin{aligned} f_{dist} =& K_{11}a_1 + K_{12}a_2 + K_{13}a_3 - K_{21}a_4 + K_{22}a_5 + K_{23}a_6 + K_{31}a_7 + K_{32}a_8 + K_{33}a_9 \\ &+ \frac{1}{2}[K_{11lm}a_1 + K_{12lm}a_2 - K_{13lm}a_3K_{21lm}a_4 + K_{22lm}a_5 + K_{23lm}a_6 \\ &+ K_{31lm}a_7 + K_{32lm}a_8 + K_{33lm}a_9]\frac{\partial n_l}{\partial x_m} \end{aligned} \tag{7.2}$$

When no symmetry constrains or distortion limitations are imposed, f_{dist} has 9 components on the linear part and 81 components on the quadratic part.

For a nematic with the director pointing along the z direction by definition, it is considered that the director variations along that direction are very small such that the n_z component does not depend on any spatial variations or in any other director components variations. Thus, it comes that $a_7 = a_8 = a_9 = 0$ and $a'_7 = a'_8 = a'_9 = 0$ such that f_{dist} ends up with 6 components on the linear part and 36 components on the quadratic part and can be simplified to,

$$\begin{aligned} f_{dist} =& K_{11}a_1 + K_{12}a_2 + K_{13}a_3 - K_{21}a_4 + K_{22}a_5 + K_{23}a_6 \\ &+ \frac{1}{2}[K_{11lm}a_1 + K_{12lm}a_2 + K_{13lm}a_3 - K_{21lm}a_4 + K_{22lm}a_5 + K_{23lm}a_6]\frac{\partial n_l}{\partial x_m} \end{aligned} \tag{7.3}$$

Further simplifying the notation with $K_{11,lm} = K_{\alpha=1,lm}$,...,$K_{23,lm} = K_{\alpha=6,lm}$, or just $K_{ij,lm} = K_{\alpha,lm}$ (considering a growing order) and $K_{ij,11} = K_{ij,\beta=1}$,...,$K_{ij,23} = K_{ij,\beta=6}$ or just $K_{ij,lm} = K_{ij,\beta}$, the compact free energy can be written as $f_{dist} = K_\alpha a_\alpha + \frac{1}{2}K_{\alpha\beta}a_\alpha a'_\beta$, with $\alpha, \beta = 1, ..., 6$ and the extended free energy comes as,

$$\begin{aligned} f_{dist} =& K_1a_1 + K_2a_2 + K_3a_3 - K_4a_4 + K_5a_5 + K_6a_6 \\ &+ \frac{1}{2}[K_{1\beta}a_1 + K_{2\beta}a_2 + K_{3\beta}a_3 - K_{4\beta}a_4 + K_{5\beta}a_5 + K_{6\beta}a_6]a'_\beta \end{aligned} \tag{7.4}$$

For the case of uniaxial symmetry, where any rotation of the coordinate system perpendicular to the director is allowed, the elastic constants of the linear and quadratic parts of the free energy, K_{ij} and $K_{\alpha\beta}$, must be equal to $-K_{ji}$ and $K_{\beta\alpha}$, respectively, after the transformations $(x_1, x_2, x_3) \rightarrow (x_2, -x_1, x_3)$ and $(n_1, n_2, n_3) \rightarrow (n_2, -n_1, n_3)$. Applying the conditions to the non-diagonal terms associated with the different quadratic elastic constants $K_{\alpha\beta}$, results that, $K_{12} = -K_{54}$, $K_{13} = K_{56}$, $K_{14} = -K_{52}$, $(K_{15} = K_{51})$, $K_{16} = -K_{53}$, $K_{21} = -K_{45}$, $K_{23} = -K_{46}$, $(K_{24} = K_{42})$, $K_{25} = -K_{41}$, $K_{26} = K_{43}$, $K_{31} = K_{65}$, $K_{32} = -K_{64}$, $K_{34} = -K_{62}$, $K_{35} = K_{61}$, $K_{36} = -K_{63}$, $K_{41} = -K_{25}$, $K_{42} = K_{24}$, $K_{43} = K_{26}$, $K_{45} = -K_{21}$, $K_{46} = -K_{23}$, $K_{51} = K_{15}$, $K_{52} = -K_{14}$, $K_{53} = -K_{16}$, $K_{54} = -K_{12}$, $K_{61} = -K_{35}$, $K_{62} = -K_{34}$, $K_{63} = -K_{36}$, $K_{64} = -K_{32}$, $K_{65} = K_{31}$. For all those that are different from $K_{\beta\alpha}$ after the transformation the corresponding elastic constants must be zero and only $K_{24} \neq 0$ and $K_{15} \neq 0$. The diagonal terms are of course equal to them selves, so there is no reason to consider them zero valued. Nevertheless, applying the same condition to the diagonal terms associated with the different quadratic elastic constants $K_{\alpha\beta}$, results that $K_{11} = K_{55}$, $K_{22} = K_{44}$ and $K_{33} = K_{66}$. The quadratic distortion energetic contribution matrix comes as,

$$K_{\alpha\beta} = \begin{bmatrix} K_{11} & 0 & 0 & 0 & K_{15} & 0 \\ 0 & K_{22} & 0 & K_{24} & 0 & 0 \\ 0 & 0 & K_{33} & 0 & 0 & 0 \\ 0 & K_{24} & 0 & K_{22} & 0 & 0 \\ K_{15} & 0 & 0 & 0 & K_{11} & 0 \\ 0 & 0 & 0 & 0 & 0 & K_{33} \end{bmatrix}$$

Applying the same conditions to the non-diagonal terms associated with the different linear elastic constants K_{ij}, results that, $K_{12} = -K_{21}$, $K_{13} = -K_{23}$ and $K_{21} = -K_{12}$, $K_{23} = K_{13}$ and only $K_{12} \neq 0$. For the diagonal terms associated with the different linear elastic constants K_{ij}, results that $K_{11} = K_{22}$. Thus, the nematic quadratic distortion energetic contribution matrix comas as,

$$K_{\alpha} = \begin{bmatrix} K_{11} & K_{12} & 0 \\ -K_{12} & K_{11} & 0 \\ 0 & 0 & 0 \end{bmatrix} = \begin{bmatrix} K_1 & K_2 & 0 \\ -K_2 & K_1 & 0 \\ 0 & 0 & 0 \end{bmatrix}$$

The distortion free energy density can now be written in the general form as,

$$\begin{aligned} f_{dist} &= K_1 a_1 + K_2 a_2 + K_2 a_4 + K_1 a_5 + \frac{1}{2}(K_{11} a_1 + K_{15} a_5) a_1' + \frac{1}{2}(K_{22} a_2 - K_{24} a_4) a_2' + \frac{1}{2}(K_{33} a_3) a_3' \\ &+ \frac{1}{2}(K_{24} a_2 - K_{22} a_4)(-a_4') + \frac{1}{2}(K_{15} a_1 + K_{11} a_5) a_5' + \frac{1}{2}(K_{33} a_6) a_6' \end{aligned} \tag{7.5}$$

Since $a_i = a_i'$, then we get,

$$\begin{aligned} f_{dist} &= K_1(a_1 + a_5) + K_2(a_2 + a_4) + \frac{1}{2}(K_{11} a_1^2 + K_{15} a_1 a_5) + \frac{1}{2}(K_{22} a_2^2 - K_{24} a_2 a_4) + \frac{1}{2}(K_{33} a_3^2) \\ &+ \frac{1}{2}(K_{22} a_4^2 - K_{24} a_2 a_4) + \frac{1}{2}(K_{15} a_1 a_5 + K_{11} a_5^2) + \frac{1}{2}(K_{33} a_6^2) \\ &= \left[K_1(a_1 + a_5) + \frac{1}{2} K_{11}(a_1 + a_5)^2 \right] + \left[K_2(a_2 + a_4) + \frac{1}{2} K_{22}(a_2 + a_4)^2 \right] + \left[\frac{1}{2} K_{33}(a_3^2 + a_6^2) \right] \\ &- (K_{24} + K_{22}) a_2 a_4 - (K_{11} - K_{15}) a_1 a_5 \end{aligned} \tag{7.6}$$

By adopting a new and lower zero for the free energy density, corresponding not to the state of uniform orientation but to that with the optimum degree of splay and twist, by defining the quantities $s_0 = -\frac{K_1}{K_{11}}$

and $q_0 = -\frac{K_2}{K_{22}}$, with,

$$\tilde{f}_{dist} = f_{dist} + \frac{1}{2}K_{11}s_0^2 + \frac{1}{2}K_{22}q_0^2 \tag{7.7}$$

the general Frank-Oseen free energy density is obtained (omitted tilde) [47],

$$\begin{aligned} f_{dist} =& \frac{1}{2}K_{11}(a_1 + a_5 - s_0)^2 + \frac{1}{2}K_{22}(a_2 + a_4 - q_0)^2 + \frac{1}{2}K_{33}(a_3 + a_6)^2 \\ & - (K_{24} + K_{22})a_2a_4 - (K_{11} - K_{15})a_1a_5 \end{aligned} \tag{7.8}$$

that can written in the explicit form according to the definition of the a_i elements,

$$\begin{aligned} f_{dist} =& \frac{1}{2}K_{11}\left(\frac{\partial n_x}{\partial x} + \frac{\partial n_y}{\partial y} - s_0\right)^2 + \frac{1}{2}K_{22}\left(\frac{\partial n_x}{\partial y} - \frac{\partial n_y}{\partial x} - q_0\right)^2 + \frac{1}{2}K_{33}\left(\frac{\partial n_x}{\partial z} + \frac{\partial n_y}{\partial z}\right)^2 \\ & - (K_{22} + K_{24})\left(\frac{\partial n_x}{\partial y}\frac{\partial n_y}{\partial x}\right) - (K_{11} - K_{15})\left(\frac{\partial n_x}{\partial x}\frac{\partial n_y}{\partial y}\right) \end{aligned} \tag{7.9}$$

If besides uniaxial symmetry, head-tail symmetry (non-polarity) is also considered, the elastic constants $K_{\alpha\beta}$ must be equal before and after the transformations $(x_1, x_2, x_3) \rightarrow (x_2, -x_1, -x_3)$ and $(n_1, n_2, n_3) \rightarrow (n_2, -n_1, -n_3)$, which results in $K_2 = -K_2 = 0$ and $q_0 = 0$. Thus, spontaneous twist is only present when some degree of polarity exists. Nevertheless, when the spontaneous twist q_0 is a small constant the system can be approximated as non-polar without loss of generality. Furthermore, spontaneous splay should only be expected when some charge gradient is present. So when head-tail symmetry is considered, $s_0 = 0$, meaning that splay energetic penalties do not have a preferred direction, such that $K_{11} - K_{15} = 0$. Also, with no polarity, there is no reason to expect any out of the plane evolution of the director field, such that too $K_{22} - K_{24} = 0$. Thus, it is possible to see that the last two terms of the above equation are directly related with the polar features of the liquid crystal such that for simplicity it can simply be stated that $K_{22} - K_{24} = K_{11} - K_{15}$. Thus, the free energy takes the general form,

$$\begin{aligned} f_{dist} =& \frac{1}{2}K_{11}\left(\frac{\partial n_x}{\partial x} + \frac{\partial n_y}{\partial y} - s_0\right)^2 + \frac{1}{2}K_{22}\left(\frac{\partial n_x}{\partial y} - \frac{\partial n_y}{\partial x} - q_0\right)^2 + \frac{1}{2}K_{33}\left(\frac{\partial n_x}{\partial z} + \frac{\partial n_y}{\partial z}\right)^2 \\ & - (K_{22} + K_{24})\left(\frac{\partial n_x}{\partial y}\frac{\partial n_y}{\partial x} + \frac{\partial n_x}{\partial x}\frac{\partial n_y}{\partial y}\right) \end{aligned} \tag{7.10}$$

Using the identities,

$$\begin{aligned} &\nabla \cdot \mathbf{n} = \frac{\partial n_x}{\partial x} + \frac{\partial n_y}{\partial y} && , \quad \nabla \times \mathbf{n} = -\frac{\partial n_y}{\partial z}\overrightarrow{e}_x + \frac{\partial n_x}{\partial z}\overrightarrow{e}_y + \left(\frac{\partial n_x}{\partial y} - \frac{\partial n_y}{\partial x}\right)\overrightarrow{e}_z \\ &\mathbf{n} \cdot \nabla \times \mathbf{n} = \left(\frac{\partial n_x}{\partial y} - \frac{\partial n_y}{\partial x}\right)n_z \approx \frac{\partial n_x}{\partial y} - \frac{\partial n_y}{\partial x} && , \quad \mathbf{n} \times \nabla \times \mathbf{n} \approx -\frac{\partial n_x}{\partial z}\overrightarrow{e}_x - \frac{\partial n_y}{\partial z}\overrightarrow{e}_y \\ &(\mathbf{n} \times \nabla \times \mathbf{n})^2 \approx \left(\frac{\partial n_x}{\partial z}\right)^2 + \left(\frac{\partial n_y}{\partial z}\right)^2 && , \quad \frac{1}{2}\nabla \cdot \Big((\mathbf{n} \cdot \nabla)\mathbf{n} - \mathbf{n}(\nabla \cdot \mathbf{n})\Big) = -\left(\frac{\partial n_x}{\partial y}\frac{\partial n_y}{\partial x} + \frac{\partial n_x}{\partial x}\frac{\partial n_y}{\partial y}\right) \end{aligned} \tag{7.11}$$

the Frank-Oseen free-energy density can be obtained,

$$\begin{aligned} f_{dist} =& \frac{1}{2}K_{11}(\nabla \cdot \mathbf{n} - s_0)^2 + \frac{1}{2}K_{22}(\mathbf{n} \cdot (\nabla \times \mathbf{n}) - q_0)^2 + \frac{1}{2}K_{33}(\mathbf{n} \times \nabla \times \mathbf{n})^2 \\ & + \frac{1}{2}(K_{22} + K_{24})\nabla \cdot \Big((\mathbf{n} \cdot \nabla)\mathbf{n} - \mathbf{n}(\nabla \cdot \mathbf{n})\Big) \end{aligned} \tag{7.12}$$

with K_{11}, K_{22}, K_{33} and K_{24} the *splay*, *twist*, *bend* and *saddle-splay* elastic constants, respectively, and with $s_0 = 0$ and $K_{22} + K_{24} = 0$ in the absence of polar features. It should be noticed that these features can arise due to external constraints, even for systems with head-tail symmetry.

Appendix B

Laplace Equation in spherical coordinates

The Laplace equation with Cartesian coordinates

$$\nabla^2 f(x,y,z) = \frac{\partial^2}{\partial x^2} + \frac{\partial^2}{\partial y^2} + \frac{\partial^2}{\partial z^2} = 0 \tag{7.13}$$

in spherical coordinates is written as,

$$\nabla^2 f(r,\theta,\phi) = \frac{1}{r^2}\frac{\partial}{\partial r}(r^2\frac{\partial}{\partial r})f + \frac{1}{r^2 sin(\theta)}\frac{\partial}{\partial \theta}(sin(\theta)\frac{\partial}{\partial \theta})f + \frac{1}{r^2 sin^2(\theta)}\frac{\partial^2}{\partial \phi^2}f \tag{7.14}$$

For $x = cos(\theta)$, $x \in [-1,1]$,

$$\nabla^2 f(r,x,\phi) = \frac{1}{r^2}\frac{\partial}{\partial r}(r^2\frac{\partial}{\partial r})f + \frac{1}{r^2}\frac{\partial}{\partial x}(1-x^2)\frac{\partial}{\partial x}f + \frac{1}{r^2(1-x^2)}\frac{\partial^2}{\partial \phi^2}f = 0 \tag{7.15}$$

Uniaxial symmetry

In this case we consider that $f(r,\theta,\phi) = f(r,\theta)$. Expanding the distribution function f into a converging power series, with $r < 1$ and $P_n(x)$ a generic function such that,

$$f(r,x) = \sum_{n=0}^{\infty} r^n P_n(x) \tag{7.16}$$

one sees that

$$\begin{aligned}
\nabla^2 f =& \frac{1}{r^2}\frac{\partial}{\partial r}(r^2\frac{\partial}{\partial r})\sum_{n=0}^{\infty} r^n P_n(x) + \frac{1}{r^2}\frac{\partial}{\partial x}(1-x^2)\frac{\partial}{\partial x}\sum_{n=0}^{\infty} r^n P_n(x) \\
=& \frac{1}{r^2}\frac{\partial}{\partial r}(r^2 n\sum_{n=0}^{\infty} r^{n-1} P_n(x)) + \frac{1}{r^2}\frac{\partial}{\partial x}(1-x^2)\sum_{n=0}^{\infty} r^n \frac{\partial P_n(x)}{\partial x} \\
=& \frac{1}{r^2} n(n+1)\sum_{n=0}^{\infty} r^n P_n(x) + \frac{1}{r^2}\frac{\partial}{\partial x}(1-x^2)\sum_{n=0}^{\infty} r^n \frac{\partial P_n(x)}{\partial x} = 0
\end{aligned} \tag{7.17}$$

which gives the Legendre equation,

$$\frac{\partial}{\partial x}(1-x^2)\frac{\partial P_n(x)}{\partial x} + n(n+1)P_n(x) = 0 \tag{7.18}$$

The generic function $P_n(x)$, called the Legendre Polynomials can be expanded in terms of x, such that,

$$P_n(x) = \sum_{k=0}^{\infty} a_k x^k \tag{7.19}$$

Substituting this series in the Legendre equation, it follows that

$$\frac{\partial}{\partial x}(1-x^2)\frac{\partial P_n(x)}{\partial x}\sum_{k=0}^{\infty} a_k x^k + n(n+1)(\sum_{k=0}^{\infty} a_k x^k) = 0 \tag{7.20}$$

$$\frac{\partial}{\partial x}(1-x^2)\sum_{k=0}^{\infty} k a_k x^{k-1} + n(n+1)\sum_{k=0}^{\infty} a_k x^k = 0 \tag{7.21}$$

$$\sum_{k=0}^{\infty} k(k-1)a_k x^{k-2} - \sum_{k=0}^{\infty} k(k+1)a_k x^k + n(n+1)\sum_{k=0}^{\infty} a_k x^k = 0 \tag{7.22}$$

$$\sum_{k=0}^{\infty} (k+2)(k+1)a_{k+2} x^k - \sum_{k=0}^{\infty} k(k+1)a_k x^k + n(n+1)\sum_{k=0}^{\infty} a_k x^k = 0 \tag{7.23}$$

from where one gets the recursion equation

$$a_{k+2} = -\frac{n(n+1) - k(k+1)}{(k+2)(k+1)} a_k \tag{7.24}$$

Since this recursion formula relates each coefficient to the one two steps before it, the two fist coefficients, a_0 and a_1 must be specified to get the formula started. With this result one can explicitly represent the values of a_k starting with $k = 2$ as,

$$\begin{aligned} a_2 =& -\frac{n(n+1)}{2} a_0 \\ a_3 =& -\frac{n(n+1) - 2}{6} a_1 \\ a_4 =& -\frac{n(n+1) - 6}{12} a_2 = \frac{n(n+1)[n(n+1) - 6]}{24} a_0 \\ a_5 =& -\frac{n(n+1) - 12}{20} a_3 = \frac{[n(n+1) - 2][n(n+1) - 12]}{120} a_1 \\ & \ldots \end{aligned} \tag{7.25}$$

Since all a_k values are explicitly represented it is possible to do the same procedure to the Legendre Polynomials,

$$\begin{aligned} P_n(x) =& a_0 + a_1 x + a_2 x^2 + a_3 x^3 + a_4 x^4 + .. \\ =& a_0[1 - \frac{n(n+1)}{2} x^2 + \frac{n(n+1)[n(n+1) - 6]}{24} x^4 + ...] + \\ & a_1[x - \frac{n(n+1) - 2}{6} x^3 + \frac{[n(n+1) - 2][n(n+1) - 12]}{120} x^5 + ...] \\ & ... \end{aligned} \tag{7.26}$$

Now one sees that: if $a_0 = a_1 = 0$ then $P_n(x) = 0$ for any $x \in [-1, 1]$; if $n(n+1) \neq k(k+1)$, i.e, if $n(n+1) \neq 2, 6, 12..$ then $Pn_(x)$ diverges; if $n(n+1) = k(k+1)$, then $Pn_(x)$ converges and one can represent it explicitly,

$$\begin{aligned} & n = 0 \Rightarrow k = 0 : P_0(x) = a_0 \\ & n = 1 \Rightarrow k = 1 : P_1(x) = a_1 \\ & n = 2 \Rightarrow k = 2 : P_2(x) = a_0(1 - 3x^2) \\ & n = 3 \Rightarrow k = 3 : P_3(x) = a_1(x - 5/3x^3)a_1 \\ & n = 4 \Rightarrow k = 4 : P_4(x) = a_2(1 - 10x^2 + 35/3x^4) \\ & \quad ... \end{aligned} \tag{7.27}$$

If one chooses $P_n(x)$ to be normalized then $P_n(1) = 1$ for any n and we takes,

$$\begin{aligned} &n = 0 \Rightarrow k = 0 : P_0(x) = 1 \\ &n = 1 \Rightarrow k = 1 : P_1(x) = 1 \\ &n = 2 \Rightarrow k = 2 : P_2(x) = \frac{1}{2}(3x^2 - 1) \\ &n = 3 \Rightarrow k = 3 : P_3(x) = \frac{1}{2}(5/3x^3 - 3x) \\ &n = 4 \Rightarrow k = 4 : P_4(x) = \frac{1}{8}(35x^4 - 30x^2 + 3) \\ &\quad ... \end{aligned} \tag{7.28}$$

which can be represented in a compact way, in the Rodriguez formula,

$$P_n(x) = \frac{1}{2^n n!}\frac{\partial^n}{\partial x^n}(x^2 - 1)^n \tag{7.29}$$

Considering two distinct solutions for the Legendre equation, $P_n(x)$ and $P_m(x)$,

$$\begin{aligned} n(n+1)P_n(x) + [(1-x^2)P_n']' = 0 \\ m(m+1)P_(x) + [(1-x^2)P_m']' = 0 \end{aligned} \tag{7.30}$$

Multiplying the first equation by $P_m(x)$, the second one by $P_n(x)$ and subtracting, we get,

$$P_m[(1-x^2)P_n']' - P_n[(1-x^2)P_m']' + n(n+1)P_n - m(m+1)P_m = 0 \tag{7.31}$$

and integrating,

$$\int_{-1}^{+1} P_m[(1-x^2)P_n']' - P_n[(1-x^2)P_m']'dx + \int_{-1}^{+1}[n(n+1)P_n - m(m+1)]P_nP_mdx = 0 \tag{7.32}$$

$$(P_n'P_m - P_nP_m')(1-x^2)|_{-1}^{+1} - \int_{-1}^{+1}(P_m'P_m' - P_n'P_m')(1-x^2)dx + \int_{-1}^{+1}[n(n+1) - m(m+1)]P_nP_mdx = 0 \tag{7.33}$$

The first term is zero in the integration limits and the second term is zero due to the difference inside the integral, leaving the third term,

$$\int_{-1}^{+1}[n(n+1) - m(m+1)]P_nP_mdx = 0 \tag{7.34}$$

Its is possible to see that if $n \neq m$ then $\int_{-1}^{+1} P_nP_mdx = 0$ and that otherwise, with $n = m$, that $\int_{-1}^{+1} P_n^2(x)dx \neq 0 = I_n(x)$. Using the Rodriguez formula, we get,

$$I_n(x) = \int_{-1}^{+1} \frac{1}{2^n n!}\frac{\partial^n}{\partial x^n}(x^2-1)^n \frac{1}{2^n n!}\frac{\partial^n}{\partial x^n}(x^2-1)^n \tag{7.35}$$

Integrating by parts, we get,

$$(2^n n!)^2 I_n(x) = \frac{\partial^{n-1}}{\partial x^{n-1}}(x^2-1)^n|_{-1}^{+1} - \int_{-1}^{+1}\frac{\partial^{n-1}}{\partial x^{n-1}}(x^2-1)^n\frac{\partial^{n+1}}{\partial x^{n+1}}(x^2-1)^n dx \tag{7.36}$$

Any differentiation of a $(x^2-1)^n$ term less than n times, the resulting expression is zero in the integration limits so,

$$(2^n n!)^2 I_n(x) = -\int_{-1}^{+1} \frac{\partial^{n-1}}{\partial x^{n-1}}(x^2-1)^n \frac{\partial^{n+1}}{\partial x^{n+1}}(x^2-1)^n dx \tag{7.37}$$

Repeating the integration by parts,

$$(2^n n!)^2 I_n(x) = \int_{-1}^{+1} \frac{\partial^{n-2}}{\partial x^{n-2}}(x^2-1)^n \frac{\partial^{n+2}}{\partial x^{n+2}}(x^2-1)^n dx \tag{7.38}$$

If this process is repeated n times, one is left with,

$$I_n(x) = \frac{(-1)^n}{(2^n n!)^2}\int_{-1}^{+1}(x^2-1)^n \frac{\partial^{2n}}{\partial x^{2n}}(x^2-1)^n dx = \frac{(-1)^n 2n!}{(2^n n!)^2}\int_{-1}^{+1}(x^2-1)^n dx = \frac{2}{2n+1} \tag{7.39}$$

or simply,

$$\int_{-1}^{+1} P_n^2(x)dx = \frac{2}{2n+1} \tag{7.40}$$

This result allows us to determine the form of the f distribution. If we multiply the distribution function by a solution of the Legendre equation, $P_m(x)$, and integrate, while using the property that the product of the Legendre polynomials with different index is zero, we end up with,

$$\int_{-1}^{+1} P_m(x)f(x)dx = \sum_{n=0}^{\infty} r^n \int_{-1}^{+1} P_m(x)P_n(x)dx \quad = r^m \int_{-1}^{+1} P_m^2(x)dx = r^m \frac{2}{2m+1} \tag{7.41}$$

which implies that the distribution function must have the following form,

$$f(x) = \sum_{n=0}^{\infty}(\frac{2n+1}{2}) < P_n(x) > P_n(x) \tag{7.42}$$

Appendix C

Landau-de Gennes functional terms expansion

Let us use the following notation for the Q_{ij} tensor,

$$Q_{ij} = \begin{bmatrix} Q_{11} & Q_{12} & Q_{13} \\ Q_{21} & Q_{22} & Q_{23} \\ Q_{31} & Q_{32} & Q_{33} \end{bmatrix} = \begin{bmatrix} Q_{11} & Q_{12} & Q_{13} \\ Q_{13} & Q_{22} & Q_{23} \\ Q_{13} & Q_{23} & Q_{33} \end{bmatrix} = \begin{bmatrix} q_1 & q_2 & q_3 \\ q_2 & q_4 & q_5 \\ q_3 & q_5 & -(q_1+q_4) \end{bmatrix}$$

$$\begin{aligned} \bullet Q_{ij}Q_{ji} &= Q_{11}Q_{11} + Q_{12}Q_{21} + Q_{13}Q_{31} + Q_{21}Q_{12} + Q_{22}Q_{22} + Q_{23}Q_{32} + Q_{31}Q_{13} + Q_{32}Q_{23} + Q_{33}Q_{33} \\ &= q_1^2 + q_2^2 + q_3^2 + q_2^2 + q_4^2 + q_5^2 + q_3^2 + q_5^2 + (q_1+q_4)^2 = 2(q_1^2 + q_2^2 + q_3^2 + q_4^2 + q_5^2 + q_1q_4) = Tr(\boldsymbol{Q}^2) \end{aligned} \tag{7.43}$$

$$\begin{aligned} \bullet Q_{ij}Q_{jk}Q_{ki} &= Q_{11}Q_{1k}Q_{k1} + Q_{12}Q_{2k}Q_{k1} + Q_{13}Q_{3k}Q_{k1} + Q_{21}Q_{1k}Q_{k2} + Q_{22}Q_{2k}Q_{k2} + Q_{23}Q_{3k}Q_{k2} \\ &+ Q_{31}Q_{1k}Q_{k3} + Q_{32}Q_{2k}Q_{k3} + Q_{33}Q_{3k}Q_{k3} \\ &= Q_{11}[Q_{1k}Q_{k1} - Q_{3k}Q_{k3}] + 2Q_{12}[Q_{1k}Q_{k2}] + 2Q_{13}[Q_{1k}Q_{k3}] + Q_{22}[Q_{2k}Q_{k2} - Q_{3k}Q_{k3}] \\ &+ 2Q_{23}[Q_{2k}Q_{k3}] \\ &= q_1[q_2^2 - q_5^2 - q_4^2 - q_1q_4] + 2q_2[q_1q_2 + q_2q_4 + q_3q_5] + 2q_3[q_2q_5 - q_3q_4] + 2q_5[q_2q_3 - q_1q_5] \\ &+ 2q_4[q_2^2 - q_3^2 - q_1^2 - q_1q_4] = 3[q_1(q_2^2 - q_4^2 - q_5^2) - q_4(q_1^2 - q_2^2 + q_3^2)] = Tr(\boldsymbol{Q}^3) \end{aligned} \tag{7.44}$$

$$\begin{aligned} \bullet(\partial_k Q_{ij})(\partial_k Q_{ij}) &= (\partial_k Q_{11})(\partial_k Q_{11}) + (\partial_k Q_{12})(\partial_k Q_{12}) + (\partial_k Q_{13})(\partial_k Q_{13}) \\ &+ (\partial_k Q_{21})(\partial_k Q_{21}) + (\partial_k Q_{22})(\partial_k Q_{22}) + (\partial_k Q_{23})(\partial_k Q_{23}) \\ &+ (\partial_k Q_{31})(\partial_k Q_{31}) + (\partial_k Q_{32})(\partial_k Q_{32}) + (\partial_k Q_{33})(\partial_k Q_{33}) \\ &= (\partial_k q_1)^2 + (\partial_k q_2)^2 + (\partial_k q_3)^2 + (\partial_k q_2)^2 + (\partial_k q_4)^2 + (\partial_k q_5)^2 \\ &+ (\partial_k q_3)^2 + (\partial_k q_5)^2 + (\partial_k q_1 + \partial_k q_4)^2 \\ &= 2[(\partial_k q_1)^2 + (\partial_k q_2)^2 + (\partial_k q_3)^2 + (\partial_k q_4)^2 + (\partial_k q_5)^2 + (\partial_k q_1)(\partial_k q_4)] \end{aligned} \tag{7.45}$$

$$\begin{aligned} \bullet(\partial_j Q_{ij})(\partial_k Q_{ik}) &= (\partial_j Q_{1j})[(\partial_1 Q_{11}) + (\partial_2 Q_{12}) + (\partial_3 Q_{13})] + (\partial_j Q_{2j})[(\partial_1 Q_{21}) + (\partial_2 Q_{22}) + (\partial_3 Q_{23})] \\ &+ (\partial_j Q_{3j})[(\partial_1 Q_{31}) + (\partial_2 Q_{32}) + (\partial_3 Q_{33})] \\ &= (\partial_1 q_1)^2 + (\partial_1 q_1)(\partial_2 q_2) + (\partial_1 q_1)(\partial_3 q_3) + (\partial_2 q_2)(\partial_1 q_1) + (\partial_2 q_2)^2 + (\partial_1 q_2)(\partial_3 q_3) \\ &+ (\partial_3 q_3)(\partial_1 q_1) + (\partial_3 q_3)(\partial_2 q_2) + (\partial_3 q_3)^2 + (\partial_1 q_2)^2 + (\partial_1 q_2)(\partial_2 q_4) + (\partial_1 q_2)(\partial_3 q_5) \\ &+ (\partial_2 q_4)(\partial_1 q_2) + (\partial_2 q_4)^2 + (\partial_2 q_4)(\partial_3 q_5) + (\partial_3 q_5)(\partial_1 q_2) + (\partial_3 q_5)(\partial_2 q_4) + (\partial_3 q_5)^2 \\ &+ (\partial_1 q_3)^2 + (\partial_1 q_3)(\partial_2 q_5) - (\partial_1 q_3)(\partial_3 (q_1+q_4)) + (\partial_3 q_5)(\partial_1 q_3) + (\partial_2 q_5)^2 - (\partial_2 q_5)(\partial_3 (q_1+q_4)) \\ &- (\partial_3 (q_1+q_4))(\partial_1 q_3) - (\partial_3 (q_1+q_4))(\partial_2 q_5) + (\partial_3 (q_1+q_4))^2 \\ &= (\partial_1 q_1)^2 + (\partial_1 q_2)^2 + (\partial_1 q_3)^2 + (\partial_2 q_2)^2 + (\partial_2 q_4)^2 + (\partial_2 q_5)^2 + (\partial_3 q_3)^2 + (\partial_3 q_5)^2 \\ &+ (\partial_3 q_1)^2 + (\partial_3 q_4)^2 + 2(\partial_3 q_1)(\partial_3 q_4) + 2[(\partial_1 q_1)(\partial_2 q_2) + (\partial_1 q_2)(\partial_2 q_4) + (\partial_1 q_3)(\partial_2 q_5)] \\ &+ 2[(\partial_1 q_1)(\partial_3 q_3) + (\partial_1 q_2)(\partial_3 q_5) - (\partial_1 q_3)(\partial_3 q_1) - (\partial_1 q_3)(\partial_3 q_4)] \\ &+ 2[(\partial_2 q_2)(\partial_3 q_3) + (\partial_2 q_4)(\partial_3 q_5) - (\partial_2 q_5)(\partial_3 q_1) - (\partial_2 q_5)(\partial_3 q_4)] \end{aligned} \tag{7.46}$$

$$
\begin{aligned}
&\bullet Q_{il}\varepsilon_{ijk}\partial_j Q_{kl} \\
&= Q_{il}\partial_1[\varepsilon_{i11}Q_{1l}+\varepsilon_{i12}Q_{2l}+\varepsilon_{i13}Q_{3l}]+Q_{il}\partial_2[\varepsilon_{i21}Q_{1l}+\varepsilon_{i22}Q_{2l}+\varepsilon_{i23}Q_{3l}]+Q_{il}\partial_3[\varepsilon_{i31}Q_{1l}+\varepsilon_{i32}Q_{2l}+\varepsilon_{i33}Q_{3l}] \\
&= Q_{il}\partial_1[\varepsilon_{i12}Q_{2l}+\varepsilon_{i13}Q_{3l}]+Q_{il}\partial_2[\varepsilon_{i21}Q_{1l}+\varepsilon_{i23}Q_{3l}]+Q_{il}\partial_3[\varepsilon_{i31}Q_{1l}+\varepsilon_{i32}Q_{2l}] \\
&= Q_{1l}\partial_1[\varepsilon_{112}Q_{2l}+\varepsilon_{113}Q_{3l}]+Q_{2l}\partial_1[\varepsilon_{212}Q_{2l}+\varepsilon_{213}Q_{3l}]+Q_{3l}\partial_1[\varepsilon_{312}Q_{2l}+\varepsilon_{313}Q_{3l}] \\
&+ Q_{1l}\partial_2[\varepsilon_{121}Q_{1l}+\varepsilon_{123}Q_{3l}]+Q_{2l}\partial_2[\varepsilon_{221}Q_{1l}+\varepsilon_{223}Q_{3l}]+Q_{3l}\partial_2[\varepsilon_{321}Q_{1l}+\varepsilon_{323}Q_{3l}] \\
&+ Q_{1l}\partial_3[\varepsilon_{131}Q_{1l}+\varepsilon_{132}Q_{2l}]+Q_{2l}\partial_3[\varepsilon_{231}Q_{1l}+\varepsilon_{232}Q_{2l}]+Q_{3l}\partial_3[\varepsilon_{331}Q_{1l}+\varepsilon_{332}Q_{2l}] \\
&= Q_{2l}\partial_1[\varepsilon_{213}Q_{3l}]+Q_{3l}\partial_1[\varepsilon_{312}Q_{2l}]+Q_{1l}\partial_2[\varepsilon_{123}Q_{3l}]+Q_{3l}\partial_2[\varepsilon_{321}Q_{1l}]+Q_{1l}\partial_3[\varepsilon_{132}Q_{2l}]+Q_{2l}\partial_3[\varepsilon_{231}Q_{1l}] \\
&= -Q_{2l}\partial_1 Q_{3l}+Q_{3l}\partial_1 Q_{2l}+Q_{1l}\partial_2 Q_{3l}-Q_{3l}\partial_2 Q_{1l}-Q_{1l}\partial_3 Q_{2l}+Q_{2l}\partial_3 Q_{1l} \\
&= -Q_{21}\partial_1 Q_{31}+Q_{31}\partial_1 Q_{21}+Q_{11}\partial_2 Q_{31}-Q_{31}\partial_2 Q_{11}-Q_{11}\partial_3 Q_{21}+Q_{21}\partial_3 Q_{11} \\
&- Q_{22}\partial_1 Q_{32}+Q_{32}\partial_1 Q_{22}+Q_{12}\partial_2 Q_{32}-Q_{32}\partial_2 Q_{12}-Q_{12}\partial_3 Q_{22}+Q_{22}\partial_3 Q_{12} \\
&- Q_{23}\partial_1 Q_{33}+Q_{33}\partial_1 Q_{23}+Q_{13}\partial_2 Q_{33}-Q_{33}\partial_2 Q_{13}-Q_{13}\partial_3 Q_{23}+Q_{23}\partial_3 Q_{13} \\
&= -q_2\partial_1 q_3+q_3\partial_1 q_2-q_4\partial_1 q_5+q_5\partial_1 q_4+q_5\partial_1 q_1+q_5\partial_1 q_4-q_1\partial_1 q_5+q_4\partial_1 q_5 \\
&+ q_1\partial_2 q_3-q_3\partial_2 q_1+q_2\partial_2 q_5-q_5\partial_2 q_2-q_3\partial_2 q_1+q_3\partial_2 q_4+q_1\partial_2 q_3+q_4\partial_2 q_3 \\
&- q_1\partial_3 q_2+q_2\partial_3 q_1-q_2\partial_3 q_4+q_4\partial_3 q_2-q_3\partial_3 q_5+q_5\partial_3 q_3
\end{aligned}
\tag{7.47}
$$

Landau-de Gennes functional rescaling

Let us consider the interface of the cholesteric with its isotropic phase defined in the $x-y$ plane, in that the scalar order parameter can only vary in the z direction, through the interface. Thus, for a director pointing perpendicular $(\perp)$ (homeotropic anchoring) and parallel $(\parallel)$ (planar anchoring) to the surface, the tensor order parameter can be written as,

$$Q_{ij}^{\perp} = S\begin{bmatrix} -1/2 & 0 & 0 \\ 0 & -1/2 & 0 \\ 0 & 0 & 1 \end{bmatrix}, Q_{ij}^{\parallel} = S\begin{bmatrix} 1 & 0 & 0 \\ 0 & -1/2 & 0 \\ 0 & 0 & -1/2 \end{bmatrix}$$

The different terms of Eq.2.41 is simplified as

$$\begin{aligned} &Tr(Q^2) = \frac{3}{2}S^2, Tr(Q^3) = \frac{3}{4}S^3, (Tr(Q^2))^2 = \frac{9}{4}S^4, \\ &(\partial_k Q_{ij})(\partial_k Q_{ij}) = \frac{3}{2}(\partial_z S)^2, (\partial_j Q_{ij})(\partial_k Q_{ik}) = (\partial_z S)^2, \epsilon_{ijk}(Q_{il})(\partial_k Q_{jl}) = 0 \end{aligned} \tag{7.48}$$

for homeotropic anchoring, and,

$$\begin{aligned} &Tr(Q^2) = \frac{3}{2}S^2, Tr(Q^3) = \frac{3}{4}S^3, (Tr(Q^2))^2 = \frac{9}{4}S^4, \\ &(\partial_k Q_{ij})(\partial_k Q_{ij}) = \frac{3}{2}(\partial_z S)^2, (\partial_j Q_{ij})(\partial_k Q_{ik}) = \frac{1}{4}(\partial_z S)^2, \epsilon_{ijk}(Q_{il})(\partial_k Q_{jl}) = 0 \end{aligned} \tag{7.49}$$

for the planar anchoring. Given these results we might look for a rescaled LdG functional we bulk terms in the form,

$$\begin{aligned} &\bullet f_{bulk} = \frac{1}{2}AQ_{ij}Q_{ji} + \frac{1}{3}BQ_{ij}Q_{jk}Q_{ki} + \frac{1}{4}C(Q_{ij}Q_{ji})^2 = \frac{3}{4}AS^2 + \frac{1}{4}BS^3 + \frac{9}{16}CS^4 \\ &\Rightarrow \tilde{f}_{bulk} = \tau\tilde{S}^2 - 2\tilde{S}^3 + \tilde{S}^4 \end{aligned} \tag{7.50}$$

in units of coherence length. In the general form, for an arbitrary director, making $f = \tilde{f}\alpha/\xi^3 and Q_{ij} = \beta\tilde{Q_{ij}}$, results in the wanted rescaled form [30],

$$\frac{\alpha}{\xi^3}\tilde{f}_{bulk} = \frac{3}{4}A\beta^2\tilde{S}^2 + \frac{1}{4}B\beta^3\tilde{S}^3 + \frac{9}{16}\beta^4\tilde{S}^4 \Longleftrightarrow \tilde{f}_{bulk} = \tau\tilde{S}^2 - 2\tilde{S}^3 + \tilde{S}^4 \tag{7.51}$$

with,

$$\Rightarrow \alpha = \frac{\xi^3 B^4}{3^6 C^3} \quad , \quad \beta = \frac{2B}{9C} \quad , \quad \tau = \frac{27AC}{B^2} \tag{7.52}$$

such that the rescaled bulk free energy takes the form,

$$f_{bulk} = \frac{2}{3}\tau Q_{ij}Q_{ji} - \frac{8}{3}Q_{ij}Q_{jk}Q_{ki} + \frac{4}{9}(Q_{ij}Q_{ji})^2 \tag{7.53}$$

As for the distortion terms, omitting the quadratic term $-2L_1q_0^2Q_{il}Q_{li}$ of Eq.2.41 that will be included in τ, with $q_0 = \tilde{q_0}/\xi$ and $\kappa = L_2/L_1$, it results that,

$$\begin{aligned} &\bullet f_{dist} = \frac{1}{2}L_1\Big(\epsilon_{ijk}\partial_k Q_{il} + 2q_0 Q_{il}\Big)^2 + \frac{1}{2}L_2\partial_j Q_{ij}\partial_k Q_{jk} \\ \Longleftrightarrow &\frac{\alpha}{\xi^3}\tilde{f}_{dist} = \frac{1}{2}L_1\frac{\beta^2}{\xi^2}\left[\left(\tilde{\partial_k}\tilde{Q_{ij}}\tilde{\partial_k}\tilde{Q_{ij}} + 4\tilde{q_0}\epsilon_{ijk}\tilde{Q_{il}}\tilde{\partial_k}\tilde{Q_{jl}} + 4\tilde{q_0}^2\tilde{Q_{ij}}\tilde{Q_{ji}}\right) + \frac{L_2}{L_1}\left(\tilde{\partial_j}\tilde{Q_{ij}}\tilde{\partial_k}\tilde{Q_{jk}}\right)\right] \\ \Longleftrightarrow &\tilde{f}_{dist} = \frac{18CL_1}{B^2\xi^2}\left[\left(\tilde{\partial_k}\tilde{Q_{ij}}\tilde{\partial_k}\tilde{Q_{ij}} + 4\tilde{q_0}\epsilon_{ijk}\tilde{Q_{il}}\tilde{\partial_k}\tilde{Q_{jl}} + 4\tilde{q_0}^2\tilde{Q_{ij}}\tilde{Q_{ji}}\right) + \kappa\left(\tilde{\partial_j}\tilde{Q_{ij}}\tilde{\partial_k}\tilde{Q_{jk}}\right)\right] \end{aligned} \tag{7.54}$$

Rescaling the omitted term of the distortion free energy that will be included in the bulk free energy, it comes that,

$$\begin{aligned} \bullet f_{dist-bulk} &= -2L_1 q_0^2 Q_{ij} Q_{ji} \\ \Longleftrightarrow \frac{\alpha}{\xi^3} \tilde{f}_{dist-bulk} &= -\frac{\beta^2}{\xi^2} 2L_1 q_0^2 \tilde{Q}_{ij} \tilde{Q}_{ji} \\ \longleftrightarrow \tilde{f}_{dist-bulk} &= -\frac{72 C L_1 q_0}{\xi^2 B^2} \end{aligned} \tag{7.55}$$

For a nematic phase with a director pointing perpendicular and parallel to the interface, it results respectively that [54],

$$\tilde{f}_{dist\perp} = \frac{18CL_1}{B^2\xi^2}(3+2\kappa)\frac{1}{2}\left(\frac{\partial \tilde{S}}{\partial \tilde{z}}\right)^2 \quad , \quad \tilde{f}_{dist\parallel} = \frac{18CL_1}{B^2\xi^2}(6+\kappa)\frac{1}{2}\left(\frac{\partial \tilde{S}}{\partial \tilde{z}}\right)^2 \tag{7.56}$$

which by dimensional analysis, yields,

$$\xi_{0\perp}^2 = \frac{18C(3+2\kappa)L_1}{B^2} \quad , \quad \xi_{0\parallel}^2 = \frac{18C(6+\kappa)L_1}{B^2} \tag{7.57}$$

Considering that $\xi_{0\perp} \simeq \xi_{0\parallel} \equiv \xi$, for the bulk, distortion-bulk and bulk the free energy densities of a cholesteric, come in the rescaled form as (omitted over bar),

$$f_{bulk} = \frac{2}{3}\tau Q_{ij}Q_{ji} - \frac{8}{3}\tilde{Q}_{ij}Q_{jk}Q_{ki} + \frac{4}{9}(Q_{ij}Q_{ji})^2 \tag{7.58}$$

$$\tilde{f}_{dist-bulk} = -\frac{4q_0^2}{3+2\kappa} Q_{ij}Q_{ji} \tag{7.59}$$

$$\tilde{f}_{dist} = \frac{1}{3+2\kappa}\left[\left(\partial_k Q_{ij}\partial_k Q_{ij} + 4q_0\epsilon_{ijk}Q_{lm}\partial_k Q_{ij} + 4q_0^2 Q_{ij}Q_{ji}\right) + \kappa\left(\partial_j Q_{ij}\partial_k Q_{jk}\right)\right] \tag{7.60}$$

Landau-de Gennes surface tension

Replacing the scalar order parameter of the LdG model by the ansatz,

$$S(z) = \frac{1}{2}\left[1 - \tanh\left(\frac{z}{z_0}\right)\right] \tag{7.61}$$

the free energy density of a nematic in units of coherence length $\xi_{0\perp}$, for homeotropic and planar anchoring, respectively, it comes that,

$$\tilde{f}_\perp = \tau\tilde{S}^2 - 2\tilde{S}^3 + \tilde{S}^4 + \frac{1}{2}\left(\frac{\partial\tilde{S}}{\partial z}\right)^2, \quad \tilde{f}_\parallel = \tau\tilde{S}^2 - 2\tilde{S}^3 + \tilde{S}^4 + \frac{1}{2}\frac{6+\kappa}{6+4\kappa}\left(\frac{\partial\tilde{S}}{\partial z}\right)^2 \tag{7.62}$$

and integrating over the z axis, gives the surface tension,

$$\gamma_\perp = \frac{z_0}{12} + \frac{1}{6z_0}, \quad \gamma_\parallel = \frac{z_0}{12} + \frac{(\frac{6+\kappa}{6+4\kappa})}{6z_0} \tag{7.63}$$

Minimizing the surface tension regarding to z_0, yields,

$$z_{0\perp} = \sqrt{2}, \quad z_{0\parallel} = \sqrt{2}\sqrt{\frac{6+\kappa}{6+4\kappa}} \tag{7.64}$$

which results in the surface tension for homeotropic and planar anchoring,

$$\gamma_\perp = \frac{\sqrt{2}}{6}, \quad \gamma_\parallel = \frac{\sqrt{2}}{6}\sqrt{\frac{6+\kappa}{6+4\kappa}} \tag{7.65}$$

Landau-de Gennes Euler-Lagrange equations

Euler-Lagrange Equation for the free energy density

$$\partial_\alpha \left[\frac{\partial f}{\partial_\alpha Q_{ij}} \right] - \frac{\partial f}{\partial Q_{ij}} = 0 \tag{7.66}$$

This equation ca calculated separately to each individual component of the symmetric, traceless matrix $\boldsymbol{Q}$, which gives five equations, with $\Sigma = \left(\tau + \frac{4}{3}(2Tr\boldsymbol{Q}^2) + \frac{6q_0^2}{3+2\kappa}) \right)$,

$$\begin{aligned}
&\bullet \left[\frac{\partial f}{\partial q_1} += \partial_x \left(\frac{\partial f}{\partial_x q_1} \right) + \partial_y \left(\frac{\partial f}{\partial_y q_1} \right) + \partial_z \left(\frac{\partial f}{\partial_z q_1} \right) \right] \Leftrightarrow \\
&\left[\frac{2}{3}(4q_1 + 2q_4) \left(\tau + \frac{4}{3} Tr(\boldsymbol{Q}^2) + \frac{6q_0^2}{3+2\kappa} \right) + 8 \left(-q_2^2 + q_4^2 + q_5^2 + 2q_1 q_4 \right) + \frac{4q_0}{3+2\kappa} \left(2\partial_y q_3 - \partial_x q_5 - \partial_z q_2 \right) = \right. \\
&\left. \frac{4\nabla^2 q_1}{3+2\kappa} + \frac{2\nabla^2 q_4}{3+2\kappa} + \frac{2\kappa}{3+2\kappa} \left(\partial_{xx} q_1 + \partial_{zz} q_1 + \partial_{yx} q_2 + \partial_{zz} q_4 - \partial_{yz} q_5 \right) + \frac{4q_0}{3+2\kappa} \left(\partial_x q_5 - 2\partial_y q_3 + \partial_z q_2 \right) \right] \Leftrightarrow \\
&\left[\frac{3+2\kappa}{6}(4q_1 + 2q_4)\Sigma + 2(3+2\kappa) \left(-q_2^2 + q_4^2 + q_5^2 + 2q_1 q_4 \right) = \right. \\
&\left. \nabla^2 q_1 - q_0 \left(2\partial_x q_5 - 4\partial_y q_3 + 2\partial_z q_2 \right) + \frac{\kappa}{2} \left(\partial_{xx} q_1 + \partial_{zz} q_1 + \partial_{yx} q_2 + \partial_{zz} q_4 - \partial_{yz} q_5 \right) + \frac{1}{2}\nabla^2 q_4 \right] \Leftrightarrow \\
&\left[\nabla^2 q_1 + \frac{\kappa}{3} \left(2\partial_{xx} q_1 + \partial_{zz} q_1 + \partial_{xz} q_3 - \partial_{yy} q_4 + \partial_{zz} q_4 - 2\partial_{yz} q_5 \right) - 4q_0 \left(\partial_y q_3 - \partial_z q_2 \right) \right. \\
&\left. = \frac{2}{3}(3+2\kappa) q_1 \Sigma - \frac{4}{3}(3+2\kappa) \left(q_1^2 + q_2^2 + q_3^2 - 2q_4^2 - 2q_5^2 - 2q_1 q_4 \right) \right]
\end{aligned} \tag{7.67}$$

$$\begin{aligned}
&\bullet \left[\frac{\partial f}{\partial q_2} = \partial_x \left(\frac{\partial f}{\partial_x q_2} \right) + \partial_y \left(\frac{\partial f}{\partial_y q_2} \right) + \partial_z \left(\frac{\partial f}{\partial_z q_2} \right) \right] \Leftrightarrow \\
&\left[\frac{2}{3}(4q_2) \left(\tau + \frac{4}{3} Tr(\boldsymbol{Q}^2) + \frac{6q_0^2}{3+2\kappa} \right) - 16 \left(q_1 q_2 + q_2 q_4 + q_3 q_5 \right) + \frac{4q_0}{3+2\kappa} \left(\partial_z q_1 - \partial_x q_3 - \partial_z q_4 + \partial_y q_5 \right) = \right. \\
&\left. \frac{4\nabla^2 q_2}{3+2\kappa} + \frac{2\kappa}{3+2\kappa} \left(\partial_{xy} q_1 + \partial_{xx} q_2 + \partial_{yy} q_2 + \partial_{yz} q_3 + \partial_{yz} q_4 + \partial_{xz} q_5 \right) + \frac{4q_0}{3+2\kappa} \left(-\partial_z q_1 + \partial_x q_3 + \partial_z q_4 - \partial_y q_5 \right) \right] \\
&\Leftrightarrow \left[\nabla^2 q_2 + \frac{\kappa}{2} \left(\partial_{xy} q_1 + \partial_{xx} q_2 + \partial_{yy} q_2 + \partial_{yz} q_3 + \partial_{yz} q_4 + \partial_{xz} q_5 \right) - 2q_0 \left(\partial_x q_5 - 2\partial_y q_3 + \partial_z q_2 \right) \right. \\
&\left. = \frac{(3+2\kappa)}{6} q_2 \Sigma - 4(3+2\kappa) \left(q_1 q_2 + q_2 q_4 + q_3 q_5 \right) \right]
\end{aligned} \tag{7.68}$$

$$\bullet \left[\frac{\partial f}{\partial q_3} = \partial_x\left(\frac{\partial f}{\partial_x q_3}\right) + \partial_y\left(\frac{\partial f}{\partial_y q_3}\right) + \partial_z\left(\frac{\partial f}{\partial_z q_3}\right)\right] \Leftrightarrow$$
$$\left[\frac{2}{3}(4q_2)\left(\tau + \frac{4}{3}Tr(\boldsymbol{Q}^2) + \frac{6q_0^2}{3+2\kappa}\right) - 16\left(q_2q_5 - q_3q_4\right) + \frac{4q_0}{3+2\kappa}\left(-2\partial_y q_1 + \partial_x q_2 - \partial_y q_4 - 2\partial_z q_5\right) =\right.$$
$$\frac{4\nabla^2 q_3}{3+2\kappa} + \frac{2\kappa}{3+2\kappa}\left(\partial_{yz}q_2 + \partial_{xx}q_3 + \partial_{zz}q_3 - \partial_{zx}q_4 + \partial_{yx}q_5\right) + \frac{4q_0}{3+2\kappa}\left(2\partial_y q_1 - \partial_x q_2 + \partial_y q_4 + \partial_z q_5\right)\Bigg] \Leftrightarrow$$
$$\Bigg[\nabla^2 q_3 + \frac{\kappa}{2}\left(\partial_{yz}q_2 + \partial_{xx}q_3 + \partial_{zz}q_3 - \partial_{zx}q_4 + \partial_{yx}q_5\right) - 2q_0\left(-\partial_y q_1 + \partial_x q_2 - \partial_y q_4 - \partial_z q_5\right)$$
$$\left. = \frac{(3+2\kappa)}{6}q_3\Sigma - 4(3+2\kappa)\left(q_2q_5 + q_3q_4\right)\right] \tag{7.69}$$

$$\bullet \left[\frac{\partial f}{\partial q_4} = \partial_x\left(\frac{\partial f}{\partial_x q_4}\right) + \partial_y\left(\frac{\partial f}{\partial_y q_4}\right) + \partial_z\left(\frac{\partial f}{\partial_z q_4}\right)\right] \Leftrightarrow$$
$$\left[\frac{2}{3}(4q_4 + 2q_1)\left(\tau + \frac{4}{3}Tr(\boldsymbol{Q}^2) + \frac{6q_0^2}{3+2\kappa}\right) + 8\left(q_1^2 - q_2^2 + q_3^2 + 2q_1q_4\right) + \frac{4q_0}{3+2\kappa}\left(\partial_z q_2 + \partial_y q_3 - 2\partial_x q_5\right) =\right.$$
$$\frac{4\nabla^2 q_4}{3+2\kappa} + \frac{2\nabla^2 q_1}{3+2\kappa} + \frac{2\kappa}{3+2\kappa}\left(\partial_{zz}q_1 + \partial_{xy}q_2 - \partial_{xz}q_3 + \partial_{yy}q_4 + \partial_{zz}q_5\right) + \frac{4q_0}{3+2\kappa}\left(-\partial_z q_2 - \partial_y q_3 + 2\partial_x q_5\right)\Bigg] \Leftrightarrow$$
$$\Bigg[\frac{3+2\kappa}{6}(4q_4 + 2q_1)\Sigma + 2(3+2\kappa)\left(q_1^2 - q_2^2 + q_3^2 + 2q_1q_4\right) =$$
$$\nabla^2 q_4 - q_0\left(2\partial_z q_2 + 2\partial_y q_3 - 4\partial_x q_5\right) + \frac{\kappa}{2}\left(\partial_{zz}q_1 + \partial_{xy}q_2 - \partial_{xz}q_3 + \partial_{yy}q_4 + \partial_{zz}q_4\right) + \frac{1}{2}\nabla^2 q_1\Bigg] \Leftrightarrow$$
$$\Bigg[\nabla^2 q_4 + \frac{\kappa}{3}\left(-\partial_{xx}q_1 + \partial_{zz}q_1 - 2\partial_{xz}q_3 + 2\partial_{yy}q_4 + \partial_{zz}q_4 + \partial_{yz}q_5\right) - 4q_0\left(\partial_y q_3 - \partial_z q_2\right)$$
$$\left. = \frac{2}{3}(3+2\kappa)q_4\Sigma - \frac{4}{3}(3+2\kappa)\left(2q_1^2 - q_2^2 + 2q_3^2 - q_4^2 - q_5^2 + 2q_1q_4\right)\right] \tag{7.70}$$

$$\bullet \left[\frac{\partial f}{\partial q_5} = \partial_x\left(\frac{\partial f}{\partial_x q_5}\right) + \partial_y\left(\frac{\partial f}{\partial_y q_5}\right) + \partial_z\left(\frac{\partial f}{\partial_z q_5}\right)\right] \Leftrightarrow$$
$$\left[\frac{2}{3}(4q_5)\left(\tau + \frac{4}{3}Tr(\boldsymbol{Q}^2) + \frac{6q_0^2}{3+2\kappa}\right) + 8\left(q_1q_5 - q_2q_3\right) + \frac{4q_0}{3+2\kappa}\left(\partial_x q_1 - \partial_y q_2 + \partial_z q_3 - 2\partial_x q_4\right) =\right.$$
$$\frac{4\nabla^2 q_5}{3+2\kappa} + \frac{2\kappa}{3+2\kappa}\left(-\partial_{zy}q_1 + \partial_{xy}q_3 - \partial_{zy}q_4 + \partial_{yy}q_5\right) + \frac{4q_0}{3+2\kappa}\left(-\partial_x q_1 + \partial_y q_2 - \partial_z q_3 - 2\partial_x q_4\right)\Bigg] \Leftrightarrow$$
$$\Bigg[\nabla^2 q_5 + \frac{\kappa}{2}\left(-partial_{zy}q_1 + \partial_{xy}q_3 - \partial_{zy}q_4 + \partial_{yy}q_5\right) - 2q_0\left(2\partial_x q_1 - \partial_y q_2 + \partial_z q_3 + \partial_x q_4\right)$$
$$\left. = \frac{(3+2\kappa)}{6}q_3\Sigma + 4(3+2\kappa)\left(q_2q_5 + q_3q_4\right)\right] \tag{7.71}$$

Bibliography

[1] E.B.Priestley, Peter J. Wojtowicz, and Ping Sheng. *Introduction to Liquid Crystals*. Plenum Press, London, 1974.

[2] Timothy J.Sluckin, David A.Dunmur, and Horst Stegemeyer. *Crystals that flow*. Taylor & Francis, 2004.

[3] O. Lehmann. On flowing crystals. *Zeitschrift fur Physikalische Chemie*, 4:462–72, 1889.

[4] Egbert F.Gramsbergen, Lech Longa, and Wim H. de Jeu. Landau theory of the nematic-isotropic phase transition. *Physics Reports*, 135(4):195–257, 1986.

[5] Geoffrey R. Luckhurst and Timothy J. Sluckin, editors. *Biaxial Nematic Liquid Crystals, Theory, Simulation and Experiment*. Wiley, 2015.

[6] Michael J. Stephen and Joseph P.Straley. Physics of liquid crystals. *Reviews of Modern Physics*, 46(4):617, 1974.

[7] David C.Wright and N.David Mermin. Crystalline liquids: the blue phases. *Reviews of Modern Physics*, 61(2):385, 1989.

[8] D. K. Yang and P. P. Crooker. Chiral-racemic phase diagrams of blue-phase liquid crystals. *Physical Review A*, 35(3):1893–1895, 1987.

[9] Introduction to liquid crystals, `http://barrett-group.mcgill.ca/tutorials/liquid_crystal/LC01.htm`.

[10] P.M.Chaikin and T.C.Lubensky. *Principles of condensed matter physics*. Cambridge University Press, 1995.

[11] Lev M.Blinov. *Structure and Properties of Liquid Crystals*. Springer, 2011.

[12] Gareth Paul Alexander. *Liquid Crystalline Blue Phases and Swimmer Hydrodynamics*. PhD thesis, University of Oxford, 2008.

[13] Nelson Rei Bernardino, Maria Carolina Figueirinhas Pereira, and Margarida Maria Telo da Gama Nuno Miguel Silvestre. Structure of the cholesteric-isotropic interface. *Soft Matter*, 10(47):9399–9402, 2014.

[14] Emre Bukusoglu Juan J. de Pablo Nicholas L.Abbott Xiaoguang Wanga, Daniel S.Millera. Topological defects in liquid crystals as templates for molecular self-assembly. *Nature materials*, 15(1):106–112, 2015.

[15] M. Tasinkevych, P. Patricio N.M. Silvestre, and M.M. Telo da Gama. Colloidal interaction in two-dimensional nematics. *The European Physical Journal E*, 9(4):341–347, 2002.

[16] National science foundation, `http://www.nsf.gov/news/mmg/mmg_disp.jsp?med_id=68657&from=mmg`.

[17] Textures of cholesteric liquid crystals, `http://www.personal.kent.edu/~bisenyuk/liquidcrystals/textures2.html`.

[18] S. Faetti and V. Palleschi. Nematic-isotropic interface of some members of the homologous series of 4-cyano-4'-(n-alkyl)biphenyl liquid crystals. *Physical Review A*, 30(6):3241, 1984.

[19] P. J. Collings D.K. Yang P.P. Crooker J. D. Miller, P. R. Battle. Temperature-concentration phase diagram for the blue phases of a highly chiral liquid. *Physical Review A*, 35(9):3959–3960, 1987.

[20] Yves Bouligand, Sven T. Lagerwall, and Bengt Stebler. Blue-phase drops on a glass interface and their decoration at the cholesteric transition. *C. R. Chimie*, 11(3):212–220, 2009.

[21] A.C. Pawsey, J.S. Lintuvuori, T.A. Wood, J.H.J. Thijseen, D.Marenduzzo, and P. S. Clegg. Colloidal particles at the interface between an isotropic liquid and a chiral liquid crystal. *Soft Matter*, 8:8422–8428, 2012.

[22] J. S. Lintuvuori, A. C. Pawsey, K. Stratford, P. S. Clegg M. E. Cates, and D. Marenduzzo. Colloidal templating at a cholesteric-oil interface: Assembly guided by an array of disclination lines. *Physical Review Letters*, 110(18):187801, 2013.

[23] Anne C. Pawsey and Juho S. Lintuvuori. Colloidal particles at chiral liquid crystal interfaces. *Liquid Crystals Today*, 23(2):32–37, 2014.

[24] B. Jerome. Surface effects and anchoring in liquid crystals. *Rep. Prog. Phys.*, 54(3):391–451, 1991.

[25] R. Meister, H. Dumoulin, M.-A. Hallé, and P. Pieranski. The anchoring of a cholesteric liquid crystal at the free surface. *J. Phys. II France*, 6(6):827–844, 1996.

[26] Yiqun Bai and Nicholas L. Abbott. Recent advances in colloidal and interfacial phenomena involving liquid crystals. *Langmuir*, 27(10):5719–5738, 2011.

[27] Nuno M. Silvestre, Maria Carolina Figueirinhas Pereira, Nelson R. Bernardino, and Margarida M. Telo da Gama. Wetting of cholesteric liquid crystals. *The European Physical Journal E*, 39(13), 2016.

[28] R. S. Zola, L. R. Evangelista, Y.-C Yang, and D.-K. Yang. Surface induced phase separation and pattern formation at the isotropic interface in chiral nematic liquid crystals. *Physical Review Letters*, 110(5):057801, 2013.

[29] J.L. West, A. Glushchenko, and Guangxun Liao. Drag on particles in a nematic suspension by a moving nematic-isotropic interface. *Physical Review E*, 66(1):012702, 2002.

[30] D. Adrienko, M.Tasinkevych, P. Patrício, and M. M. Telo da Gama. Interaction of colloids with a nematic-isotropic interface. *Physical Review E*, 69(2):021706, 2004.

[31] Bohdan Senyuka Ivan I. Smalyukh Mykola Tasinkevych Nuno M. Silvestre, Qingkun Liu. Towards template-assisted assembly of nematic colloids. *Physical Review Letters*, 112(22):225501, 2014.

[32] J.M Romero-Enrique P.Patrício, C.-T. Pham. Wetting transition of a nematic liquid crystal on a periodic wedge-structured substrate. *The European Physical Journal E*, 26(1):97–101, 2008.

[33] L. Harnau, F. Penna, and S. Dietrich. Colloidal hard-rod fluids near geometrically structured substrates. *Physical Review E*, 70(2):021505, 2004.

[34] Jose Manuel Romero-Enrique, Chi-Tuong Pham, and Pedro Patricio. Scaling of the elastic contribution to the surface free energy of a nematic liquid crystal on a sawtoothed substrate. *Physical Review E*, 82(1):011707, 2010.

[35] P. Patricio, J. M. Romero-Enrique, N. M. Silvestre, N. R. Bernardino, and M. M. Telo da Gama. Complex fluids at complex surfaces: Simply complicated? *Molecular Physics*, 109(7-10):1067–1075, 2011.

[36] P. Patricio, N. M. Silvestre, C.-T. Pham, and J. M. Romero-Enrique. Filling and wetting transitions of nematic liquid crystals on sinusoidal substrates. *Physical Review E*, 84(2):021701, 2011.

[37] N. M. Silvestre, Z. Eskandari, P. Patricio, J. M. Romero-Enrique, and M. M. Telo da Gama. Nematic wetting and filling of crenellated surfaces. *Physical Review E*, 86(1):011703, 2012.

[38] Maria Carolina Figueirinhas Pereira. Wetting of cholesteric liquid crystals. Master's thesis, Faculty of Sciences, Lisbon University, 2015.

[39] Anne Claire Pawsey. *Colloids at Liquid Crystal Interfaces*. PhD thesis, The University of Edinburgh, 2014.

[40] Anne C. Pawsey and Paul S. Clegg. Colloidal particles in blue phase liquid crystals. *Soft Matter*, 11:3304–3312, 2015.

[41] T. J. Dingemansa L. A. Madsen, M. Nakata, and E. T. Samulski. Thermotropic biaxial nematic liquid crystals. *Physical Review Letters*, 92(14):145505, 2004.

[42] D.Demus, J.Goodby, H.-W. Spiess G.W.Gray, and V.Vill, editors. *Handbook of Liquid CrCrystals Vol2A, Low Molecular Weight Liquid Crystals*. Wiley, 1998.

[43] Epifanio G Virga. *Variational Theories for Liquid Crystals*. Chapman & Hall, 1994.

[44] J. Thoen. Adiabatic scanning calorimetric results for the blue phases of cholesteryl nonanoate. *Physical Review A*, 37(5):1754–1759, 1988.

[45] Maurice Kleman and Oleg D. Lavrentovich. *Soft Matter Physics: An Introduction*. Springer, 2001.

[46] P. W. Anderson W. F. Brinkman S. Meiboom, James P. Sethna. Theory of the blue phase of cholesteric liquid crystals. *Physical Review Letters*, 46(18):1216, 1981.

[47] F.C.Frank. I. liquid crystals. on the theory of liquid crystals. *Discussions of the Faraday Society*, 25:19–28, 1958.

[48] Iancu Pardowitz and Siegfried Hess. Elasticity coefficients of nematic liquid crystals. *Journal of Chemical Physics*, 76(3):1485, 1982.

[49] S. Chandrasekhar. The structure and energetics of defects in liquid crystals. *Advances in Physics*, 35(6):507–596, 1986.

[50] Ian W.Stewart. *The Static and Dynamic Continuum theory of Liquid Crystals - A Mathematical Introduction*. Taylor & Francis, 2004.

[51] O.D. Lavrentovich. Defects in liquid crystals: Surface and interfacial anchoring effects. *NATO Science Series*, 127(3):161–195, 2003.

[52] Jonathan V. Selinger. *Introduction to the Theory of Soft Matter: From Ideal Gases to Liquid Crystals*. Springer, 2015.

[53] W.H.de Jeu G.Vertogen. *Thermotropic Liquid Crystals, Fundamentals*. Springer, 1988.

[54] P. G. De Gennes. Short range order effects in the isotropic phase of nematics and cholesterics. *Molecular Crystals and Liquid Crystals*, 12(3):193–214, 1971.

[55] V. Popa-Nita, T. J. Sluckin, and A. A. Wheeler. Static and kinetics at the nematic-isotropic interface: Effects of biaxiality. *J. Phys. II*, 7(9):1225–1243, 1997.

[56] P.G. de Gennes and J. Prost. *The Physics of Liquid Crystals*. Oxford University Press, New York, 1993.

[57] George E. Andrews, Richard Askey, and Ranjan Roy. *Special Functions*. Cambridge University Press, 1999.

[58] George B. Arfken and Hans J. Weber. *Mathematical Methods for Physicists*. Elsevier Academic Press, 2005.

[59] Shri Singh. *Phase transitions in liquid crystals*. Elsevier, 2000.

[60] Richard. A. L. Jones. *Soft Condensed Matter*. Oxford University Press, 2002.

[61] A. Poniewierski and T.J. Sluckin. On the free energy density of nonuniform nematics. *Molecular Physics*, 55(5):1113–1127, 1985.

[62] N. Schopohl and T. J Sluckin. Defect core structure in nematic liquid crystals. *Physical Review Letters*, 59(22):2582, 1987.

[63] C. Blanc, D. Svensek, S. Zumer, and M. Nobili. Dynamics of nematic liquid crystal disclinations: The role of the backflow. *Physical Review Letters*, 95(9):097802, 2005.

[64] P. E. Cladis and M. Kléman. Non-singular disclinations of strength s = + 1 in nematics. *Le journal de physique*, 33(5-6):591–598, 1972.

[65] L. Longa, D. Monselesan, and H.-R. Trebin. An extension of the landau-ginzburg-de gennes theory for liquid crystals. *Liquid Crystals*, 2(6):769–796, 1987.

[66] E. de Miguel L.F. Rull E.Martin de Rio, M.M. Telo da Gama. Surface-induced alignment at model nematic interfaces. *Physical Review E*, 52(5):5028–5039, 1995.

[67] Ping Sheng. Phase transition in surface-aligned nematic films. *Physical Review Letters*, 37(16):1059, 1976.

[68] G. Barbero and G. Durand. On the validity of the rapini-papoular surface anchoring energy formin nematic liquid crystals. *J. Physique*, 47(12):2129–2134, 1986.

[69] J.-B. Fournier and P. Galatola. Modeling planar degenerate wetting and anchoring in nematic liquid crystals. *Europhysics Letters*, 72(3):403–409, 2005.

[70] Jian-Ming Jin. *The Finite Element Method in Electromagnetics*. John Willey & Sons, Inc, Urbana-Champaign, Illinois, second edition edition, 2002.

[71] The finite element method (fem), comsol multiphysics cyclopdeia, `https://www.comsol.com/multiphysics/finite-element-method`.

[72] J.D.Parsons. Ordering and distortion at the nematic-isotropic fluid interface. *Molecular Crystals and Liquid Crystals*, 31(1-2):79–91, 1975.

[73] Hitoshi Mada. Study on surface alignment of nematic liquid crystals, temperature dependece of pretilt angles. *Molecular Crystals and Liquid Crystals*, 51(1-2):43–56, 1979.

[74] Alfred Saupe. Disclinations and properties of the directorfield in nematic and cholesteric liquid crystals. *Molecular Crystals and Liquid Crystals*, 21:211–238, 1973.

[75] Timothy J. Bunning, Deborah L. Vezie, Pamela F. Loyd, Peter D. Haaland, Edwin L. Thomas, and W. Wade Adams. Cholesteric liquid crystals: image contrast in the tem. *Liquid Crystals*, 16(5):769–781, 1994.

[76] Jun Yoshioka, Fumiya Ito, Hiroaki Takahashi Yuto Suzuki, Hideaki Takizawa, and Yuka Tabe. Director/barycentric rotation in cholesteric droplets under temperature gradient. *Soft Matter*, 10(32):5869–77, 2014.